Interface Characterization of Multilayer Mirrors

By

Sanjay Kumar Rai

Enrollment No. PHYS 03 2007 04 016

Raja Ramanna Centre for Advanced Technology, Indore

Indore – 452013, India

A thesis submitted to the
Board of Studies in Physical Sciences

In partial fulfillment of requirements
For the Degree of

DOCTOR OF PHILOSOPHY

Of

HOMI BHABHA NATIONAL INSTITUTE

October 2013

Homi Bhabha National Institute

Recommendations of the Viva Voce Board

As members of the Viva Voce Board, we certify that we have read the dissertation prepared by Sanjay Kumar Rai entitled "Interface characterisation of multilayer mirrors" and recommend that it may be accepted as fulfilling the dissertation requirement for the Degree of Doctor of Philosophy.

Chairman Dr.L.M. Kukreja Date: 30.06.2014.

Guide Dr. G.S.Lodha Date 30.06.14

Member 1 Dr. S.K. Gupta Date

Member 2 Dr. H.S.Rawat Date 30/06/2014.

Member 3 Dr.C.Mukharjee Date 30/06/14

Prof. A.Subrahmanyam
(External Examiner) IIT Madras. Date 30.06.14.

Final approval and acceptance of this dissertation is contingent upon the candidates submission of the final copies of the dissertation to HBNI. I hereby certify that I have read this dissertation prepared under my direction and recommend that it may be accepted as fulfilling the dissertation requirement.

Date : 30.06.14

Place RRCAT, Indore

Guide: Dr. G. S. Lodha

STATEMENT BY AUTHOR

This dissertation has been submitted in partial fulfilment of requirements for an advanced degree at Homi Bhabha National Institute (HBNI) and is deposited in the Library to be made available to borrowers under rules of the HBNI.

Brief quotations from this dissertation are allowable without special permission, provided that accurate acknowledgement of source is made. Requests for permission for extended quotation from or reproduction of this manuscript in whole or in part may be granted by the Competent Authority of HBNI when in his or her judgment the proposed use of the material is in the interests of scholarship. In all other instances, however, permission must be obtained from the author.

Sanjay Kumar Rai

DECLARATION

I, hereby declare that the investigation presented in the thesis has been carried out by me. The work is original and has not been submitted earlier as a whole or in part for a degree/diploma at this or any other Institution/ University.

Sanjay Kumar Rai

Publications Based on the work

In Journals

1. “NbC/Si multilayer mirror for next generation EUV light sources”, Mohammed H. Modi, **S. K. Rai,** Mourad Idir, F. Schaefers, and G. S. Lodha, Optics Express 20, (2012) 1514.

2. “Ion beam sputter deposited W/Si multilayers: Influence of re-sputtering on the interface structure and structure modification at ultra short periods” **S.K. Rai**, Arijeet Das, A.K. Srivastava, G.S. Lodha, Rajnish Dhawan. Applied Surface Science 257, (2011) 10704.

3. “X-ray characterization of thin foil gold mirrors of a soft X-ray telescope for ASTROSAT Characterization of SXT mirrors by X-ray reflectivity” Archna Sagdeo, **S. K. Rai**, Gyan S. Lodha, K. P. Singh, Nisha Yadav, R. Dhawan, Umesh Tonpe and M. N. Vahia, Experimental Astronomy 28, (2010) 11.

4. “Oxidation studies of niobium thin films at room temperature by X-ray reflectivity” K.J.S. Sokhey, **S.K. Rai**, G.S. Lodha, Applied Surface Science 257, (2010) 222.

5. “Effect of surface roughness on multilayer film growth” Modi M.H., **Rai S.K.,** Thomasset A., Lodha G.S. and Idir M. The European Physical Journal 168, (2009) 27.

6. “Effect of Si layer thickness on structural properties of Co/Si multilayer system” Archna Jaiswal, **Sanjay K. Rai**, MK Tiwari1, V R Reddy, G S Lodha, and R V Nandedkar, J of Phys : Condens Matter 19 (2007) 016001

7. “Surface and Interface study of pulsed-laser-deposited off-stociometric NiMnSb thin films on Si(100) substrate” **S. K. Rai,,** S. Rai, M.K.Tiwari, G. S. Lodha, M. H. Modi, M. K. Chattopadhyay, S. Majumdar, S. Gardelis, Z. Viskadourakis, J.Giapintzakis, R. V. Nandedkar, S. B. Roy, and P. Chaddah. Physical Review B 73, (2006) 034517.

In conference Proceedings

8. “Growth of Short period multilayers for x-ray mirror” **Sanjay K. Rai**, Arijeet Das, R. Dhawan and G. S. Lodha, 53 DAE Solid State Physics Symposium (2008) Mumbai, 367.

9. “Hard x-ray reflectometer/ diffractometer station” **Sanjay K. Rai**, Archna Jaiswal, B.Gowrishankar and G. S. Lodha 52nd DAE Solid State Physics Symposium held at Mysore University, Mysore (2007), 421.

10. "Ion-Beam Sputtering System for depositing thin films and multilayers" Rajnish Dhawan, **Sanjay K. Rai**, M.H.Modi, B.Gowri Sankar, Shradha Tiwari, Anand Valecha, M.A.Ansari, V.P. Bhanage, C.P.Navathe,G.S.Lodha, RRCAT report reference no. RRCAT/2012-02

DEDICATION

माता जी और

पिता जी को समर्पित

Acknowledgement

I must confess that writing the acknowledgement is simultaneously most interesting and difficult part of the thesis writing. You get a nice feeling that now the writing process which was keeping you busy for long time is finally going to be over. But at same time it gives a feeling of emptiness, somewhere I had started liking this busy schedule where I have to maintain a balance between regular office works and write the thesis also.

It is my pleasure to acknowledge here the efforts of many people who have made possible the works described in this dissertation. First I would like to thank my Guide Dr. G. S. Lodha who has encouraged me to pursue the work in this area and gave very useful suggestion. I have learnt from him a very important lesson of life, to always remain hopeful about the future. I wish to record my deepest gratitude to him for his erudite guidance and active support at every step of this work. I thank him for his patience and cooperation during the work and giving shape to my thesis.

I am extremely thankful to Dr. S.K. Deb, for his constant encouragement. I am grateful to Dr. S.K. Gupta, BARC and Dr. L.M. Kukreja members of Doctoral Committee for their constructive criticism, motivation and guidance. I also want to thank Dr. S.B. Roy for guiding me during my course work report preparation.

I wish to record my deep sense of gratitude to Prof. Ullrich Pietsch (University of Siegen, Germany) and Prof. A. Subrahmanyam (IIT Madras , Chennai) for extensively reviewing my thesis and giving very useful advice on improving the quality of thesis presentation.

Research is a team work and it cannot be done alone. I got lot of help from my colleagues during this work I am thankful to Mr. Nageswararao Pothana and Mr. Rajnish Dhawan and Mr. Praveen Yadav for helping me in doing my experiments and lots of other support which I got from them time to time. I am thankful to Dr. M.H. Modi, Dr. Arvind Srivastava, Ms. Pragya Tiwari, Dr. Maheswar Nayak and Dr. M.K. Tiwari, for various experimental assistance and fruitful discussion to carry out my work. I would like thank Mr. Pushpen Mondal, Mr. R. K. Gupta, for helping me in TEM and soft x-ray reflectivity measurements.

I am thankful to Mr. B. Gowrisankar for mechanical engineering support in assembling the reflectometer and Ion beam sputtering system. I want to thank Mr.

Viraj Bhange, Ms. Shradha and her team for helping me in automation of developed systems.

I specially thank Dr. Archna Sagdev and Dr. Pooja Gupta for their help, support, fruitful discussions and friendly environment. Both helped me extensively in finishing my thesis work fast by reading the chapters in a tight schedule.

Lots of other colleagues of my Division have helped me at various moments. Listing names of everybody is not possible but I profusely thank the entire ISUD members who have joyfully supported me in concluding my work.

I cannot forget to thank my tea club members Dr. Kanwaljeet Singh Sokhey , Dr. Tapas Ganguli and Dr. M.A. Manekar for the various interesting and thought provoking discussion we had during our tea breaks.

I am thankful to all the collaborators who work in other places. I thank Dr. Franz Schaefers, BESSY, Germany and colleagues in Nagoya University Japan, for soft x-ray measurements of some of the samples used in this work. Thanks are due to Prof K. P. Singh and Prof. M.N. Vahia of TIFR for giving me opportunity to work on replicated gold mirrors of ASTROSAT Indian x-ray Telescope.

Last, but not the least, I want to thank, from the depth of my heart, my beloved wife Rashmi, who has endured with me, through this arduous journey; our kids Suyash and Kritika for being a source of constant joy to us and my mother and my father, for making me what I am.

Contents

SYNOPSIS

Thrust of this thesis is centered on development of short period grazing incidence hard x-ray mirrors and soft x-ray normal incidence mirrors with an aim that they can be used in Indus-1 and Indus-2 beamlines. To reach this objective we have developed moderate resolution reflectometer capable of carrying out x-ray reflectivity, grazing incidence diffraction and powder diffraction with very little modification. We also carried out development of Ion Beam Sputtering based thin film deposition system. This deposition system was used for fabricating thin film structures, x-ray mirrors and various other multilayers studied. We have carried out detailed investigations on the surface and interface of few single and bilayer structures initially, using the developed system, before carrying out fabrication and characterization of targeted multilayer mirrors. X-ray reflectivity, grazing incidence x-ray diffraction and cross-sectional TEM are the main probes used for characterizing these multilayer mirrors and thin film structures.

X-ray multilayer structure consists of alternating layers of high and low electron density materials. In x-ray multilayer the reflectivity from each interface add up coherently and produce maximum reflectivity at certain scattering vectors [1]. X-ray multilayers with small periods around ~ 2nm are of great significance. This is because of their widespread use as radiation-stable dispersive optical elements, polarizers for synchrotron radiation, dispersive elements for x-ray diagnostics of high-temperature plasmas, normal incidence reflectors for (soft-) x-ray microscopy in the water window (2 to 4 nm), for applications in x-ray astronomy and for experiments with x-ray free electron lasers (XFEL) [1-6]. Our centre has two synchrotron sources Indus-1 and Indus-2 operating at 450 MeV and 2.5 GeV electron energy respectively. Various beamline on these sources would find multilayer based x-ray optics quite useful. Worldwide, use of multilayer mirrors at synchrotron beamlines has increased significantly in recent times [7]. Using multilayer optics in a beamline enhances the range of experiments with increased flux. Usefulness of these structures is governed primarily by the practically achievable interface perfection. An interaction between extrinsic and intrinsic interface roughness induced by the base substrate and growth process, respectively, controls the interface morphology while thermodynamic characteristics of the forming layers determine interface reactions such as mixing, inter diffusion or compound formation. Compositionally sharp and topologically smooth

interfaces with good optical contrast are required for high reflectivity. Atomic-scale surface or interface roughness causes scattering losses and can significantly lower the reflectivity. Influence of the interface structure becomes prominent on the reflectivity performance when period of the multilayer is reduced. Furthermore, a multilayer with steep concentration gradients at the interfaces is inherently unstable and may experience interface degradation under high radiation loads and/or high temperatures to which x-ray optics are often exposed (e.g. synchrotron beam lines, intense plasma source diagnostics). Multilayers, when exposed to high intense synchrotron radiation, show quick rise in local temperature up to 600^0C [8,9]. The rise in temperature in metallic multilayers leads to structural modification like crystallization, formation of intermetallic compounds, inter diffusion between layers, and change in layer roughness. Their performance is thus limited by the degradation of quality in high temperature environment. In present scenario, recently developed free electron laser (FEL) sources like Stanford, DESY, SACLA and Fermi@elettra [10] generate x-ray pulses of very high intensity induce radiation damage in optical components [11,12]. Hence, it becomes important to study the thermal stability of optical elements before it is exposed to intense synchrotron radiation.

We have undertaken development of short period multilayer, which can be used as monochromator for hard x-rays on Indus-2 beamline and normal incidence mirrors for soft x-rays on Indus-1/ Indus-2 source. Details of optimization process and issues related with the growth of short period sputter deposited W/Si and W/B_4C multilayer mirrors have been described in the report. Changes in the interface structure on reducing the multilayer period have been analyzed. In all sputtering deposition techniques it is known that large number of sputtering gas ions and neutrals get reflected from the target and hit the freshly growing film surface. This process of back scattering is equivalent to that of ion/neutral beam hitting the growing surface as if ion assisted deposition is happening. These neutrals and ion hitting the film have sufficient energy to modify the growth and interface nature of the film [13]. This study was focused on the role of reflected sputter gas neutrals on the growth mechanism of short period multilayer mirrors. Information about influence of reflected neutrals on growth of short period multilayers are not available in the literature. It this study we found that with W/Si the shortest period which can be deposited with a continuous layer is 2.8 nm

whereas with W/B_4C it is possible to go upto 1.8 nm periods. Thermal stability of W/B_4C multilayer with change in period has been examined.

Additionally, we have also carried out work on development of normal incidence mirror in VUV soft x-ray region. Mo/Si multilayers are currently the most promising reflective coating for extreme ultraviolet (EUV) lithography operating at near normal incidence angles above 12.6 nm wavelength. However, it has a severe drawback of poor thermal stability caused by negative heat of mixing between Mo and Si. Resultantly this structure undergoes interface degradation right after the deposition process. Different approaches have been adopted in the past to overcome the inter diffusion and structural degradation problem by inserting a barrier layer of boron carbide or carbon between Mo and Si to prevent intermixing [14] and increase the thermal stability to 300 ^{0}C. However, all these efforts lead to significant compromise in reflectivity performance. In this study we report a new multilayer combination comprised of refracting layers of Niobium carbide with spacer layers of silicon as a more stable and high reflecting combination for the 10-20 nm wavelength region. The reflectivity of the new combination is comparable to Mo/Si conventional mirrors. This combination has remained stable upto 700 ^{0}C compared to Mo/Si which was stable upto 100 ^{0}C only and upto 300 ^{0}C with barrier layers [15]. This is a significant improvement towards developing high reflectivity high thermal stability soft x-ray normal incidence multilayer optics.

For undertaking the above research targets we developed (1) A moderate resolution hard X- ray reflectometer for thin films/multilayer characterization and (2) Ion beam sputtering system for deposition of short period multilayers.

X-ray reflectivity is a powerful tool for the characterization of surfaces and interfaces. The technique measures spatial variations in the electron density on length scales from 2-3 nm to 200 nm. It is sensitive to atomic scale roughness, interdiffusion in buried layers, the thickness of multilayer stacks, and in-plane correlations in each of these cases [16,17]. Development of hard X-ray reflectometer helped in characterization of the thin films and multilayers grown in our group for x-ray optics application. This also helped us to generate the expertise needed for development of experimental station on the beamline. We have assembled the X-ray reflectometer/diffractometer on a sealed tube source with a flexibility to shift the assembled system on synchrotron beam line.

The other major motivation for assembling this system was that we required a system capable of handling large size / odd shaped samples for testing in house developed large size optics. As a calibration exercise the developed reflectometer was used to carry out interface studies on various thin films, and multilayers and some of these studies are included. This system was also used to characterize large size (12 cm long and 6 cm wide) Au coated mirrors to be used for x-ray space telescope.

We have also developed a custom designed Ion Beam Sputtering (IBS) system for fabrication of short period x-ray multilayer optics for x-ray monochromators, normal incidence mirrors for x-ray microscopes and multilayer polarizers. Development of the automated system has enabled fabrication of high periodicity x-ray multilayer mirrors. It has also enhanced capabilities to fabricate various other thin films and multilayer structures with repeatable quality.

Outline and layout of thesis chapters

This thesis covers three major works (a) Development of hard-x-ray reflectometer and Ion Beam Sputtering system. These systems are used for fabricating and characterizing thin films structure, x-ray mirrors and various other multilayers (b) Development of short period multilayer mirrors of W/Si and W/B_4C and testing the performance of theses mirrors (c) Development of normal incidence soft x-ray mirrors of NbC /Si and comparing its performance with Mo/Si mirror. Outline of various chapters is described below

1. Introduction

This chapter contains literature survey highlighting usefulness of x-ray multilayer mirrors in x-ray and VUV region, discussion about normal incidence mirrors in VUV range, discussion about short period grazing incidence hard x-ray mirrors. Details of possible uses of multilayer mirrors in Indus-1 and Indus-2 have been reported. Various deposition issues and role of reflected neutrals on growth mechanism of short period multilayer mirrors have been described. Use of hard-x-ray reflectivity measurements in characterization of thin films has been emphasized. Need for in-house development of hard x-ray reflectometer capable of handling odd shaped samples has been explained.

2. Experimental techniques and development of instruments

This chapter describes the details of developed instruments and other experimental techniques used for sample preparation and characterization. It covers theoretical aspect of x-ray reflectivity measurements, discussion about optical response of materials in x-ray region, theory of reflectivity data analysis and issues related with the development of x-ray reflectometer. Design of multilayer based moderate resolution x-ray reflectometer setup capable of doing XRR, GIXRD and powder XRD and details of hardware needed for integration of x-ray reflectometer are presented. Description, of alignment procedure of a reflectometer and sample for correct reflectivity measurements have been elaborated. The developed system has also been used for diffuse scattering measurement, powder diffraction and GIXRD. Procedures, to carry out data processing to arrive at unique solution by model fitting have been described. Details about installation of reflectometer on Indus-2 beamline and initial experiments have also been discussed.

Details of development of Ion Beam Sputtering (IBS) based thin film deposition system have been described. Some examples showing the optimization of the system have been discussed. IBS has advantage over other physical vapor deposition processes like e-beam evaporation and magnetron sputtering. In e-beam evaporation the energy of adatoms reaching the substrate are below 1 eV, hence it is difficult to deposit films with smooth morphology and mostly films grow with columnar structure. This problem of low adatom energy is not present in magnetron sputtering. However, in magnetron sputtering plasma has to be generated and sustained in the sputtering zone and the deposition takes place at higher Ar partial pressure leading to contamination of Ar trapping inside the growing film surface. In ion beam sputtering technique ions are generated inside an independent source which is kept away from sputtering zone and ions are made incident on the target by using extraction mechanism. Hence deposition takes place at a lower working pressure of at least one order below than that in magnetron sputtering. Deposition by IBS technique produce films with better morphology and packing density.

Details of other systems used for characterization and deposition like Magnetron sputtering, Cross sectional Transmission Electron Microscopy have also been described in this chapter.

3. Studies carried out using developed reflectometer and Ion beam sputtering system

This chapter gives details of various case studies carried out using the developed reflectometer as a part of optimization and calibration of the developed systems. As a first study we carried out a detailed study of surface and interface properties of pulsed-laser deposited NiMnSb films on Si (100) substrate as a function of film thickness. As the thickness of films is reduced below 35 nm formation of a porous layer is observed. Porosity in this layer increases with decrease in NiMnSb film thickness. These morphological changes of the ultra thin films are reflected in the interesting transport and magnetic properties of these films. There are no influences of compositional in-homogeneity and surface/interface roughness in these films.

In our investigation on Co/Si we have found that the Co layer in Co/Si multilayer system is highly oriented only for the multilayer containing low thickness of Si layers and this texture is lost as we increase the thickness of the Si layer, this thickness is ~5.6 nm. No XRD peak due to silicide phase in the as-deposited Co/Si ML suggests that silicide phase is not present and even if it is present its volume fraction is so low that its presence is not seen in the XRD pattern.

We also report studies carried out on oxidation behavior of Nb thin films with successful use of x-ray reflectivity to non -destructively probe the structure of Nb thin film deposited on Si substrates and variation in the thickness of oxide layer in the film with time scales of 2 hours to 1.5 years. We report the results of growth kinetics of oxidation process on niobium thin film surfaces exposed to air at room temperature. We have observed that 40% increase in the contact potential increases the growth rate for the first few mono layers of Nb2O5 from 0.22 to 279nm/s. The growth rates of oxidation on these samples become similar after the oxide thicknesses of 2.5nm are reached. It is concluded on the basis of this study that a protective layer should be grown in situ to avoid oxidation of Nb thin film surface for getting good performance.

We also carried out measurements of reflectivity of Au coated thin foil mirrors using Cu Kα, Cr Kα and measurements at Indus-1 reflectivity beamline. These gold mirrors were fabricated in TIFR for a national Astrosat project of fabricating soft x-ray Imaging Telescope. It was found that the roughness of the low-density top gold layer as

obtained from the fitting of X-ray reflectivity data for CuKα radiation is relatively more as compared to that obtained from the CrKα radiation. This indicates that in the mirrors made by this process, the upper surfaces are smoother as compared to the deeper layers This study helped in optimizing the fabrication process with repeatable quality.

4. Development of short period x-ray mirrors

This chapter gives general introduction on short period multilayer mirrors and difficulties faced while depositing short period mirrors. Studies were carried out on W/Si short period multilayers by changing the period from 6 nm to 1.7 nm. Problems encountered on reducing period below 4nm have been discussed. Reason of asymmetry in interface roughness in W/Si multilayer has been explained. Issue of re-sputtering and its influence on a putting limit on lowest thickness of deposition and influencing interface intermixing has been explained. Minimum continuous layer of W and Si has been estimated by XRR data analysis and has been confirmed by CSTEM. This study has demonstrated that at shorter period's role of reflected neutrals hitting the growing films becomes the controlling factor. This observation has been supported with help of Monte-Carlo based SRIM (SRIM 2008 "The Stopping and Range of Ions in Solids", by J. F. Ziegler, J. P. Biersack and M. D. Ziegle) simulations. In these simulations we have shown how these low energy reflected neutrals can re-sputter the films and also produce intermixing. Further it has been explored how B_4C as spacer layer can help in reducing this limit..

Second part of this chapter discusses study on deposition of W/B_4C multilayer mirrors in range of 4 nm to 1.3 nm. It focuses on the interface structure changes on reducing the period thickness. Influence of thickness reduction on interface modification has been experimentally observed using XRR and observed changes have been explained with help of Monte-Carlo based simulation using SRIM. Thermal stability of these, structures has been examined. Annealing studies with period reduction are presented. Minimum continuous layer by XRR data analysis for W/B_4C has been estimated and confirmed by CSTEM. We also report performance of large layer pair (100-300) multilayer mirrors at the minimum continuous layer thickness found in the study. Issues of stress in depositing higher period, large layer pair ML have been described. Normal incidence measurement of these 2nm structures in soft x-ray and its performance evaluation has been reported. These studies have concluded that that with

W/Si the shortest period which can be deposited with a continuous layer is 2.8 nm whereas with W/B_4C it is possible to go upto 1.8 nm periods. Also W/B_4C multilayers with 2 nm period show good thermal stability.

5. Development of normal incidence VUV, soft x-ray mirrors

This chapter is focused on development of normal incidence mirror in soft x-ray regime. There is a discussion about stability problems with Mo/Si normal incidence mirrors, efforts by various groups to increases the thermal stability of this system, and how NbC /Si compares with Mo/Si normal incidence mirrors in 12.5 to 14 nm region. Description of deposition of various NbC /Si samples to analyze growth issues has been reported. High temperature performance of NbC/Si mirrors has been reported. Deposition at various higher temperatures and its influence on interface structure has been described. In this study we have successfully demonstrated that NbC /Si based multilayer mirrors have remained stable upto 700 ^{0}C. This is a considerable improvement compared to Mo/Si mirrors which are stable upto 100 ^{0}C only and upto 350 ^{0}C with barrier layers. This is important development towards fabricating high reflectivity high thermal stability soft x-ray normal incidence multilayer optics.

6. Conclusion Future scope

This chapter briefly discusses final conclusion of the whole work. It also discusses future directions for improving the limits of short period multilayer mirrors, ways to attain large area thickness uniformity and importance of stress reduction in multilayers.

References

1. *E. Spiller, Soft X-Ray Optics 1994 SPIE, Optical Engineering Press.*
2. *S.V. Bobashev, A.V. Golubev, Yu.Ya. Platonov, L.A. Shmaenok, G.S. Volkov, N.N. Salashchenko, V.I. Zayzev, Phys. Scripta 43, (1991) 356.*
3. *J. Kirz, C. Jacobsen, M. Howells, Quart. Rev. Biophys. 28, (1995) 33.*
4. *N.M. Ceglio, D.G.Stearns, D.P. Gaines, A. M. Hawrkluk, and J.E. Trebes, Opt. Lett. 13, (1988) 108.*
5. *M.A. MacDonald, F. Schafers, R. Pohl, and A. Gaupp, Opt. Exp. 17, (2009) 23290.*
6. *J.F. Seely, G. Gutman, J. Wood, G.S. Herman, M.P. Kowaski, J. C. Rife, and W. R. Hunter, Appl. Opt. 32, (1992) 3541.*

7. *Alexande Kazimirov, D.M. Smilgies, Q. Shen, X. Xiao, Q. Hao, E.Fontes, S.H.Bilderback, Sol M. Gruner Y.Platonov and V.V.Martynov, J. Synchrotron Radiation,13, (2006), 204.*

8. *A.F.Jankowski, D.M.Makowiecki, Optical Engineering30, (1991) 2003.*

9. *A. F. Jankowski, L. R. Schrawyer, and M. A. Wall, J. Appl. Phys. 68, (1990) 5162.*

10. *Primoz Rebernik Ribic and G Margaritondo, J. Phys. D: Appl. Phys. 45, (2012), 213001.*

11. *A. R. Khorsand, R. Sobierajski, E. Louis, S. Bruijn, E. D. van Hattum, R. W. E. van de Kruijs, M. Jurek, D. Klinger, J. B. Pelka, L. Juha, T. Burian, J. Chalupsky, J. Cihelka, V. Hajkova, L. Vysin, U. Jastrow, N. Stojanovic, S. Toleikis, H. Wabnitz, K. Tiedtke, K. Sokolowski-Tinten, U.Shymanovich, J. Krzywinski, S. Hau-Riege, R. London, A. Gleeson, E. M. Gullikson, and F.Bijkerk, Opt. Express 18, (2010) 700.*

12. *F. Barkusky, A. Bayer, S. Döring, P. Grossmann, and K. Mann, Opt. Express 18, (2010) 4346.*

13. *E.Franke . H.Neumann, M.Zeuner,W.Frank, F.Bigl, Surf. Coat. Technol. 97, (1997) 90.*

14. *H. Maury, P. Jonnard, J.-M. André, J. Gautier, M. Roulliay, F. Bridou, F. Delmotte, M.-F. Ravet, A. Jérome, P. Holliger, Thin Solid Films 514, (2006) 278.*

15. *T. Bottger , Dirk C. Meyera, Peter Pauflera, Stefan Braunb, Matthew Mossb, Hermann Maib, Eckhard Beyerb , Thin Solid Films 444, (2003) 165.*

16. *Chason E. and Mayer T: M., Critical Reviews in Solid State And Materials Sciences, 22, (1997) 1.*

17. *"High-Resolution X-Ray Scattering: From Thin Films to Lateral Nanostructures" Ullrich Pietsch, Vaclav Holy, Tilo Baumbach, Springer Book , 2004.*

Details of publications produced from different Chapters

Publications from chapter 2

"Hard x-ray reflectometer/ diffractometer station"
Sanjay Rai, Archna Jaiswal, B.Gowrishankar and G. S. Lodha 52nd DAE Solid State Physics Symposium held at Mysore University, Mysore (2007), 421.

"Ion-Beam Sputtering System for depositing thin films and multilayers"
Rajnish Dhawan, **Sanjay Rai**, M.H.Modi, B.Gowri Sankar, Shradha Tiwari, Anand Valecha, M.A.Ansari, V.P. Bhanage, C.P.Navathe,G.S.Lodh RRCAT report reference no. RRCAT/2012-02

Publications from chapter 3

"X-ray characterization of thin foil gold mirrors of a soft X-ray telescope for ASTROSAT Characterization of SXT mirrors by X-ray reflectivity"
Archna Sagdeo, **S. K. Rai**, Gyan S. Lodha, K. P. Singh, Nisha Yadav, R. Dhawan, Umesh Tonpe and M. N. Vahia, Experimental Astronomy 28, (2010) 11.

"Oxidation studies of niobium thin films at room temperature by X-ray reflectivity"
K.J.S. Sokhey, **S.K. Rai**, G.S. Lodha, Applied Surface Science 257, (2010) 222.

"Effect of Si layer thickness on structural properties of Co/Si multilayer system"
Archna Jaiswal, **Sanjay Rai**, MK Tiwari1, V R Reddy, G S Lodha, and R V Nandedkar, J of Phys : Condens Matter 19 (2007) 016001.

"Surface and Interface study of pulsed-laser-deposited off-stociometric NiMnSb thin films on Si(100) substrate"
S. Rai,, S. Rai, M.K.Tiwari, G. S. Lodha1, M. H. Modi, M. K. Chattopadhyay, S. Majumdar, S. Gardelis, Z. Viskadourakis, J.Giapintzakis, R. V. Nandedkar, S. B. Roy, and P. Chaddah, Physical Review B 73, (2006) 034517.

Publications from chapter 4

*"*Role of Reflected neutrals on interface structure of ultra short period W/B_4C multilayer x-ray mirrors*"*
***S.K. Rai**, P.N. Rao, Puspen Mondal ,A.K. Srivastava, Maheswar Nayak, and , G.S.Lodha , To be Submitted*

"Ion beam sputter deposited W/Si multilayers: Influence of re-sputtering on the interface structure and structure modification at ultra short periods"
S.K. Rai, Arijeet Das, A.K. Srivastava, G.S. Lodha, Rajnish Dhawan. Applied Surface Science 257, (2011) 10704.

"Growth of Short period multilayers for x-ray mirror"
Sanjay Rai, Arijeet Das, R. Dhawan and G. S. Lodha , 53 DAE Solid State Physics Symposium (2008) Mumbai, 367.

Publication from chapter 5

"NbC/Si multilayer mirror for next generation EUV light sources",
Mohammed H. Modi, **S. K. Rai,** Mourad Idir, F. Schaefers, and G. S. Lodha, Optics Express 20, (2012) 1514.

"Effect of surface roughness on multilayer film growth"
Modi M.H., **Rai S.K.,** Thomasset A., Lodha G.S. and Idir M. The European Physical Journal168, (2009) 27.

List of Figure

List of Tables

Chapter 1

1.0 Introduction

This chapter contains a general introduction to x-ray multilayer mirrors and their increasing use in instrumentation operating in the soft and hard x-ray range. In the following sections of this chapter, we briefly introduce the necessary concept and the existing information on the subject required for the commencement of this work, our motivation and details of the work.

Since discovery of x-rays by W.C. Roentgen in 1895 it was realized that due to high energy of these radiations, it would be possible to do imaging at much higher resolutions compared to visible light. Roentgen also observed in his initial experiments that these rays do not deviate from their path on passing through most of the materials. Quest to see much smaller objects of nm sizes compared to micrometer size possible with visible light started a rapidly growing field of research, covering all areas from x-ray source development to x-ray imaging and spectroscopy instrumentation. Conventional optical elements, lenses or coated mirrors were not useful in the case of x-rays. This is mainly due to the fact that refractive index of x-rays is close to one for all materials. The refractive index for electromagnetic wave shows anomalous behavior at resonant frequencies corresponding to the electronic transition in atoms and molecules. The following equation shows dependence of refractive index n on ω the frequency of incident wave[1].

$$n(\omega) = 1 - \frac{1}{2}\frac{e^2 n_a}{\varepsilon_0 m}\sum_s \frac{g_s}{\left(\omega^2 - \omega_s^2\right) + i\gamma\omega}$$

Where g_s, n_a, ε_o ,m and γ are oscillator strength, atomic density, permittivity of free space, mass of electron and damping factor respectively.

On low frequency side of a resonance n increases with ω which is normal dispersion and immediately above the natural resonance frequency ω_s it decreases. In the x-ray region frequencies are usually higher than transition frequencies of most of the materials as a result the refractive index turns out to be less than 1 as shown in figure (1.1). Furthermore it leads to phenomena of total external reflection from a flat and sharp interface. The deviation of n from unity is extremely small hence, the angle (called critical angle) up to which total external

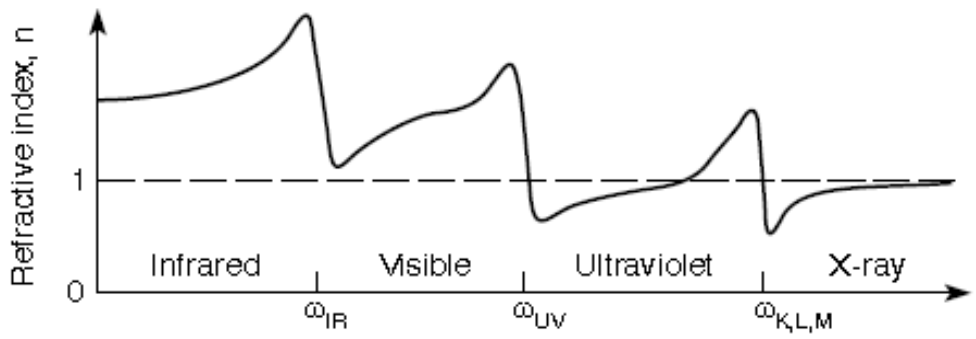

Fig. 1.1 Variation of refractive index of in the frequency range from infra red to x-rays, in x-ray region it is approaching one.

reflection happens is extreme grazing. Initially the development of x-ray optical technology had relied upon the properties of total external reflection and upon the use of natural crystals to obtain reflection of beam by diffraction process. For a long time, surfaces in total external reflection region and crystals were used to reflect x-rays. Since, total external reflection of the x-rays happens at very low grazing incident angles for most materials (0.2 to 0.5 deg for 8 keV x-ray), one needs to use large sized mirrors to accept the source with stringent condition on surface roughness and slope errors. On the other hand, use of natural crystals as optical element for x-rays was mostly limited to using them as monochromator to collimate a beam from a diverging source and to select a desired wavelength. Common crystals used were silicon, germanium and graphite for shorter wavelengths (0.05-0.3 nm), and for slightly longer wavelengths (up to 0.5nm), mica and potassium acid phthalate (KAP). However, this method had its own limitations. First, all single crystals have very sharp diffraction peaks hence it is very difficult to align them correctly. Any small misalignment would destroy the beam intensity. Second, attempts to focus beam by bending crystals generates aberrations and the optics is under huge stress. Third problem with crystals is the available d-spacings between the scattering planes which are limited to the natural periods of the crystals. The principle of a diffractive optic, however, using constructive interference from many weak scattering planes to produce strong reflectivity, can be extended if a crystal can be made at any desired d spacing. If the crystal consists of periodic stack of films instead of periodic array of planes of atoms then it would be possible to make crystals as per the requirements as shown in figure (1.2).

First multilayer diffraction was reported by Dumond and Youtz [2] using Mo Kα source on Au/Cu multilayers, deposited by evaporation. The multilayer diffraction however decayed after

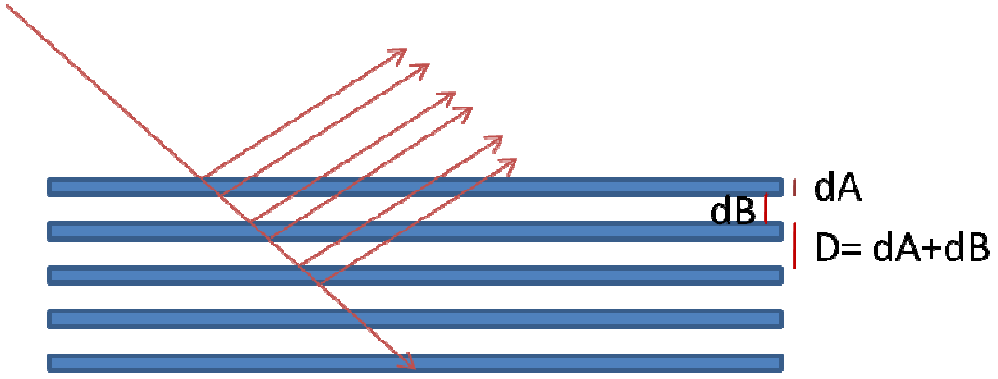

Figure 1.2 Schematic reflection of X-ray by a multilayer mirror

few weeks due to inter diffusion between gold and copper. This was the beginning of long body of research on fabrication and characterisation of multilayers and their application as optical element in x-ray region. After a long time, from first multilayer attempt, in mid 70s improvement in deposition methods made it possible to fabricate such structures with better control. Significant early advances were made by Spiller and his coworkers [3,4], an early review of theory was published by Underwood and Barbee [5]. Since then many groups around the world now work on x-ray multilayer optics from glancing incidence to normal incidence, and fabrication techniques and mirror performance have been studied in detail. A general review book covering theory and many applications has been published by Spiller [6].

X-ray multilayer mirrors are fabricated by sequential layer deposition of materials with a large contrast in x-ray refractive index (figure 1.2). These structures are called artificial Bragg structures. The parameters which can be varied in a multilayer are, two different layer materials, A and B, the order of the layer (ABAB.. or BABA..), total number of bilayers, N, and finally the individual layer thicknesses, dA and dB. Among the multilayer community, combinations of these parameters like the vertical repetition of the bilayers i.e., multilayer period, D = dA+dB, and the multilayer thickness ratio Γ= dA/(dA + dB), between the top high Z layer thickness and the period, are the most commonly used expressions for differentiating multilayers. Sometimes deposition of a buffer layer on the substrate is also done for enhanced multilayer adhesion or a capping layer at the top for protection from oxidation etc. In multilayers, which are one dimensional analogue to 3D crystal, reflection occurs at each interface due to difference in refractive index of the two layers A and B. High reflectivity is

obtained by a multilayer when reflection from all bilayers are optimized to add in phase at a desired angle. Refractive index of a material for energies above 30eV can be written as

$$n = 1 - \delta + i\beta = 1 - \frac{r_e}{2\pi}\lambda^2 N_{at}(f_1 - if_2) \ ,$$

Where δ is the deviation of the refractive index from unity, β is the absorption index and f_1 and f_2 are the real and imaginary part of atomic scattering factors, N_{at} is the number atoms per unit volume and r_e is classical electron radius $r_e = e^2/4\pi\varepsilon_o mc^2 = 2.82\text{x}10^{-6}$ nm. The atomic scattering factor, f tells the strength of the electric field scattered by an atom to that of a single free electron. The values of atomic scattering factors for Z up to 90 are tabulated by Henke[7] in the energy range 50-30000 eV. f_1 is close to the number of free electrons per atom, i.e. electrons with binding energy less than the incident photon energy, N_{at} .f_1 is the effective number of free electrons per unit volume. For large photon energies and away from absorption edges we have approximately $\delta \propto \lambda^2$ and $\beta \propto \lambda^3$. In case of high energy hard x-rays, number of free electrons become equal to Z the atomic number.

To get highest reflectivity one should choose two materials to get highest refraction contrast and lowest absorption. Period of multilayer can be calculated using modified Bragg equation to account for refraction correction. Modified Bragg equation is given as

$$m\lambda = 2D\sin\theta\sqrt{1 + \frac{(1-\bar{\delta})^2 - 1}{\sin^2\theta}}$$

Where $(1-\bar{\delta})$ is the average real part of the refractive index which in case of bilayers is

$$\bar{\delta} = \frac{d_a\delta_a + d_b\delta_b}{d_a + d_b}$$

Period is decided depending on the wavelength region and angle of incidence it is going to be used. As a straightforward guide shorter the operating wavelength shorter is the period. Γ is adjusted to minimize the absorption and maximize the number of layer pairs participating in the interference to increase the resolution and reflectivity.

X-ray multilayers have been used for variety of applications such as monochromator, mirror, polarizing element for synchrotron radiation, dispersive elements for x-ray diagnostics of high-temperature plasmas, normal incidence reflectors for (soft-) x-ray lithography, normal incidence mirrors for microscopy in the water window (2 to 4 nm) and as grazing incidence mirrors in x-ray telescopes applications for x-ray astronomy [8,9,10,11,12,13,14]. The advantages of using the multilayer optics are that the multilayer period thickness can be tailored according to operating wavelength and incidence angle and can be coated on curved substrate for focusing/collimating the x-rays.

Synchrotron (SR) source gives continuous radiation from infrared to hard x-ray region. Various energy regions can be loosely defined as $\lambda < 0.3$ nm is called hard x-ray (HXR), $0.3 < \lambda < 10$ nm is called soft x-ray (SXR) and $10 < \lambda < 50$ nm is called extreme ultra violet radiation. Synchrotron radiation has high intensity, brightness, polarizence, directionality, and pulse structure, which makes it a unique light source. These sources are used for variety of experiments for material science, biological and industrial applications. Because of broad band of wavelengths available at a synchrotron one requires multilayer structures with bilayer thickness varying from 1nm to 15 nm. Worldwide, use of multilayer mirrors at synchrotron beamlines has increased significantly in recent times[13]. Increased need of short period stable multilayer mirrors has kicked off research in developing newer and newer multilayer combinations for various applications. Present day multilayers require ultra short period structure (<2nm) with large number of layer pairs and long term stability of interface under high heat load [14]. Indian SR sources Indus-1 operating at 450 MeV emits radiation upto VUV/ soft x-ray region, and Indus-2 with 2.5 GeV energy emits radiation up to hard x-ray region[15]. In this thesis we have undertaken development of short period multilayer, which can be used as monochromator for hard x-rays and normal incidence mirrors for EUV/soft x-rays in 10-20 nm region on Indus-1/ Indus-2 source. Both these requirements need multilayer in periods range from 6 nm to 1.5 nm. At periods below 3nm it becomes difficult to get measured reflectivity close to theoretically possible values due to various issues related with growth. In practice, the structures of most short period multilayers are far from the assumed ideal structures. Diffusion and intermixing of the materials at their interfaces cause imperfection in the definition of the layers. These issues suggest a careful investigation of changes in interface structure with multilayer period reduction.

1.2 Concern of short period multilayers

Usefulness of short period (~ 2nm) structures is governed primarily by the practically achievable interface perfection. Compositionally sharp and topologically smooth interfaces with good optical contrast are required for high reflectivity. In practice the theoretical performance of multilayer systems is reduced by the occurrence of roughness at the interfaces. The effect of roughness on the reflectivity is usually described by a Debye-Waller factor, given by $e^{-q^2\sigma^2}$, where σ is the root mean square (r.m.s.) value of the roughness and $q = 4\pi\sin\theta / \lambda$. Note that $q = 2\pi/d$ when the Bragg condition is fulfilled. This factor expresses the decrease in the reflected intensity of an interface with roughness σ, compared to that of a perfectly smooth interface, at an angle of incidence θ and wavelength λ. As an example, the influence of a 0.4 nm r.m.s. roughness on the Debye-Waller factor is calculated for multilayers with a period of 4, 3 and 2 nm for the reflectivity of the first Bragg peak. This results in fall of reflectivity upto 91, 82 and 35% from ideal reflectivity with zero roughness. These calculations show that how much important it is to minimize interface roughness at shorter periods.

Interface roughness results from three main imperfections in the multilayer structures: roughness of the substrate surface that may propagate into the multilayer, variation of the layer thicknesses and imperfections at the interfaces due to growth mechanism used. The first two factors are extrinsic to the formation of the multilayers, while the last factor is an intrinsic parameter, which depends on the materials characteristics and reactions between the constituents of the multilayers during and after deposition. Imperfections at interfaces can be divided into two different categories: one is the composition gradient across the two materials resulting from interdiffusion of the constituents, and the other is structural roughness at the interfaces. In calculations of the reflectance, the compositional gradient is treated using a step approximation representing the gradient of the optical constants from one layer to the next[16]. Such gradients reduce the calculated reflectance. The effects of the structural roughness at the interfaces are analogous to the thermal diffuse scattering of x-rays in crystals. Structural roughness introduces a diffuse component in the scattering, and reduces the specular reflectance. Optimization of the multilayer performance thus includes choosing constituent materials that undergo minimum

inter-layer diffusion and intermixing and that form smooth and uniform interfaces, choosing appropriate starting substrate and deposition method.

Furthermore, a multilayer with shorter periods is inherently unstable and may experience interface degradation under high radiation loads and/or high temperatures to which x-ray optics are often exposed (e.g. synchrotron beam lines, intense plasma source diagnostics). Multilayers, when exposed to high intense synchrotron radiation, show quick rise in local temperature up to 600^0C [17,18]. Interdiffusion in multilayer structures results from the presence of steep chemical gradients at the interfaces, which provide a driving force for interdiffusion and homogenization of the structures. Depending on the thermodynamic characteristics of the constituent materials in multilayers, different products may develop under a thermal activation. Interdiffusion and reactions in multilayers usually lead to the formation of new phases, which may crystallize or recrystallize from the original crystalline phases in the structures. Broadening of one of the layers in the structures due to reaction at high temperature has been observed in some materials. Their performance is thus limited by the degradation of quality in high temperature environment. In present scenario, recently developed free electron laser (FEL) sources like Stanford, DESY, SACLA, FLASH, LCLS and Fermi@elettra [19] generate x-ray pulses of very high intensity which induce radiation damage in optical components [20]. Hence, it becomes important to study the thermal stability of optical elements before it is exposed to intense synchrotron radiation.

In real structures, it is often unclear which of the interfacial imperfections, compositional gradients or structural roughness, has a greater effect on the performance and characteristics of the multilayers. Studies to separate the effects of the intermixing and the structural roughness components on the reduction of the multilayer reflectivity are important because by understanding which effects limit the reflectance, fabrication of improved performance multilayers may be possible. Attempts to determine these effects have been reported by different groups. Auger depth profiling [21,22] and cross-sectional TEM analysis[23,24] have been used to study the concentration gradients across the interfaces, and specular and non-specular x-ray scattering have been used to quantify the interfacial roughness[25,26,27,28,29]. Techniques like cross-sectional TEM, Auger, and depth resolved x-ray photoelectron spectroscopy give details with nm level resolution but this information is highly localized which may not represent the average behavior. In x-ray reflectivity measurement information is collected from area as large as 10 mm

in length and 0.05 mm in width which represents average behavior of the structure. X-ray reflectivity has been used extensively in this thesis work.

1.3 Influence of reflected neutrals

Other than issues discussed above there is one more problem which has not been addressed adequately in the past. That is, how the reflected neutrals influence the interface structure of multilayer at shorter periods? In all sputtering deposition techniques it is known that large number of sputtering gas neutrals and ions get reflected from the target and hit the freshly growing film surface. This process of back scattering is a kinematical effect of ion bombardment on a target. If mass M of the incident ion is less than the target atom mass, law of momentum conservation allows the ion to be reflected from the target atom. The angular distribution of the reflected neutrals is also approximately cosine distribution same as for sputtered atoms. The most significant problem with the reflected neutrals is that they have 2-6 times the energy of the sputtered atoms and their number density also could be as high as 0.6-0.8 of sputtered atoms from the target. Results of simulation using TRIM code of SRIM 2008[30] to estimate the reflected neutrals when Ar ions of varying energy are hitting a W target are shown in the figure 1.3. Figure 1.3 (a) shows the number density and energy value distribution of sputtered W atoms and as well as reflected Ar ions/neutrals when incident energy of the Ar ions is 500 eV. This figures shows that total numbers of reflected neutrals is high and comparable to numbers of sputtered atoms. Also energy of reflected neutrals can be very high compared to sputtered atoms. Figure 1.3 (b) shows changes in mean energy of sputtered atoms (red line) and reflected neutrals with the incident Ar ion energy. This graph shows that on increasing the Ar ion energy the energy of sputtered atoms does not change but mean energy of reflected neutrals increases significantly. This high energy is equivalent to that of ion/neutral beam hitting the growing surface as if ion assisted deposition is happening. Flux and energy of reflected neutrals was measured by Rossangel et.al [31]. The paper concludes that bombardment of depositing film during sputtering should be considered as an unavoidable artifact of sputtering deposition technique. A review by Mattox [32] covers the range of modifications which can happen in the film due to bombardment of energetic particles. These neutrals and ion hitting the film have sufficient energy to re-sputter the

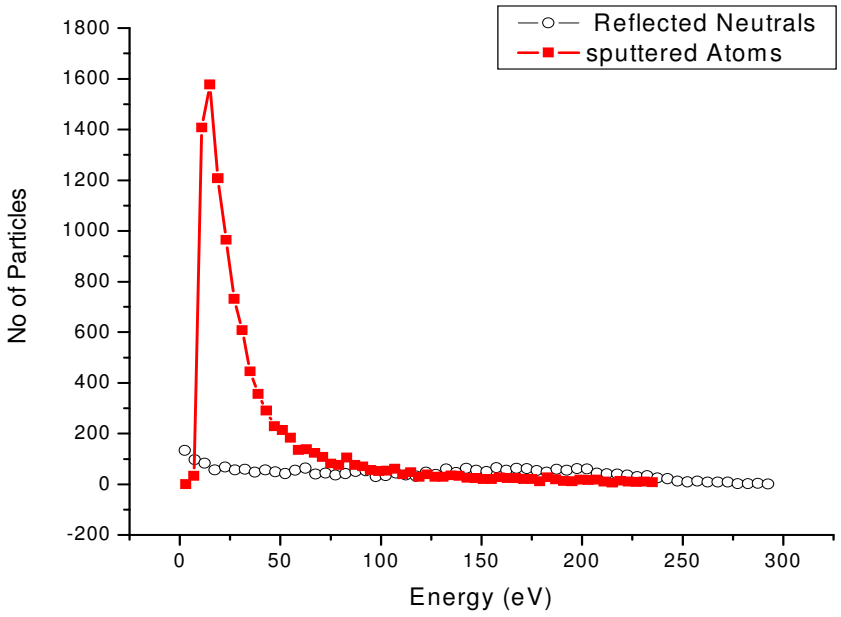

(a)

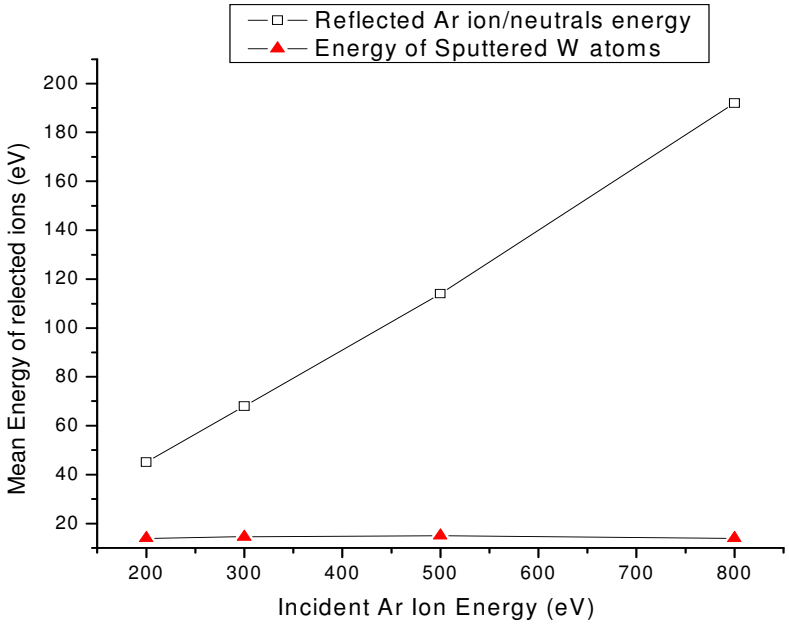

(b)

Fig. 1.3 Top (a) number density and energy distribution of sputtered atoms (red line) and reflected ar ions/neutrals (black line) (b) (bottom)Changes in mean energy of sputtered W atoms (red triangle) and reflected neutrals with the incident Ar ion energy

growing film, modify growth morphology, density, adhesion, interface mixing and can also generate residual stresses in the film. In case of multilayers, as we are depositing High Z and Low Z materials sequentially and the bombardment of neutrals seen by both interfaces is not same. It becomes important to understand the influence of these neutrals. At shorter periods these neutrals pose a challenge in fabricating a thin continuous layer itself.

This study has focused on to understand the role of reflected sputter gas neutrals on the growth and interface modification of short period multilayer mirrors. We have studied W/Si, W/C and W/ B_4C combination by depositing multilayers of various periods starting from 9 nm to 1.5 nm. We have examined the influence of these reflected neutrals as how they affect the interface structure in these combinations. In this study we have demonstrated that these neutrals not only re-sputter the low Z layer but also produce intermixing during deposition which is more serious at shorter periods. This puts a limit on the lowest period which can be deposited without intermixing. In this study we have estimated the shortest period which can be deposited with a continuous layer for both W/Si and W/B_4C combinations. It is found that W/Si is more susceptible to damage due to reflected neutrals. Multilayers with continuous layers could show better thermal stability than intermixed multilayer mirrors. This aspect we examined by annealing W/B_4C multilayer of varying periods.

1.4 Limitations of Normal Incidence mirror in EUV region

Another goal of the thesis was development of thermally stable, normal incidence mirror above Si L edge (12.6nm) in EUV region. Presently, Mo/Si multilayers combination gives highest reflectivity in extreme ultraviolet (EUV) region. This combination is used for lithography applications in near normal incidence mode above 12.6 nm wavelength. However, it has a severe drawback of poor thermal stability caused by negative heat of mixing between Mo and Si. The reflective properties of Mo/Si multilayers are directly correlated to the structure of the interface. Broadening of the interface due to interdiffusion processes and roughness development significantly reduces the reflectivity [33,34]. Resultantly this structure undergoes interface degradation right after the deposition process. A number of studies have been performed to investigate the origin of Mo/Si intermixing and its dependence on the deposition parameters [35,36,37]. This has resulted, in minimizing the intermixing but not totally eliminating it. This suggests that interlayer formation is an intrinsic property of the Mo/Si material pair and

could present a fundamental barrier to achieve maximum optical performance [38]. Different approaches have been adopted in the past to overcome the inter diffusion and structural degradation problem by inserting a barrier layer of boron carbide or carbon between Mo and Si to prevent intermixing [39] and increase the thermal stability to 300^0C [40]. However inserting an extra layer leads to phase variation in the waves reflecting from different interfaces at Bragg condition and thereby resultant phase mismatch reduces the overall reflectivity.

In an effort to explore some other combination for achieving high reflectivity as well as high thermal stability we decided to try for a new combination. Carbides of refractory metals (Mo, Nb) are known to exhibit excellent physical properties like high melting point, good electrical conductivity and extreme hardness. In the 10-20 nm wavelength regions, the refractive index properties of these metal carbides are almost identical to their metallic constituents. Therefore, it is expected that a multilayer comprised of a refracting layer of metal carbide with a spacer layer of Si should exhibit a similar high reflectivity performance. Previous studies on carbide layers suggest that these carbides are non-stoichiometric and contain vacancies in the carbon lattice sites [41,42]. From multilayer point of view, the presence of unsaturated carbon in near vicinity of the metal species (Nb, Mo) may act as a barrier for direct chemical mixing with Si. This approach may yield better results than earlier attempts of putting a barrier layer of B_4C or C between Mo and Si to prevent the chemical mixing of two species.

In the present study, NbC/Si multilayer is deposited on a Si substrate to carry out high temperature annealing studies to investigate interfacial properties at elevated temperatures. We have compared the performance of NbC/Si multilayer mirror with Mo/Si from the thermal stability point of view in this study. We have also examined the performance of this combination while depositing it at high temperature.

1.5 Developed Instruments

Most of the studies carried out on short period multilayers have utilized tools like cross-sectional TEM, Auger spectroscopy and depth resolved x-ray photoelectron spectroscopy etc. for finding out structural details. These tools are good to get details of the interface but they are destructive in nature and they give only specific information in a much localized area. No tool gives details like period thickness, interface roughness and layer density in one measurement

simultaneously. X-ray reflectivity can give these details with high resolution and information is collected from area as large as 10 mm in length which represents the average behavior of the structure. In this thesis we have used x-ray reflectivity to get details about the interface structure and used other tools to confirm the observations. X-ray reflectivity is sensitive to atomic scale roughness, interdiffusion in buried layers and in-plane correlations of roughness. The technique measures variations in the electron density on length scales from 3-4 nm to 200 nm. This makes XRR a very good tool for non-destructive structural analysis of thin films and multilayers [43,44]. The accuracy of density and roughness determination by XRR is ~5% and thickness can be estimated within 1% depending on the roughness of the interface. Two excellent books by Holy[45] and Tolan[46] cover the subject on how to analyze x-ray reflectivity data in great detail. Chason and Mayer[43] have used XRR for studying surface and interface morphology of various interfaces, estimation of diffusion using a marker layer in a buried interface and dynamic studies like interfacial reactions, scaling of roughness during growth etc. A recent round robin study carried out on XRR characterization involving 20 laboratories around the world established XRR as a reproducible and repeatable technique to evaluate quantitatively electron density, thickness and roughness of thin layers[47].

Moderate resolution x-ray reflectometer was designed and developed as part of the thesis to carry out reflectivity measurements. We have assembled the x-ray reflectometer/ diffractometer on a sealed tube source with a flexibility to shift the assembled system to a synchrotron beam line. Commercially available systems lack flexibility of use. It is not possible to handle large size and odd shaped samples on them. Developed system is capable of handling large size / odd shaped samples for testing large size optics. Reflectivities over six orders of dynamic range could be obtained with good resolution. This instrument can also be used for doing grazing incidence x-ray diffraction (GIXRD) as well as powder diffraction with minimum changes required in the optics. Performance of the system was compared with commercial systems and was found better for x-ray reflectivity measurements. We started out our work by examining single layer films of various thicknesses estimated the structural details and confirmed those interpretations using other tools. The developed methodology was used for analysis of structures of bilayers, trilayers and finally multilayers using x-ray reflectivity. In this thesis we have demonstrated that by systematic and watchful investigation of XRR data obtained from samples it is possible to get comprehensive structural details. This system was also used to

characterize large size (12 cm long and 6 cm wide) Au coated mirrors to be used for first Indian x-ray space telescope planned to be launched in a year.

During the course of this work we have also developed a custom designed ion beam sputtering (IBS) system for fabrication of short period multilayer for hard x-ray monochromators, normal incidence mirrors for soft x-ray applications. This deposition system was used for fabricating thin film structures, x-ray mirrors and various other multilayers studied in this thesis Development of the automated system has enabled fabrication of high periodicity x-ray multilayer mirrors.

1.6 References

1 *" The Optical Principles of the Diffraction of X-rays" R.W. James, (Bell, London 1948)*

2 J. DuMond and J.P. Youtz, J. Appl. Phys. 11, (1940), 357.

3 E. Spiller, Applied Optics 15 ,(1976), 2333.

4 R. P. Haelbich, A. Segmuller, and E. Spiller, Applied Physics Letters 34 (3), (1979), 184.

5 J. H. Underwood and T. W. Barbee, Applied Optics 20,(1981) ,3027.

6 "Soft X-Ray Optics" Eberhard Spiller, (SPIE Optical Engineering Press, Bellingham, USA, 1994).

7 "X-ray interactions: photoabsorption, scattering, transmission, and reflection at E = 50-30 000 eV, Z = l-92," B. L. Henke, E. M. Gullikson, and J. C. Davis, Atom. Data and Nucl. Tables, vol. 54,(1993), 18 l-424.

8 "Soft X-rays and Extreme Ultraviolet Radiation", David Attwood, Cambridge University Press. (1999).

9 J. Kirz, C. Jacobsen, M. Howells, Quart. Rev. Biophys. 28, (1995), 33.

10 N.M. Ceglio, D.G.Stearns, D.P. Gaines, A. M. Hawrkluk, and J.E. Trebes, Opt. Lett. 13, (1988), 108.

11 M.A. MacDonald, F. Schafers, R. Pohl, and A. Gaupp, Opt. Exp. 17, (2009), 23290.

12 J.F. Seely, G. Gutman, J. Wood, G.S. Herman, M.P. Kowaski, J. C. Rife, and W. R. Hunter, Appl. Opt. 32, (1992), 3541.

13 A. Rack, T. Weitkamp, M. Riotte, D. Grigoriev, T. Rack, L. Helfen, T. Baumbach, R. Dietsch, T. Holz, M. Kra¨mer, F. Siewert, M. Medunˇa, P. Cloetens and E. Ziegler, J. Synchrotron Rad. 17, (2010), 496.

14 Alexande Kazimirov, D.M. Smilgies, Q. Shen, X. Xiao, Q. Hao, E.Fontes, D.H.Bilderback, Sol M. Gruner Y.Platonov and V.V.Martynov, J. Synchrotron Radiation,13, (2006), 204.

15 www.rrcat.gov.in.

16 J. H. Underwood and T. W. Barbee, Nature 294 (1981), 429.

17 A.F.Jankowski, D.M.Makowiecki, Optical engineering30, (1991), 2003.
18 A. F. Jankowski, L. R. Schrawyer, and M. A. Wall, J. Appl. Phys. 68, (1990), 5162.
19 Primoz Rebernik Ribic and G Margaritondo, J. Phys. D: Appl. Phys. 45, (2012), 213001.
20 A. R. Khorsand, R. Sobierajski, E. Louis, S. Bruijn, E. D. van Hattum, R. W. E. van de Kruijs, M. Jurek, D. Klinger, J. B. Pelka, L. Juha, T. Burian, J. Chalupsky, J. Cihelka, V. Hajkova, L. Vysin, U. Jastrow, N. Stojanovic, S. Toleikis, H. Wabnitz, K. Tiedtke, K. Sokolowski-Tinten, U.Shymanovich, J. Krzywinski, S. Hau-Riege, R. London, A. Gleeson, E. M. Gullikson, and F.Bijkerk, Opt. Express 18, (2010), 700.
21 S.S. Chao, D.A. Pawlik, J. Gonzalez-hernandez, Q. Wang, and D.D. Alired, Solid State Comm. 79, (1991), 205.
22 J. Gonzalez-Hernandez, B.S. Chao, D.A. Pawlik, D.D. Allred, and Q. Wang, J. Vac. Sci. Technol. A101, (1992), 145.
23 W.C. Shih and W.M. Stobbs, Ultramicros. 32, (1990), 219.
24 T.D. Nguyen, R. Gronsky, and J.B. Kortright, ICEM Proc. 4 (1990), 442.
25 J. B. Kortright, J. Appl. Phys. 70, (1991), 3620.
26 D. E. Savage, J. Kleiner, N. Schimke, Y.-H. Phang, T. Jankowski, J. Jacobs, R. Kariotis, and M. G. Lagally, J. Appl. Phys. 69, (1991) 1411.
27 D. E. Savage, N. Schimke, Y.-H. Phang, and M. G. Lagally, J. Appl. Phys. 71, (1992), 3283.
28 D. G. Steams, J. Appl. Phys. 65, (1989), 491.
29 D. G. Steams, J. Appl. Phys. 71, (1992), 4286.
30 "The Stopping and Range of Ions in Solids", by J. F. Ziegler, J. P. Biersack and M. D. Ziegler, SRIM 2008 Book.
31 S.M.Rossangel J. Vac. Sci and Tech. (A) 7, (1989), 1025.
32 D.M.Mattox J. Vac. Sci and Tech. (A) 7, (1989), 1105.
33 S. Yulin, in: N. Kaiser, H. Pulker (Eds.), Optical Interference Coatings, Springer Series in Photonics, 2003.
34 M. Slaughter, P.A. Kearney, D.W. Schulze, C.M. Falco, C.H. Hills, E.B. Saloman, R.N. Watts, Proc. SPIE 1343, (1999), 73.
35 D.L. Windt, R. Hull, K. Waskiewicz, J. Appl. Phys. 71, (1992), 2675.
36 S. Bajt, D.G. Stearns, P.A. Kearney, J. Appl. Phys. 90, (2001) ,1017.
37 S. Yulin, T. Feigl, T. Kuhlmann, N. Kaiser, A.I. Fedorenko, V.V.Kondratenko, O.V. Poltseva, V.A. Sevryukova, A.Y. Zolotaryov, E.N. Zubarev, J. Appl. Phys. 92, (2002), 1216.
38 D.G. Stearns, R.S. Rosen, Proc. SPIE 1547, (1991), 2.
39 T. Bottger , Dirk C. Meyera, Peter Pauflera, Stefan Braunb, Matthew Mossb, Hermann Maib,Eckhard Beyerb , Thin Solid Films 444, (2003) ,165.
40 H. Maury, P. Jonnard, J.-M. André, J. Gautier, M. Roulliay, F. Bridou, F. Delmotte, M.-F. Ravet, A. Jérome, P. Holliger, Thin Solid Films 514, (2006), 278.
41 M.Y. Liao, Y. Gotoh, H. Tsuji, J. Ishikawa, "Compound-target sputtering for niobium carbide thin film deposition," J. Vac. Sci. Tehnolol. B 22, (2004), L24-L27.

42 S. Barzilai, M. Weiss, N. Frage, A. Raveh, Surface and Coatings Technology 197, (2005), 208.

43 Chason E. and Mayer T: M., Critical Reviews in Solid State And Materials Sciences, 22, (1997), 1.

44 "High-Resolution X-Ray Scattering: From Thin Films to Lateral Nanostructures" Ullrich Pietsch, Vaclav Holy, Tilo Baumbach, Springer Book, (2004).

45 'High-Resolution X-ray Scattering from Thin flims and Multilayer`, V. Holy, U. Pietsch, T. Baumbach, , Springer Heidelberg Germany (1999).

46 "X-ray Scattering from Soft Matter Thin Films", Metin Tolan, Springer, Germany, 1999.

47 P. Colombi, D. K. Agnihotri, V. E. Asadchikov, E. Bontempi, D. K. Bowen, C. H. Chang, L. E. Depero, M. Farnworth, T. Fujimoto, A. Gibaud, M. Jergel, M. Krumrey, T. A. Lafford, A. Lamperti, T. Ma, R. J. Matyi, M. Meduna, S. Milita, K. Sakurai, L. Shabel'nikov, A. Ulyanenkov, A. Van der Lee and C. Wiemer, J. Appl. Cryst. 41, (2008), 143.

Chapter 2

Characterization and Deposition techniques

This chapter describes the details of developed instruments and other experimental techniques used for sample preparation and characterization. As discussed earlier we have used hard x-ray reflectivity as a main tool for characterization of all the thin films and multilayers studied in this thesis. To reach this objective we have developed moderate resolution reflectometer capable of carrying out x-ray reflectivity, grazing incidence diffraction and powder diffraction with very little modification. We also carried out development of ion beam sputtering based thin film deposition system. This deposition system was used for fabricating thin film structures, x-ray mirrors and various other multilayers studied. Other than this we have also used cross sectional TEM and annealing setup. All the developed and commercial experimental tools used for the work are discussed in this chapter.

2.1.1 Principles of X-ray reflectivity

As discussed earlier x-ray reflectivity is a powerful tool to extract the information about the buried layers and interlayers in thin film structure[1,2]. It is a nondestructive technique and has wide applicability [3,4,5,6,7,8]. In XRR technique, depth sensitivity can be varied from nanometer to hundreds of nanometer range by controlling the momentum transfer vector of incident beam[1,9,]. In x-ray region refractive index is close to unity so at extreme grazing angles XRR technique is surface sensitive. It gives information about thicknesses, roughness, and optical behavior of buried layers in thin film structure.

Refractive index of a material for x-rays is written as

$$n = 1 - \delta + i\beta = 1 - \frac{r_e}{2\pi}\lambda^2 N_{at}(f_1 - if_2)$$

This implies that

$$\delta = \frac{r_e}{2\pi}\lambda^2 N_{at} f_1 \quad \text{and} \quad \beta = \frac{r_e}{2\pi}\lambda^2 N_{at} f_2$$

For high energy x-ray f_1 takes value equal to Z (atomic no). Hence, if we measure δ and β using x-ray reflectivity we can get estimate of electron density/ bulk density of the material and absorption coefficient of the material.

When light beam falls on boundary between two media (surface/interfaces), then reflection and transmission of beam occur. Reflection and transmission of beam from a

surface/interfaces is shown in Fig (2.1). Amplitudes of reflected and transmitted beams are given by Fresnel's equations[10], which are.

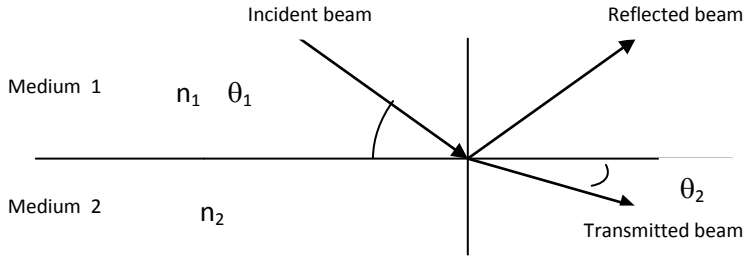

Fig 2.1 Reflection and transmission of light beam from a surface/interfaces

$$r_{12}^{s} = \frac{n_1 \sin\theta_1 - n_2 \sin\theta_2}{n_1 \sin\theta_1 + n_2 \sin\theta_2} \quad ; \quad r_{12}^{p} = \frac{n_1 \sin\theta_2 - n_2 \sin\theta_1}{n_2 \sin\theta_1 + n_1 \sin\theta_2}$$

$$t_{12}^{s} = \frac{2n_1 \sin\theta_1}{n_1 \sin\theta_1 + n_2 \sin\theta_2} \quad ; \quad t_{12}^{p} = \frac{2n_1 \sin\theta_1}{n_2 \sin\theta_1 + n_1 \sin\theta_2}$$

Where, n_1 and n_2 are the refractive indexes of 1st and 2nd medium, r_{12}^{s}, t_{12}^{s}, and r_{12}^{p}, t_{12}^{p} are reflected and transmitted amplitudes of s and p polarized beams. One can also express these reflected and transmitted amplitudes in terms of momentum transfer vector $q = \frac{4\pi n \sin\theta}{\lambda} = 2k_z$ (along the normal direction).

$$r_{12}^{s} = \frac{q_1 - q_2}{q_1 + q_2} = \frac{k_{i,z} - k_{t,z}}{k_{i,z} + k_{t,z}} \quad ; \quad r_{12}^{p} = \frac{n^2 k_{i,z} - k_{t,z}}{n^2 k_{i,z} + k_{t,z}}$$

Reflected intensity (reflectivity) is given as $|r_{12}|^2$

$$\Rightarrow \quad |r_{12}|^2 = \left|\frac{q_1 - q_2}{q_1 + q_2}\right|^2 = \left|\frac{\sqrt{1-\left(\frac{q_{cr1}}{q}\right)^2} - \sqrt{1-\left(\frac{q_{cr2}}{q}\right)^2}}{\sqrt{1-\left(\frac{q_{cr1}}{q}\right)^2} + \sqrt{1-\left(\frac{q_{cr2}}{q}\right)^2}}\right|^2 ;$$

$$\Rightarrow \text{ Where } q_{cr} = \frac{4\pi}{\lambda} n \sin\theta_{cr}$$

For angle much higher than critical angle $q >> q_{cr}$

$$\Rightarrow \qquad |r_{12}|^2 \propto \frac{1}{q^4}$$

$$\Rightarrow \qquad \text{So reflectivity decreases as } \frac{1}{q^4} \text{ with } q.$$

Similarly we can calculate transmission coefficients also for s and p polarizations as

$$t_{12}^{s} = \frac{2k_{i,z}}{k_{i,z} + k_{t,z}} \qquad ; \qquad t_{12}^{p} = \frac{2k_{i,z}}{n^2 k_{i,z} + k_{t,z}}$$

Propagation angle θ_2 inside the medium can be obtained by propagation angle in incident medium using Snell's law $\sin\theta_2 = \left(1 - \frac{n_1}{n_2}\cos^2(\theta_1)\right)^{1/2}$.

2.1.2 Reflectivity from a finite thickness slab

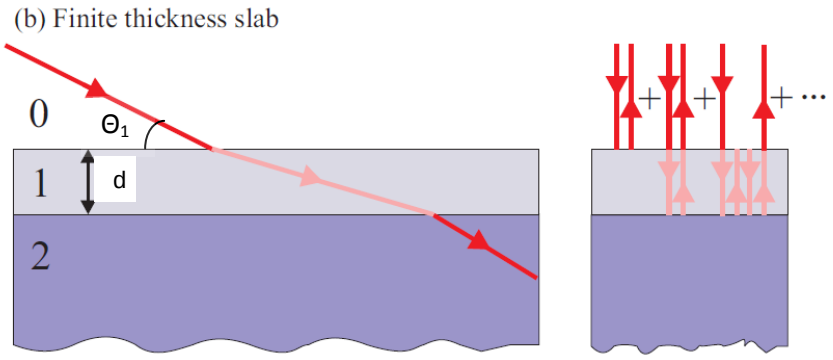

Fig 2.2 Reflection and transmission from a slab of finite thickness. The thickness of the slab is d and total reflectivity is the sum of infinite number of reflection as shown on the right side (figure taken from[2])

In this section the reflectivity from a slab of finite thickness is discussed. Consider a slab of finite thickness shown in Fig. (2.2). The side view depicts only the transmitted wave vectors across the two interfaces from medium 0 to 1, and from 1 to 2, whereas the right panel shows the z components of the wave vectors. In contrast to the case of the infinite slab there is now an infinite series of possible reflections, and the first three of these are drawn in the figure:

(1) Reflection at interface 0 to 1, amplitude r_{01}.

(2) Transmission at interface 0 to 1, t_{01}, then reflection at interface 1 to 2, r_{12}, followed by transmission at interface 1 to 0, t_{10}. In adding this wave to the above it is necessary to include the phase factor $p^2 = e^{iqd}$.

In such thin film structure, successive reflection and transmission of beam occur at both top and bottom surfaces, these factors form a geometric progression series with higher order multiples of phase factor. After summing up all the reflections and transmission coefficients we can calculate that the total reflected amplitudes from thin film as

$$r_{slab} = \frac{r_{01} + r_{12}\, p^2}{1 + r_{01} r_{12}\, p^2}$$

The phase factor p^2 , of the rays reflected from top and bottom face of the slab is e^{iqd} where $q = 2k_1 \sin\theta_1$ and r_{01} and r_{12} are Fresnel reflection coefficient of top and bottom surface the reflected intensity for a finite thickness is plotted in figure (2.3)

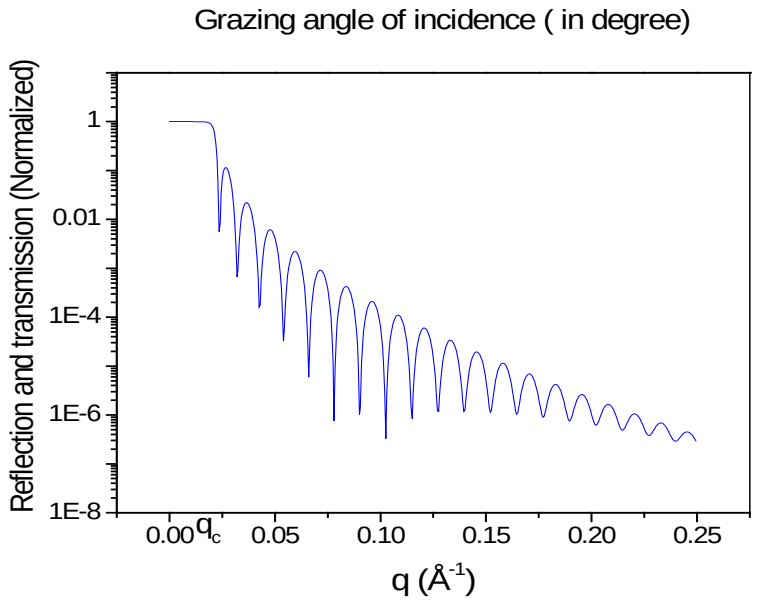

Fig 2.3 Reflectivity pattern of finite thickness slab showing Kiessig oscillations due to thickness of the film

We should note here that the Fresnel reflectivity is specular. This means that the reflected intensity is confined to the plane spanned by the incident wave vector and the interface normal, and that within this plane the angle of the reflected beam equals the angle of the incident beam.

2.1.3 Reflectivity from Multilayers

A method to extend the exact result for a single slab to the case of a stratified medium has been described by by L. G. Parratt[11] in 1954, which is based on a recursive formalism.The medium is imagined as being composed of N strata, or layers, sitting on top of an infinitely thick substrate. By definition the N'th layer sits directly on the substrate. Each layer in the stack has a refractive index $n_j = 1 - \delta_j + i\beta_j$ and is of thickness d_j. It follows from Fig. (2.1) that the z component of the wavevector, $k_{z,j}$, in the slab labeled j is determined from the total wavevector $k_j = n_j k$ and the x component, $k_{x,j}$, which is conserved through all layers so $k_{x,j} = k_x$ for all $_j$. The value of $k_{z,j}$ is found from

$$k_{z,j}^2 = (n_j k)^2 - k_x^2 = (1-\delta_j + i\beta_j)^2 k^2 - k_x^2 \approx k_x^2 - 2\delta_j k^2 + i2\beta_j k^2$$

Noting that $q_j = 2k_j \sin\theta_i = 2k_{x,j}$ the wave vector transfer in j^{th} layer is

$$q_j = \sqrt{q^2 - 8k^2\delta_j + i8k^2\beta_j}$$

In absence of the multiple reflections, the reflectivity of each interface is obtained from Fresnel equations as

$$r_{j,j+1} = \frac{q_j - q_{j+1}}{q_j + q_{j+1}}$$

This expression does not include the multiple reflection effects.

The first step is to calculate the reflectivity from the interface between the bottom of the N^{th} layer and the substrate. As the substrate is infinitely thick so there is no reflections from below the subststrate to consider and

$$r_{N,\infty} = \frac{q_N - q_\infty}{q_N + q_\infty}$$

The reflectivity from top of the N^{th} layer is then evaluated using equation for reflectivity from a finite slab described earlier as

$$r_{N-1,N} = \frac{r_{N-1,N} + r_{N,\infty}\, p_N^2}{1 + r_{N-1.N} r_{N,\infty}\, p_N^2}$$

Which allows that the multiple scattering and refraction in the N'th layer and where P^2_N is the phase factor $e^{iq_n d_n}$. or in general $P^2_j = e^{iq_j d_j}$. It follows that the reflectivity from next interface up in the stack is

$$r_{N-2,N-1} = \frac{r_{N-2,N-1} + r_{N-1,N}\, p_{N-1}^2}{1 + r_{N-2,.N-1} r_{N-1,N}\, p_{N-1}^2}$$

and it is clear that the process can be continued recursively until the total reflectivity amplitude, R, at the interface between the vacuum and first layer is obtained.

2.1.4 Treatment of roughness

Practically, in thin films, surfaces and interfaces are not perfectly sharp but have some roughness as is shown in Fig (2.4). This roughness could be both chemical and physical. In specular reflectivity both types of roughness are treated as same and it is not possible to separate the effects of chemical and physical roughness. Roughness of interfaces affects the reflectivity. It decreases the reflectivity by a factor $DW = e^{-\sigma^2 q^2}$ called Debye Waller factor[9,10], where σ is the roughness of that surface. So the actual reflectivity of surface (or interface) with σ roughness is $|R|^2_{real} = |R|^2 e^{-\sigma^2 q^2}$, instead of $|R|^2$. This factor based on the assumption that momentum transfer vector q is constant in whole thin film, but in reality, the value of q depends on the refractive index of material. In multilayer, value of q changes from layer to layer. Replacing the q^2 in Debye Waller factor by the geometric average $q_1 q_2$, where q_1 and q_2 are values of q in two media forming the surface gives a very good approximation to a rigorous theory (Nevot Croce factor) and yields for the reflectivity reduction in amplitude and in intensity. So reflection amplitude and reflectivity is given by $R = R_0 e^{\frac{-q_1 q_2}{2}\sigma^2}$ (known as Nevot Croce factor[12,13]) and $|R|^2_{real} = |R|^2 e^{-q_1 q_2 \sigma^2}$, respectively.

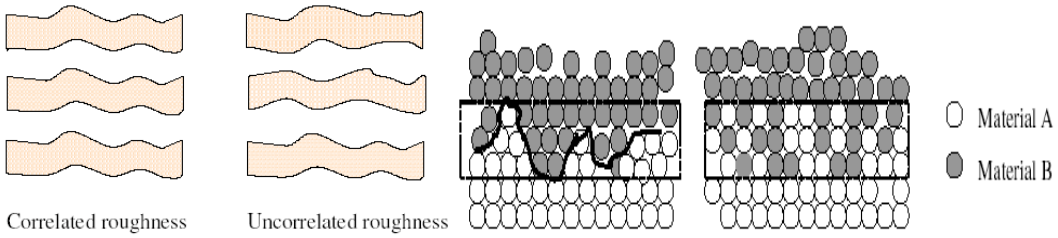

Fig 2.4: Surfaces and interfaces in thin films are not perfectly sharp but have some roughness.

Simulated reflectivity reflectivity pattern of multilayer $|R|^2$ calculated using recursive formalism for a W/Si multilayer with t_w= 15 Å, t_{Si}= 25 Å, $\sigma_W = \sigma_{Si} = \sigma_s$ = 3 Å and N=10 is shown using IMD software[14] in Fig (2.5). In multilayer, reflectivity is ~1 before the critical angle. After critical angle reflectivity decreases and Keissig oscillation appear of $\Delta q = \frac{2\pi}{t_{total}}$ width. Where, t_{total} is multilayer's total thickness. In this region, reflected beam from various interfaces may interfere constructively or destructively depending on the grazing angle of incidence. Due to interferences, between reflected beams from various interfaces, high intensity peaks appear at an angle where all the reflected components add in phase and Bragg condition is satisfied. These peaks are known as Bragg peaks. Separation between two adjacent Bragg peaks are $\Delta q = \frac{2\pi}{d}$, where d is multilayer stack thickness ($t_A + t_B$). Intensity of various Bragg peaks depends on the gamma ratio $\Gamma = t_A/t_A + t_B$. By knowing this ratio one can calculated the density of individual layers participating in the multilayer. Number of Kiessig oscillations between two adjacent Bragg peaks is N-2, where N is the number of repetitions of bilayer stack. m^{th} peak in the reflectivity vanishes, if $m = p\left(\frac{t_A}{t_B} + 1\right)$, where p is an integer

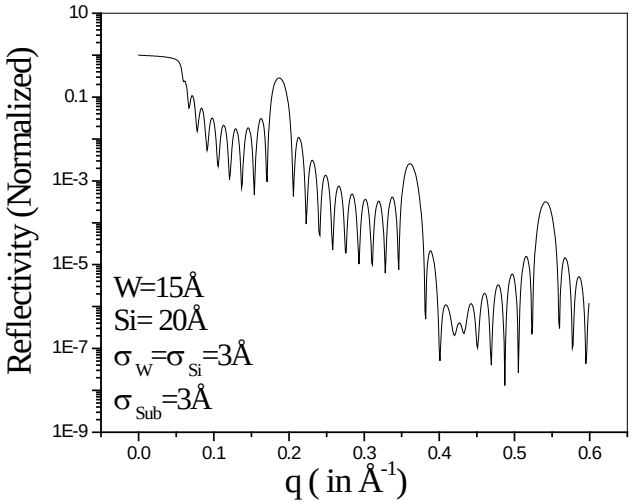

Fig 2.5 Simulated reflectivity for W/Si multilayer with t_W= 15 Å, t_{Si}= 20 Å, σ_W= σ_{Si} = σ_s = 3 Å and N=10, by using IMD program based on recursive formalism.

2.2.1 Details of In-house Developed reflectometer

The design of developed system is a very simple. Instrument consists of essentially a tube based x-ray source, collimation system, goniometer, multilayer monochromator for incident beam monochromator assembly, detector and a PC for controlling and data acquisition. In this system x-ray source used is a Philips x-ray tube with Cu target. The source operates in a horizontal line focus. The effective size of the focus at a take off angle of 3° is 10 mm X 0.05 mm. The x-ray beam is filtered using 50-micron Ni foil to suppress the Cu K_β line before it enters reflectometer.

In the collimation system, near-parallel incident beam is realized by using two slits of width 0.1 mm and 0.05 mm slit at the source and a knife edge slit is kept close to the sample surface to further reduce the beam size. Schematic of the setup is shown in the figure (2.6). In the beginning of slit mounting we have provision for inserting number of Nickel foils for attenuating the incident beam intensity when measurements are being performed at the lowest angle. Soller slit with 0.4° divergence is used in the incident beam to control axial divergence. In this system we have an in house developed incident beam multilayer monochromator. This multilayer consists of 40 layer pair of Pt / C, the reflectivity of this multilayer is 80% for Cu K_α at an

incidence angle (θ) of 1.1°. By using this multilayer we are able to achieve very high intensity incident parallel beam on the sample with a reasonable resolution. The direct beam width achieved with this arrangement is 0.035°.

The goniometer used in this system has minimum step size of 0.001 ° for ω / θ movement and 0.001° for 2θ movement. Sample holder is mounted on the goniometer, which has provision for moving the sample in z direction with a minimum step size of 5 micron. This is required to bring the sample exactly in the beam path. The sample holder is capable of holding sample of size 10 mm X 10 mm to 100 mm X 100 mm. There is a provision for inserting a knife-edge on the sample for reducing the incident beam divergence. This helps in reducing the footprint of the incident beam at grazing angles. The most critical requirement for getting best performance from

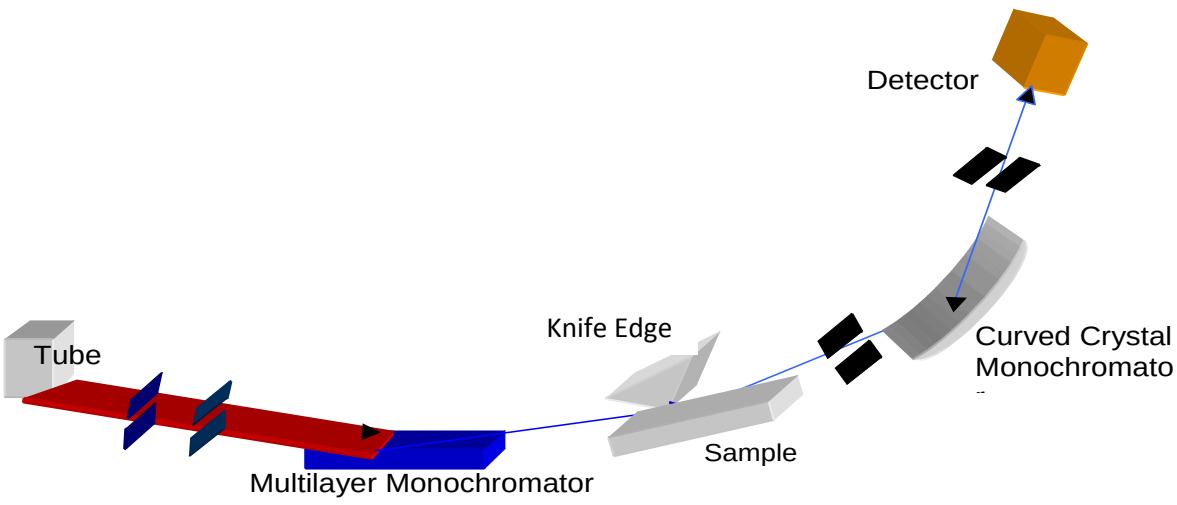

Fig. 2.6 Schematic of the multipurpose reflectometer diffractometer.

the system is alignment of goniometer. The rotational axis of the sample circle i.e. ω circle should coincide with the center of primary beam path. In case of powder diffraction setup, if ω axis is within ± 0.5 mm, it is acceptable, but for reflectivity measurement where beam size is 50 micron we have to make sure that ω axis is within ± 0.005 mm. This is the reason for not getting good reflectivity pattern if a normal powder diffraction setup is used for reflectivity measurement. To align the ω axis with the beam path, initially detector is kept at zero position and intensity of the beam is recorded. After this sample is brought up in the beam such that we get half intensity. To check if rotation axis of ω circle is in the path of the beam, sample is

rotated by 180°, if we get counts less or more than before rotation this indicates that ω axis is not in the path of the beam. In this case sample is moved up or down to get the same count. After this goniometer height is adjusted by half of the movement required of the sample to get the same counts. This process needs to be repeated several times before one is able to exactly align the ω axis with center of beam path.

In the reflected beam arm, curved pyrolytic graphite crystal is used as a monochromator. After the monochromator NaI scintillation counter is placed for recording the reflected beam intensity. The detector is capable of handling 10^6 cps and the background count of the detector is less than 0.5 cps. A variable slit of 0.01 to 5 mm is placed before the detector to collect the full-reflected beam. The system can be operated with both incident beam monochromator and reflected beam monochromator or with only one monochromator as per the requirement. The schematic of the system with both incident beam monochromator and diffracted beam monochromator is shown in figure (2.6).

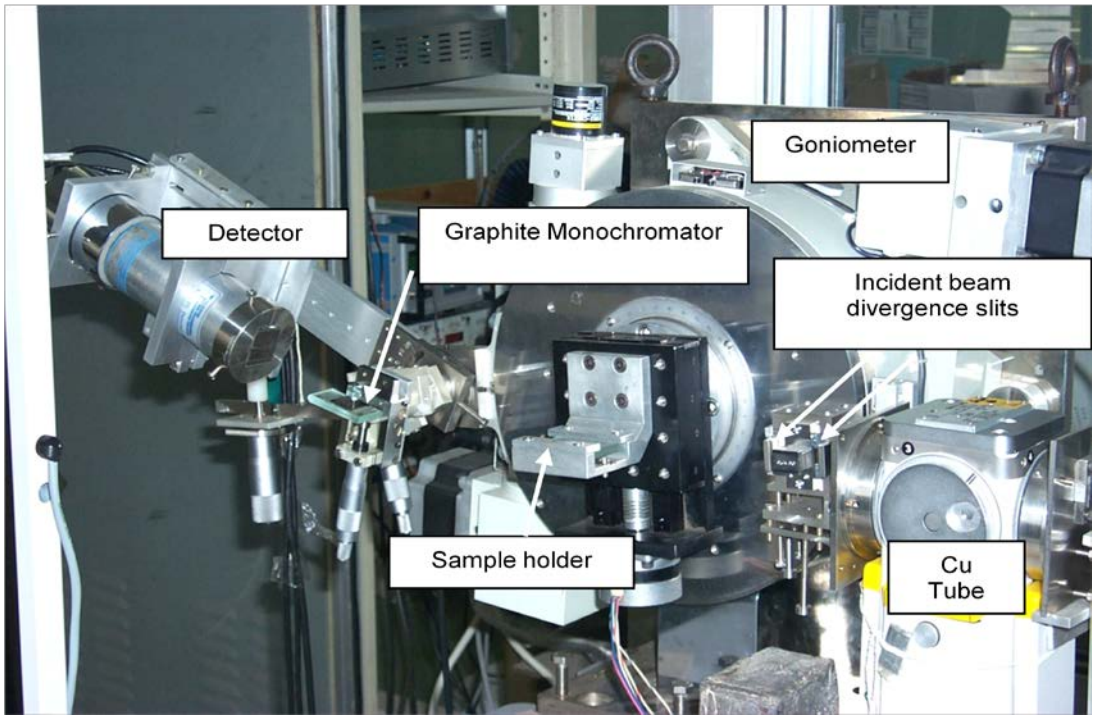

Fig. 2.7 Actual photograph of the developed system showing different components.

Figure (2.7) shows actual setup consisting of scintillation counter detector, graphite monochromator, incident beam slits, sample holder and x-ray tube used for the reflectometer.

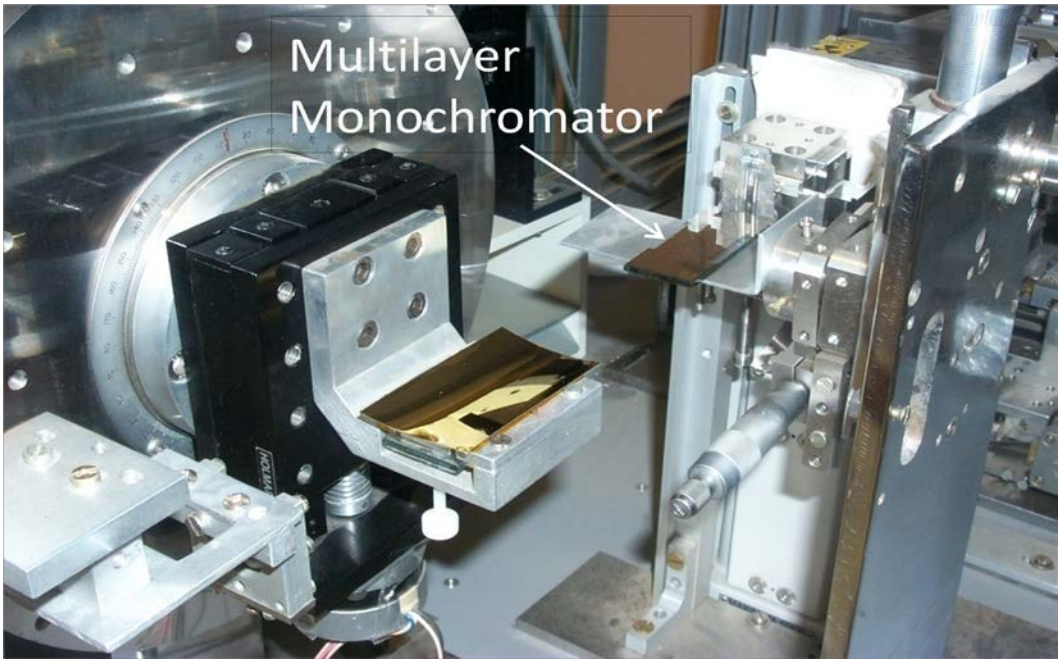

Fig. 2.8 photograph of the reflectometer showing incident beam multilayer monochromator.

Figure (2.8) shows the photograph of the system with incident beam multilayer monochromator. In the figure test piece of gold foil mirror of x-ray telescope is seen. The mirror sample is mounted on the sample holder for reflectivity measurements. The flexibility of sample holder makes it possible to hold odd size and shaped samples for measurements.

2.2.2 Measurement Procedure

To carry out reflectivity measurements accurately it is important to make sure that rotational axis of the sample (ω axis) matches precisely (better than 1/10 of the incident beam width) with the sample surface and sample surface zero angle matches with the zero of the ω rotation. This is achieved by bringing the sample precisely at the half height of the maximum beam intensity. After this we choose an incidence angle α_i below critical angle α_c of the sample and angular position of the specularly reflected beam is found by moving the detector circle 2θ. If 2θ does not coincide with $2\alpha_i$ it indicates that sample surface zero is not matching with the ω circle. The offset observed is adjusted in ω circle. Repeating this procedure at different α_i's improves the alignment of the system. In our system reflectivity measurement is carried out

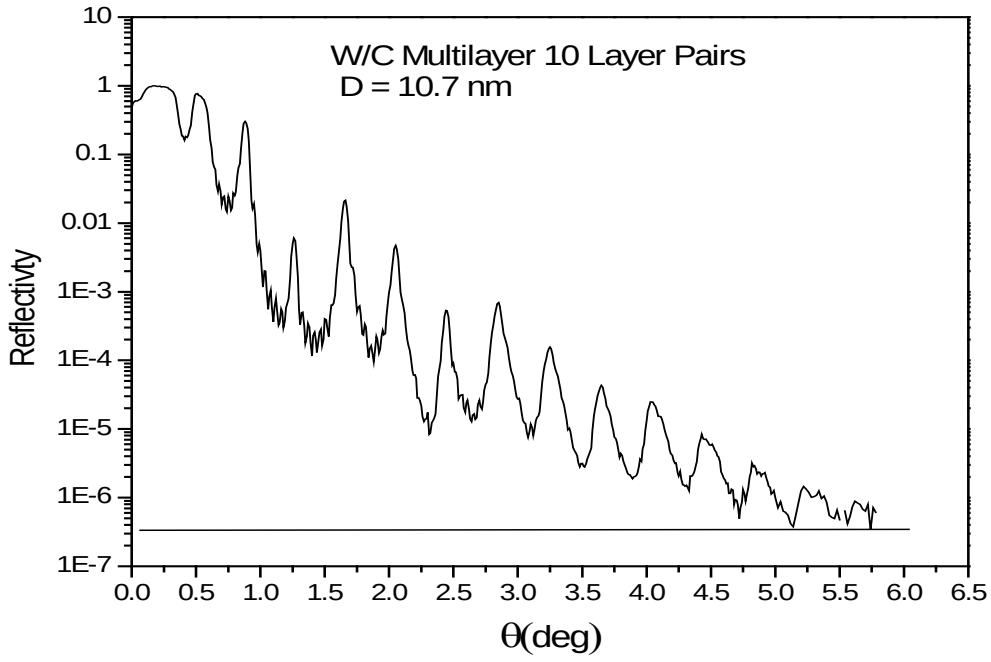

Figure 2.9 Reflectivity pattern of W/C multilayer showing more than six orders of dynamic range achieved

mostly with only incident beam multilayer monochromator as it gives high intensity parallel beam. In case sample fluoresces with Cu K_α we use monochromator in reflected beam arm. Incident beam slit size is kept at 0.05 mm and receiving slit before the detector is fixed at 0.1 mm. With this arrangement we are able to resolve films of thickness as low as 5 nm and as high as 150nm.The dynamic range of measurement achieved is more than six orders as shown in figure (2.9). This figure shows reflectivity pattern of a W/C multilayer with 10 layer pairs of 10.7 nm thickness, showing more than six orders of dynamic range measured.

Due to fine intense incident beam and precise alignment we are able to get the best possible resolution as well as high dynamic range. High flux gives us additional angular range (larger q space) allowing us to probe short length scales which helps us in getting the details of interface structure and tightening the constraints on the model used for fitting. Resolution in vertical direction in reciprocal space (q space) depends on incident beam divergence, monochromaticity of the beam and acceptance angles $\Delta\theta_{in}$ and $\Delta\theta_{sc}$. This relationship is given as

$$\delta q_Z = k_o \sqrt{\Delta\theta_{in}^2 + \Delta\theta_{sc}^2}$$

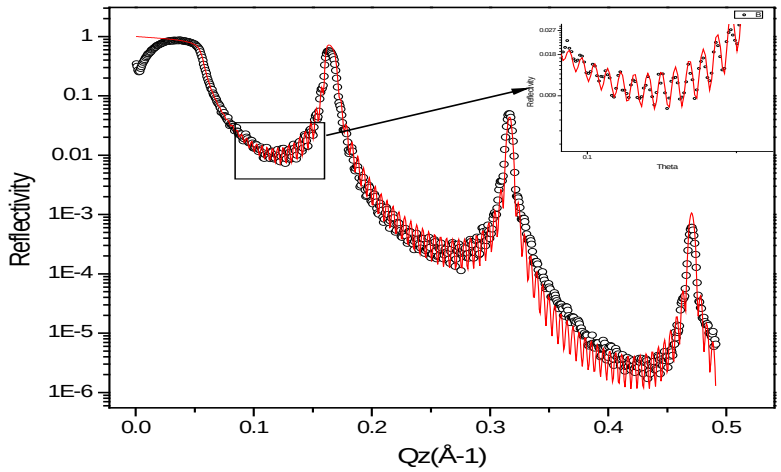

Figure 2.10 Reflectivity pattern of Pt/C multilayer Inset shows clear Kissing oscillation with fitting

The resolution in q determines the maximum length scale that can be coherently probed by the experiment. Figure (2.10) shows reflectivity pattern obtained reflectivity measurements of Pt/C x-ray multilayer along with the fitting line. This multilayer had N = 30 layer pairs of Pt (15Å) and C(25Å). Well resolved Kissing oscillation from a total stack thickness of 1200 Å in the reflectivity pattern indicates good alignment and resolution of the system.

2.2.3 Error in sample Alignment

If ω/θ axis is parallel to the sample surface but a distance δ_z away (fig. 2.11) from the centre of the rotation axis than the incidence angle changes from θ to θ+Δθ. Where it can be shown that $\Delta\theta = \sim \cos(\theta)$. $\delta_z /L = \delta_z /L$. L being the distance between the x-ray source and the sample due to this misalignment R vs θ curve would be shifted from the true value by the misalignment angle Δθ. A displacement of 50 micron for measurement radius of 200 mm would shift the angle by 0.01° which can destroy the reflectivity measurement. Hence, it is very important to correctly align the sample with respect to goniometer rotation axis.

Other than specular scattering measurements we have also used the developed system for diffuse scattering measurements. Such as (a) *Off-specular scan:* In off-specular scan, detector is kept at an offset of 2θ+Δθ . Sample and detector both rotate simultaneously with the offset Δθ.

(b) *Rocking scan:* In rocking scan, detector is positioned at fixed position 2θ and sample is rotated around position θ and (c) *Detector scan:* - In detector scan sample is positioned at fixed position θ, and detector is rotated around position 2θ. These scan help is getting information about in-plane and out of plane correlation in roughness at various interface in a multilayer sample.

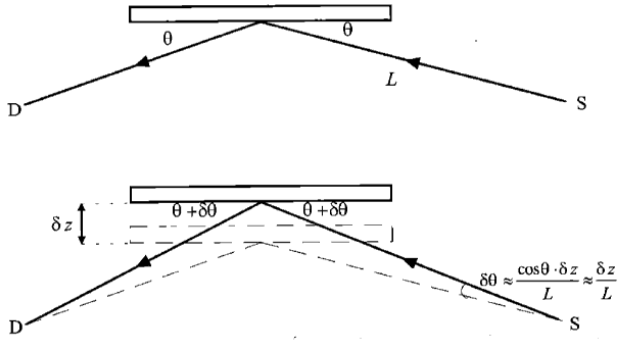

*Fig 2.11**Top** sample surface aligned correctly with the rotation axis for reflectivity measurement **bottom** same measurement but sample shifted by a distance δ_z from the rotation axis.*

2.2.4 Data Normalization

Normalization of the reflectivity data is a critical aspect of reflectivity measurement. Any error in this process would lead to misleading fitting models. The best way to normalize data is to measure the intensity of direct beam and divide the measured reflectivity with this number. But many a times due to size constrains of the sample and beam size, beam intensity etc., there are possibilities of error. If incident beam width is ***l,*** than its foot print on the sample at a grazing angle θ would be ***l/sinθ*** *for* a beam incident at an angle of 0.2 deg the size would be ~300 times larger the beam width. This large variation in size of the beam on sample is biggest source of normalization error. Using a knife edge as proposed by Holy [1] is of huge help in this situation. Knife edge is placed directly above the sample such that it forms a slit of 50 micron with the sample surface to reduce the foot print of the beam on sample. Figure (2.12) shows reflectivity of sample carried out with and without knife edge. In this graph, measurement

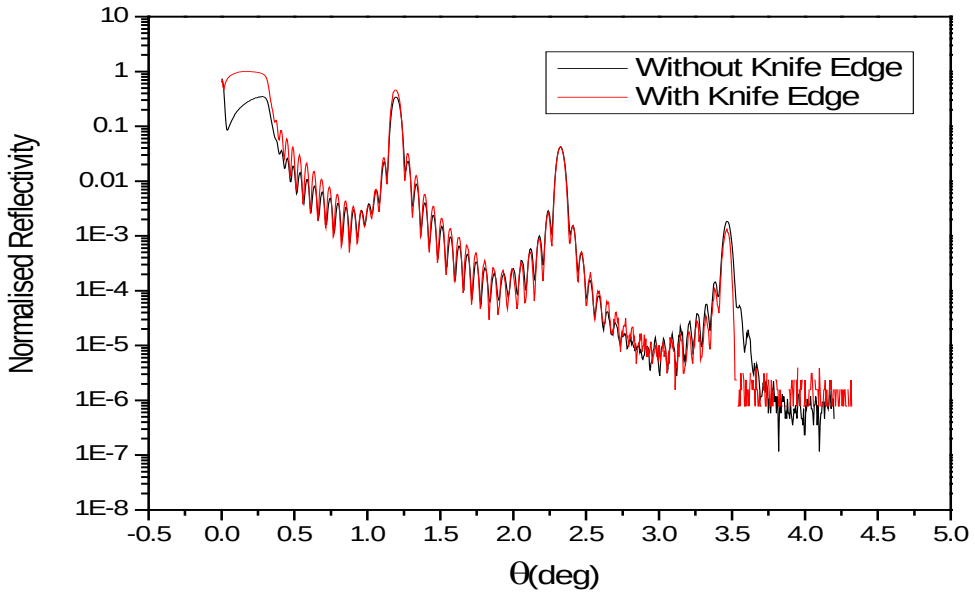

Fig 2.12 Measurement done on same sample with and without knife edge

carried out without knife edge was normalized with respect to direct beam counts and measurement with knife edge was normalized with respect to maximum beam count observed in critical angle region. It is clear from the graph that both measurements are equivalent and normalization is very easy on using knife edge where as any error in measuring of direct beam can spoil the normalization process and incorrect graph would be generated. It is found good to repeat the measurement after removing and replacing the sample again to check the repeatability of the data as well as of the sample. For all the measurements reported in this thesis we have followed this practice.

2.2.5 Performance Comparison

We had also done the comparison of x-ray reflectivity measurement on a multilayer sample with our instrument and with a measurement on a commercial Bruker system. Figure (2.13) shows a comparison of the two measurements on same sample. One can clearly see that more features are visible with a measurement done on developed system indicating that resolution and alignment of the developed system is better than the commercial system. This improvement in the performance is mainly due to precise alignment of the goniometer axis and all the optical elements including slits etc.

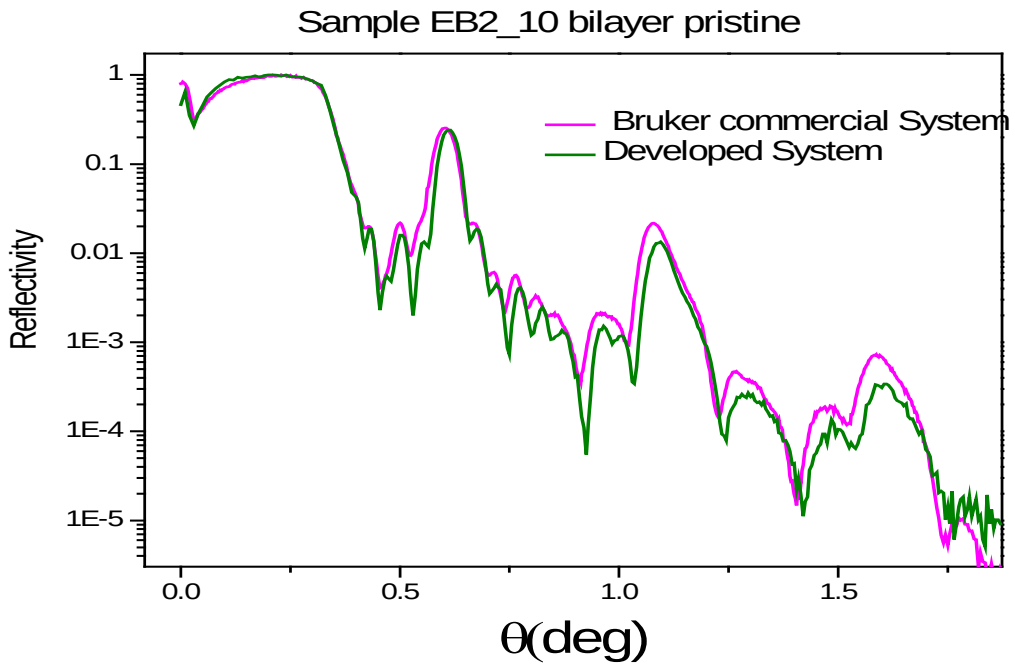

Fig. 2.13 Comparison of x-ray reflectivity measurement carried out on same sample with developed system and commercial Bruker system

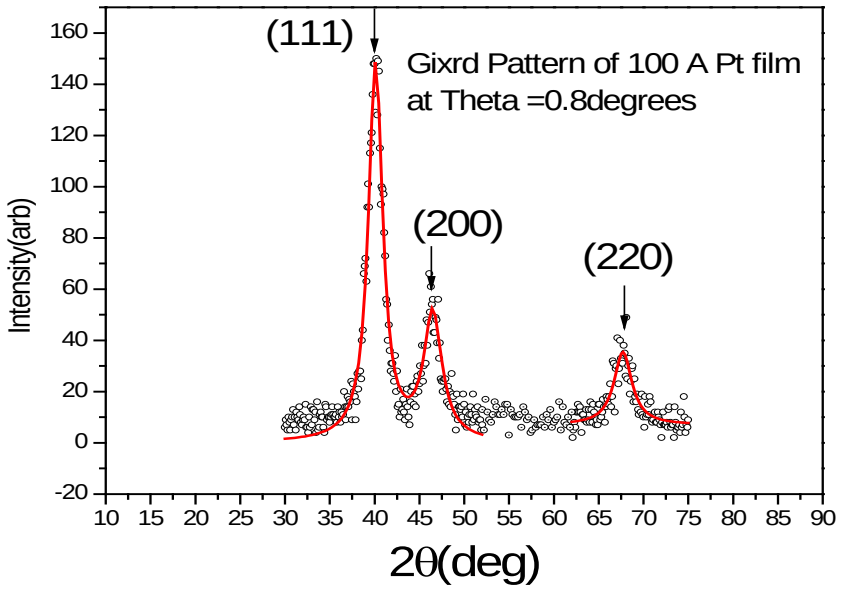

Fig 2.14 GIXRD Pattern of a 10 nm film of Pt on SiO_2 substrate

2.2.6 Grazing Incidence X-ray diffraction measurements

To carry out GIXRD first sample is aligned as the procedure defined for reflectivity measurements. It helps in accurately positioning the incidence angle theta. After alignment we fix the angle of incidence below 1 ° and insert a soller slit in diffracted beam path and open the receiving slit before detector to approximately 4-5 mm. The curved graphite monochromator is also removed and monchromatisation of the incident beam is done with only incident beam multilayer monochromator and Ni filter. This gives us intense parallel beam on the sample, which gives us good signal from the film. Figure (2.14) shows GIXRD pattern of a 10 nm Pt film deposited on float glass substrate. We have obtained very good signal from film and very low background from the substrate. All three peaks of film are visible indicating that film is polycrystalline. The measurement was done with angle of incidence fixed at 0.8°. Position of peaks observed matches with the expected pattern of Pt. The measurement was carried out with steps of 0.05° in 2θ and data acquisition time was 4 sec per step.

2.2.7 Powder Diffraction

We also carried out powder diffraction using this system after doing some changes in the optical system. To carry out powder diffraction we removed both incident beam monochromator and diffracted beam monochromator and only Ni filter was used for suppressing

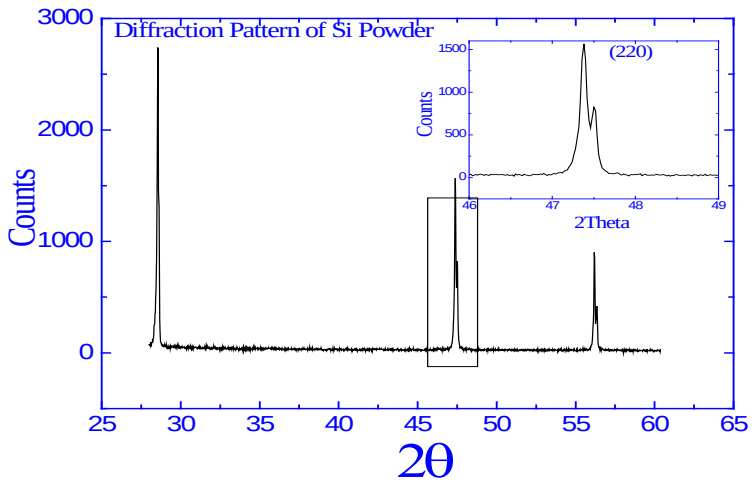

Fig. 2.15 Diffraction pattern of Si powder inset (220) peak of Si is shown showing that $K_{\alpha 1}$ and $K_{\alpha 2}$ are well separated

Cu K_β. After removing both monochromators the distances between source, sample and detector were kept same so the measurement geometry was maintained as Bragg-Brentano. This gave us good intensity of the diffraction peaks and peak shapes were Lorenztian. Figure (2.15) shows powder pattern of Si powder taken on the system. Inset of figure (2.15) shows magnified view of 220 peak of the pattern, it shows that $K\alpha_1$ and $K\alpha_2$ peak are well resolved indicating that alignment of the goniometer is correct. Peak positions and relative peak heights matched with the standard JCPDS Cards.

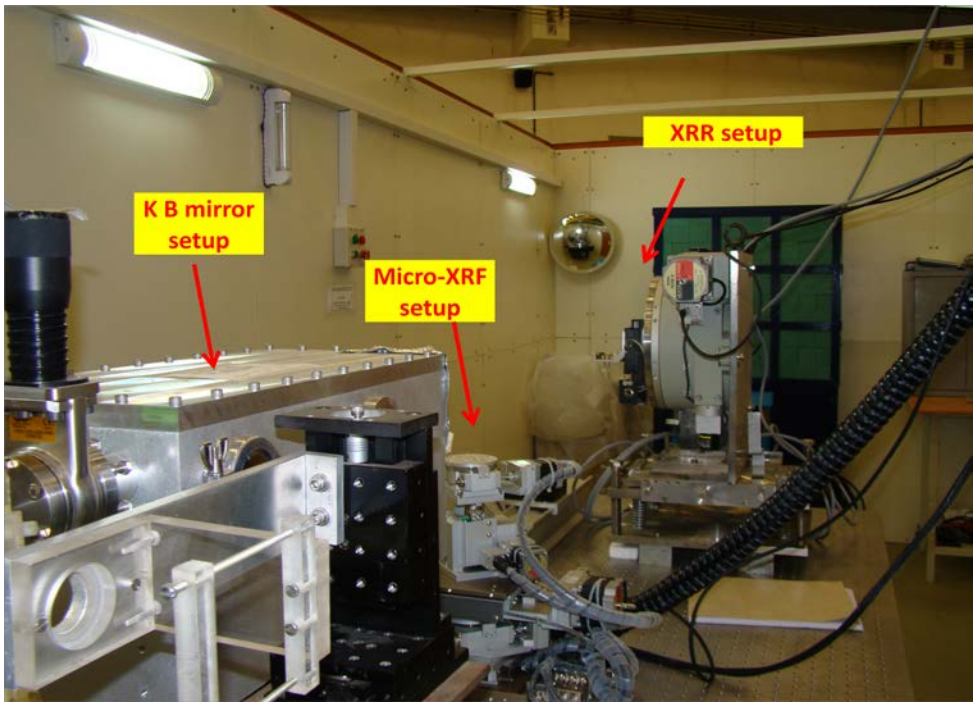

Fig.2.16 X-ray reflectivity setup installed on Indus-2 beam line.

After all the performance testing of developed system we used this system to carry out reflectivity and GIXRD studies on thin film and multilayer samples used for this thesis. All the optimization procedure for sample fabrication was carried out using this system. In the later part of the thesis work we shifted this instrument to Indus -2 beamline and carried out initial experiments. Figure (2.17) shows the photograph of the setup after installation on the beanline along with other setups. Results from the initial experiments are shown in the figure (2.17). Figure (2.17 a) shows reflectivity pattern of a Pt film measured at 10 keV energy x-ray along with the fit line. Figure (2.17 b) shows reflectivity pattern of W/B_4C 2 nm period 20 layer pair multilayer measured at 15 keV along with simulated pattern. These results show that

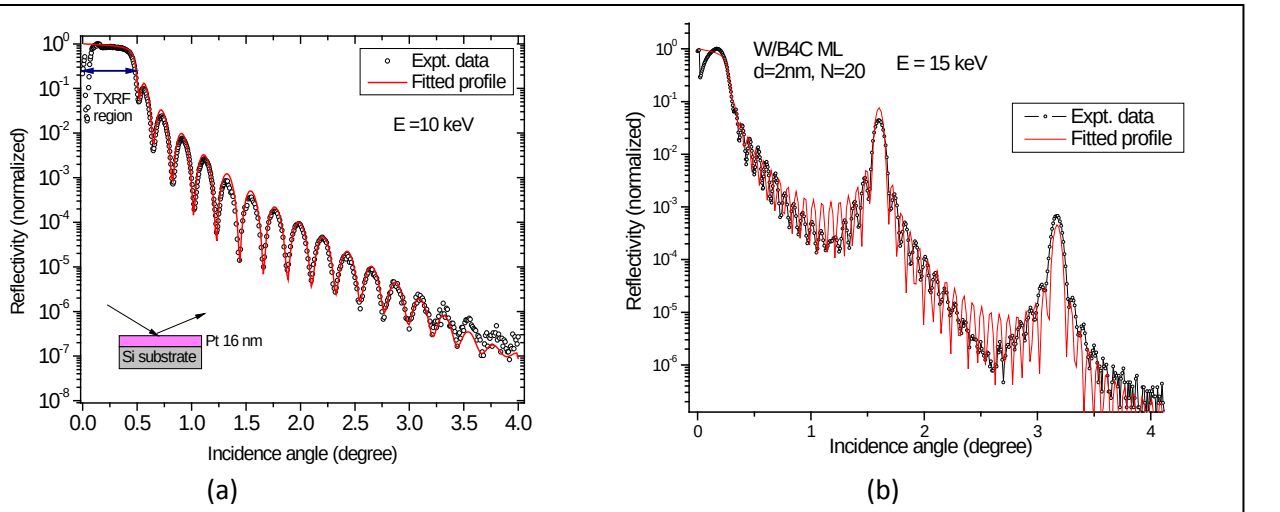

Fig 2.17 (a) reflectivity pattern of a Pt film measured at 10 keV energy x-ray along with the fit line (b) reflectivity pattern of 2 nm period W/B_4C multilayer measured at 15 keV.

reflectometer is working fine, more work will be carried out in future on this system.

2.3.1 Deposition techniques

To fabricate thin film various deposition techniques[15] are used such as thermal evaporation, electron beam evaporation, DC/RF/Magnetron/Ion beam sputtering, Pulse laser deposition, chemical vapor deposition etc. These techniques are either purely physical processes as evaporation method or purely chemical processes as gas and liquid phase chemical reactions or based on both physical and chemical processes as glow discharge and sputtering. We used ion beam sputtering techniques and DC/RF sputtering technique to deposit our thin film structures.

Sputtering and evaporation techniques are widely used for the fabricating multilayers for EUV/soft x-rays. The advantage of sputter deposition system is its stability. Gas flow and power to the plasma can be very well stabilized. Thickness errors well below 0.2 Å per layer have been achieved with accumulated thickness errors below 0.5 Å after the deposition of more than 100 layers[16]. Evaporation sources cannot be stabilized up to this level because of varieties of reasons; big changes in vapor pressure for small changes in temperature; long time constants in any feed back loop due to thermal mass of the evaporant and the crucible; temperature variation over the evaporant produced by changes in the surface geometry of evaporant. Evaporation with pulse laser, where film thickness is controlled by number of pulses eliminates some of above problems and gives good multilayer quality[17]. Successful deposition of x-ray mirrors has been obtained by Ion assisted electron beam deposition technique[18].

The kinetic energy of evaporated particles is a major difference between deposition methods. For conventional evaporation, the evaporated particle energy cannot be adjusted, and is below the 0.5eV. An advantage of this low energy is the damage of growing film is minimized. Crystallization of amorphous films can more easily be avoided and amorphous films usually have better boundaries than polycrystalline films. On the other hand, bombardment of the film by other higher energy particles (known as ion beam assisted deposition) can enhance sideways diffusion of the surface atoms and help them to settle in the valleys of the structure, thus producing smoother films. Bombardment of the film during or after diffusion with ions has successfully been used to obtain smoother boundaries[19,20]. In sputter deposition, kinetic energy of evaporated particles is >10eV, and can be adjusted and in addition, the growing film can be bombarded by secondary electrons and inert gas ions and atoms. For many materials optimized sputter deposition have produced much sharper boundaries than evaporation[21].

Sputtering is the method of choice where a large number of similar coatings have to be fabricated routinely. Thermal deposition with insitu monitoring is the choice where a single large and expensive substrate, like the mirror of x-ray telescope has to be coated.

2.3.2 General discussion about Sputtering

In sputtering technique, inert gas ions are accelerated by an electric field. Accelerated ions are bombarded on target material to sputter the target atoms. Sputtered target atoms are deposited on substrate in the form of thin film. Ions are generated either by glow discharge or by separate ion source. Depending on the method by which the discharge is produced and sustained, sputtering can be classified into DC/RF/Magnetron/Ion beam sputterings.

DC sputtering is the simplest form of sputter deposition. DC sputtering system is consists of planer cathode and anode. Target material and substrate are mounted on the surface of cathode and anode, respectively. Chamber is filled with inert gas of $\sim 10^{-2}$ mbar pressure. Few hundred volts voltage is applied between cathode and anode to produce the glow discharge. Generated positive ions of gas are accelerated towards the cathode and sputter the target material. Sputtered target material is deposited on substrate mounted at anode. This deposition technique works well for metallic targets. In the case of insulating targets, a positive charge is developed on target surface, which repel the incoming positive ions. So this technique is not suitable for insulating materials.

To avoid the charge accumulation in DC sputtering a RF voltage is applied between anode and cathode instead of DC voltage. This is called RF sputtering. In this case target material is alternatively bombarded by positive ions and electrons, which remove the charge accumulation problem on insulating targets. Another advantage of RF voltage is that the collision probability between gas molecules and electrons is increased, so discharge can occur at relatively lower pressure ($\sim 10^{-3}$ mbar).

In DC and RF sputtering methods discharges exist over the entire chamber. Pressure of gas in chamber is also of the order of $\sim 10^{-3}$ mbar. So in these methods deposition rate is very low and contamination of film is high. To obtain high deposition rate at lower pressure magnetron sputtering is used. Deposition rate depends on the incident ion beam flux, which is proportional to the density of ions in plasma. Limitation of ion density in plasma is due to recombination of ions with electrons. These recombinations mainly occur at the walls of chamber. To prevent this, a transverse magnetic field of few hundred gauss is applied. Due to the presence of magnetic and electric fields, electrons of plasma are confined near the target. Electron confinement increases the ion flux. Hence magnetron sputtering can be operated at relatively lower pressure with high sputtering rate.

In ion beam deposition technique, separate ion source is used to produce a focused ion beam, which is incident on a target material for sputtering. The most commonly used source is Kaufman broad beam ion source[22]. It consists of a discharge chamber in which plasma is magnetically confined. The ions are extracted from the source by a multi-aperture accelerator system. To avoid the defocusing of beam due to the space charge effects, electrons are mixed with extracted ions to neutralize the ion beam. Such an energetic ion beam is made to impinge on a target. In this method, deposition can be carried at much low pressure. Ion beam energy and angle of incidence on target can be optimized. Multiple targets can be mounted and positioned in the beam path. In this method deposition rate is smaller than magnetron sputtering. Ions are generated in ion beam sputtering technique inside an independent source which is kept away from sputtering zone and these ions by using extraction mechanism are made incident on the target. Hence deposition takes place at a lower working pressure, at least one order below than that in magnetron sputtering. Deposition by IBS technique produce films with better morphology and packing density.

2.3.3 SRIM Simulation

The sputtering process can be evaluated theoretically by Monte Carlo method based simulations of interaction of large number of incident ions with target atoms. The most widely used computer code is SRIM[23] previously known as TRIM. SRIM is a group of programs which calculate he stopping range of ion (10 eV to 2 GeV/amu) into matter using a quantum mechanical treatment of ion atom collision. During collisions the ions and atom have screened Coulomb collision including exchange and correlation interactions between the overlapping electron shells. The ions also have long range interaction with target atoms creating electron excitations and plasmons within the target. The charge state of ion within the target is characterized by an effective charge, which include a velocity dependent charge state and long range screening due to collective electron sea of the target. The probability of atomic collision and angular distribution of recoils are determined by a Monte Carlo randomization procedure. One of the options of the code is to follow the history of each collision until all atoms have energy less than the displacement energy in respective target material. The detailed collision history mode was used in all our sputtering, re-sputtering simulation with the SRIM code.

In sputtering process, in addition to sputtered target atoms other particles can also get ejected. In all sputtering deposition techniques it is known (as shown in Fig. 2.18) that large number of sputtering gas neutrals and ions get reflected from the target and hit the freshly growing film surface. This process of back scattering is a kinematical effect of ion bombardment on a target. If mass M of the incident ion is less than the target atom mass, law of momentum conversation allows the ion to be reflected from the target atom. The angular distribution of the reflected neutrals is also approximately a cosine distribution. Flux and energy of reflected neutrals was measured by Rossangel et.al [24]. He had concluded that bombardment of depositing film during sputtering should be considered as an unavoidable artifact of sputtering deposition technique. A review by Mattox [25] covers the range of modifications which can happen in the film due to bombardment of energetic particles. It is possible to model theoretically and calculate the energy and angular distribution of these reflected neutrals using Monte Carlo based SRIM. Our simulations for 10^5 Ar^+ ions incident at normal to target with energies between 800-200 eV,

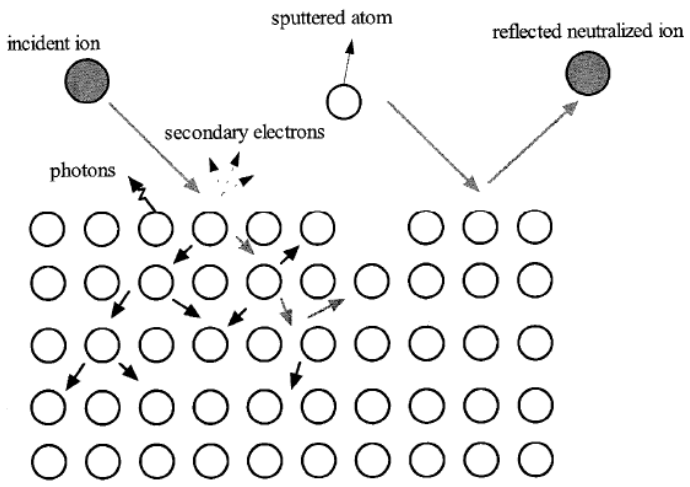

Fig. 2.18 Schematic of physical sputtering process. Incident ion creates a cascade of atomic collisions in the surface layer of target and target atoms are ejected along with reflected neutral/ions , photons and secondary electron

showed that the reflected neutrals have 2-6 times the energy of the sputtered atoms and their number density also could be as high as 0.6-0.8 of sputtered atoms from the target. These neutrals and ion hitting the film have sufficient energy to re-sputter the growing film, modify growth morphology, density, adhesion, interface mixing and can also generate residual stresses in the film. In case of multilayer growth, as we are depositing High Z and Low Z materials sequentially and the bombardment of neutrals seen by both interfaces is not same. It becomes important to understand the influence of these neutrals. At shorter periods these neutrals could pose a challenge in fabricating a thin continuous layer itself.

2.3.4 Development of Ion Beam Sputtering system

As mentioned earlier we have assembled an ion beam sputtering system based on Kaufman focused beam ion source. The schematic diagram of the IBS thin film deposition system is shown in fig.(2.19).The chamber has a diameter of 560mm, a height of 665mm and a wall thickness of 5.0mm which is sufficient to incorporate ion source using suitable ports. The ion gun is mounted on a supporting assembly at port Φ203 CF (conflate flange). The angle of

gun with respect to the target is 50 degree. During sputtering, the target is kept horizontal with

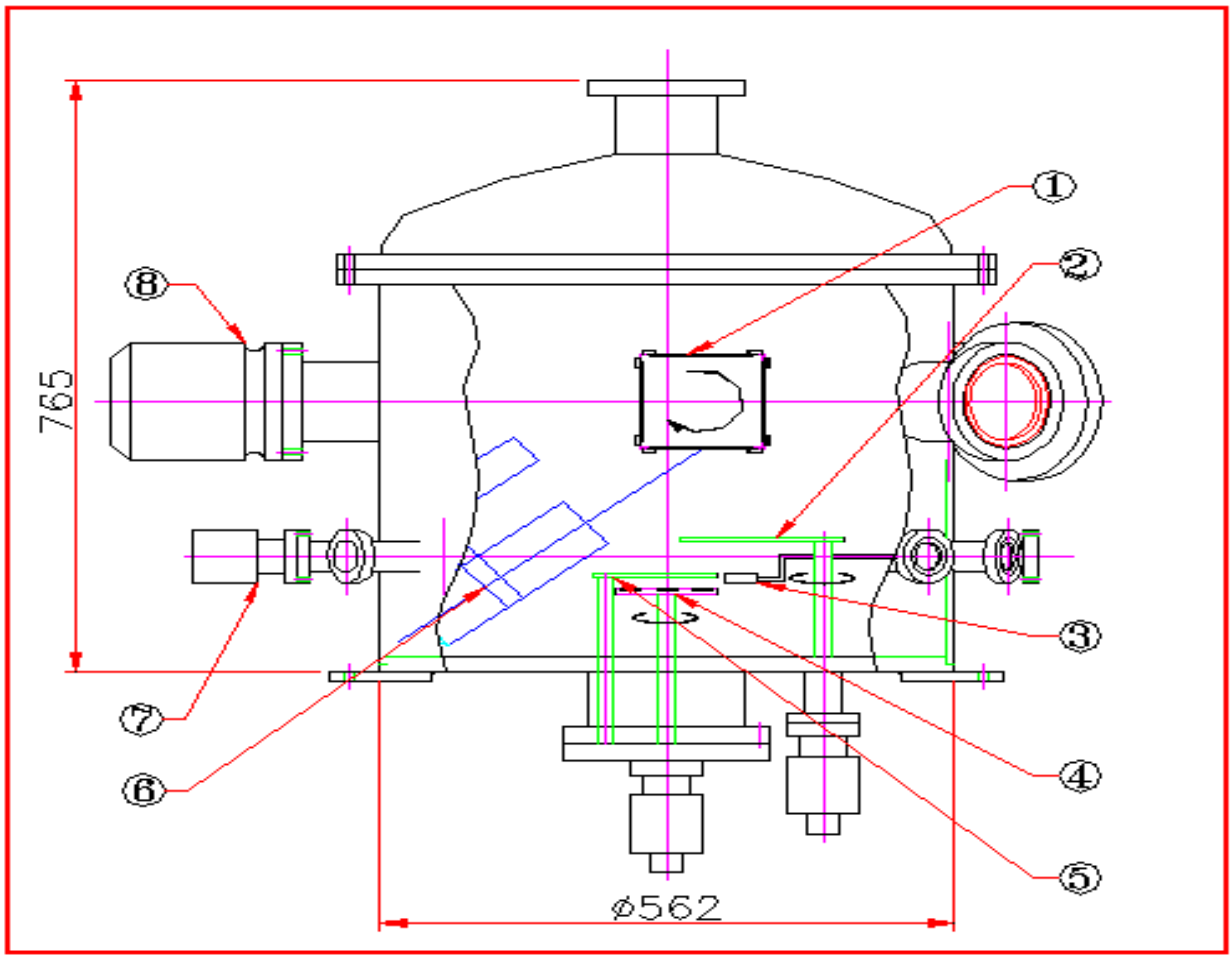

Fig. 2.19 Schematic diagram of main chamber of ion beam sputtering system
1: Target holder, 2: Motorized shutter for substrate, 3: Thickness monitor, 4: Substrate holder, 5: Fixed shutter for substrate, 6: Kauffman Ion gun, 7: Residual gas analyzer (RGA), 8: Turbo molecular pump

respect to the substrate inside the chamber. This geometry allows maximum sputtering yield [26].A four target holder (square block) is installed on port Φ152 KF (Klein flange) in which we can load four targets at a time for depositing thin film and multilayers of various materials. A substrate holder is also mounted on a rotary feed through on port Φ70 CF which can hold four substrate at a time therefore we can fabricate four samples in a single or multiple operations without breaking the vacuum of the chamber. A substrate heater is also installed that can be used in place of substrate holder for fabricating of thin films and multilayers at high temperature (max. up to 700 ^{o} C). Thickness of the film can be monitored using quartz crystal thickness

monitor (INFICON IC/5) which is mounted on port Φ152 CF. Various other ports have been kept to incorporate other accessories in future.

The ion source used in the present system is a 3cm diameter Kauffman-type hot cathode gridded source (Commonwealth Scientific Corporation). Thermionically emitted electrons by hot tantalum (or tungsten) cathode ionize the Ar gas molecules. Ar ions are formed into small beamlets by passing through apertures in the screen grid. These beamlets are accelerated by accelerator grid. Accelerating voltage can be varied from 50-1000 V. After accelerating grid, energetic ions are neutralized using neutralizer cathode. This ion beam is bombarded on target material to produce sputtering.

In the system target holder and shutter for substrate can be rotated through motorized rotary feed throughs which are mounted at separated port Φ70 CF of the chamber. These motorized feed throughs are operated through a controller with specified motors, one for target holder and other for shutter. A user friendly software (Labview) is developed to control the whole operation of the IBS system.

Turbo molecular pump (TMP 500 l/s capacity backed by a rotary) pumping system has been used for evacuation. The designed chamber has a volume of about 200 liter and the internal surface area including all components and ports exposed to vacuum is about 15000 cm^2. Considering the gas load due to surface area and installed components like substrate heater, substrate holder, shutter for substrate, quartz crystal thickness monitor, Gun supporting components, components for automation, target holder, electrical cable for getting signals etc.

The base vacuum obtained is of the order of 2×10^{-7} mbar within a few hours without any baking. After installing all the ports the vacuum of the chamber was tested using a TMP backed by rotary pump. The ultimate vacuum obtained in the chamber is 8×10^{-8} mbar (with baking).
At the same time, the pump can be operated at a constant pumping speed in order to maintain a pressure of the order of 4×10^{-4} to 6×10^{-4} mbar after introducing the flow of Argon gas in the chamber. We have used a mass flow controller (Brooks Instrument 5850E) with an accuracy of 1% for this purpose. The MFC can be operated in the range of 1-20 cm^3/min with most of the commonly used sputtering gas e.g. Ar, Xe, etc. but for 3cm DC ion source the MFC optimized range is 3-5 cm^3/min for sputtering gases.

Most of the samples used in this study have been fabricated using the same system after proper optimization of all the deposition parameters like discharge current, acceleration voltage and beam voltage etc.

2.3.5 Magnetron Sputtering System

Some samples of W/B_4C multilayer were made using customized magnetron sputtering system purchased from Germany. This magnetron sputtering system has both DC and RF compatibility. There are two rectangular cathodes of size 500 mm × 100 mm each. This sytem can be used for deposition on 300 mm X 150mm area fig. (2.20). The sputtering process is in a horizontal configuration. Sample movement is fully software controlled from load lock to main processing chamber. The base pressure in main chamber and load lock system is 1×10^{-8} mbar and 8×10^{-8} mbar, respectively. Load lock chamber contains a RF ion etcher for substrate cleaning. All test samples are fabricated on Si and float glass substrates. Substrate moves linearly over sputter sources with variable speed. The deposited material thickness is determined by the time of substrate exposure to the source, which, in turn depend on the velocity of the substrate. Purity of W and B_4C target is 99.9 and 99.99, respectively. High purity (99.999%) argon is used as sputtering gas. DC power is used for sputtering of W and RF power is used for B_4C. During optimization of the sputtering parameters, sputtering power for W and B_4C was varied from 80 to 200 W and 200 to 700 W, respectively. Ar flow is varied from 4 to 12 sccm, resulting in pressure variation of the process chamber between 1.0 $x10^{-3}$ to 8 $x10^{-3}$ mbar. The target-substrate distance

Fig. 2.20 Photograph of DC/ RF magnetron sputtering system showing main deposition chamber on left and load lock chamber with ion etcher on right

can be varied from 50 mm to 150 mm. Our samples were at 70 mm target-substrate distance.

2.4.1 Transmission Electron Microscopy (TEM)

Transmission electron microscopy[27] is a powerful tool to see the microstructures (~ few Å). In TEM, electron beam is used as a probe to find the information about structure of materials[28]. In this method, sample is illuminated by high energy (accelerated by 100-400KV) electron beam and transmitted/diffracted beam is observed, which gives information about the structure of material. Two types of scattering between electrons and sample are possible. (1) Elastic scattering. (2) Inelastic scattering. Using elastic scattering between electrons and material (electron diffraction), structural information about material as crystal structure, periodicity, grain sizes, grain location etc are obtained, in TEM. Electron diffraction has its own advantages. Electrons can be focused easily compared with x-rays. The optics of electron microscope is used to make images of the intensity emerging from the sample. Variation in the intensity of electron due to diffraction across a thin specimen is called 'diffraction contrast' and is useful to make the images of defects as dislocations, imperfections and second phase particle. In high resolution TEM, transmitted and diffracted beam from specimen interferes and give information is called 'phase contrast imaging'.

Schematic of TEM is shown in Fig (2.21). Emitted electron beam (current 10-100 microampere) from electron gun accelerated by 100-400 KeV. Electron beam is focused using magnetic lenses. Generally, parallel electron beam is used to illuminate the sample. Diffracted

and transmitted beams from sample are focused using objective lens. In the back focal plane of objective lens, one can select either diffracted or transmitted beam by placing objective aperture at suitable position. After the objective aperture intermediate lens make the correct image of specimen. By changing the focusing strength of intermediate lens by increasing current in intermediate lens TEM can switch from ‘diffraction mode’ to ‘image mode’. Further magnification of the diffraction/image is performed using subsequent intermediate and projector lenses.

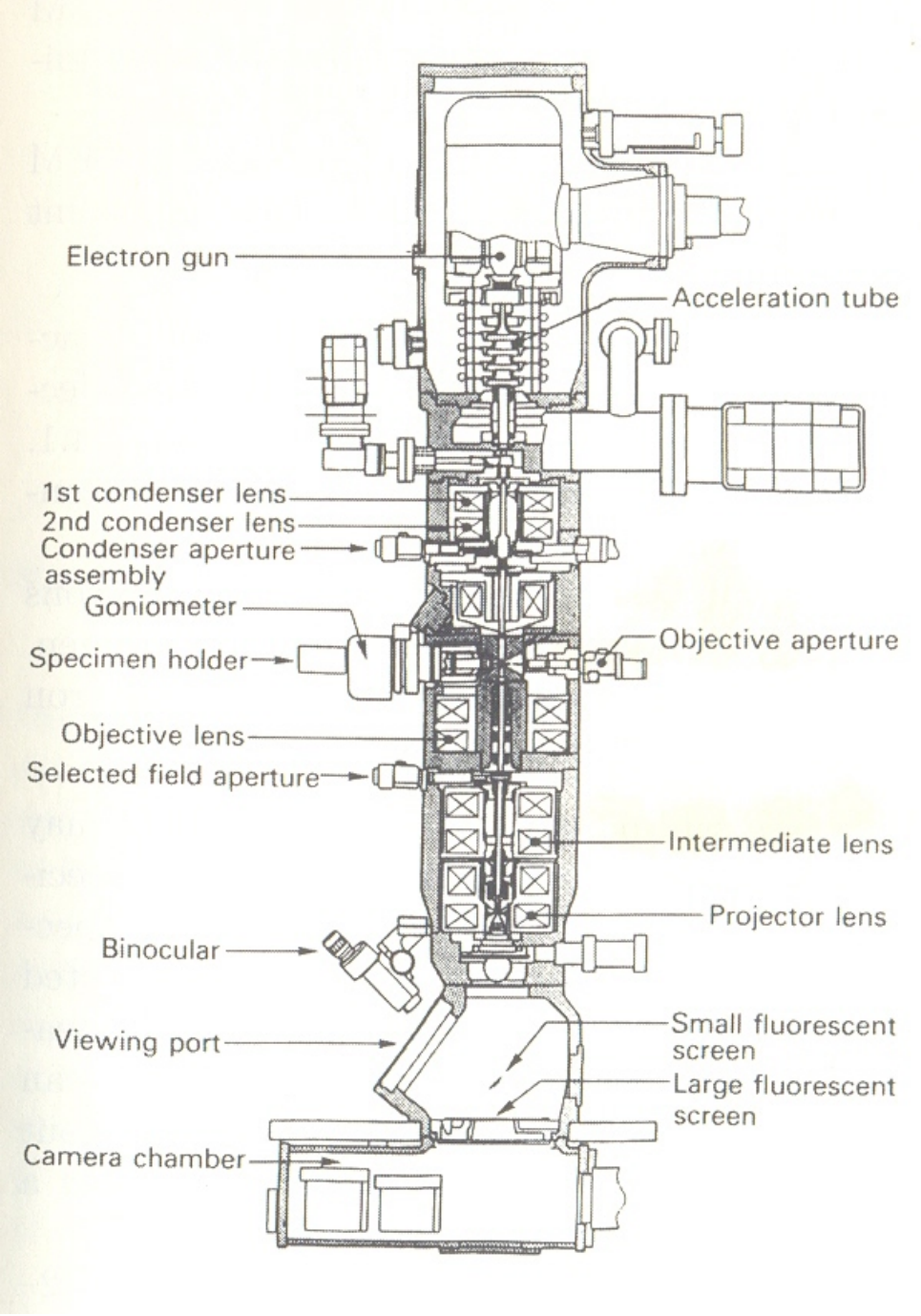

Fig 2.21 Schematic diagram of TEM.

2.4.2 Modes of Operation of TEM: TEM can be operated in different modes as follows;

(a) Imaging Mode

Dark field and bright field imaging

Fig (2.22) shows the ray diagram of a conventional TEM making dark and bright field images. In these images intermediate lens is focused in the image plane of objective lens. When objective aperture is positioned to pass only the transmitted beam then bright field image is formed as is shown in fig (2.22a). In bright field image the area of specimen, which diffract the beam is dark and rest is bright. In this image, the gross morphology of specimen can be seen. We can see the grains and measure the grain size. When objective aperture is positioned to pass only diffracted beam then dark field image is formed as is shown in fig (2.22b). In dark field image the area of specimen, which diffract the beam is bright and rest is dark. In dark field image we can position the objective aperture at different diffraction spots of various orientations and see the corresponding oriented grains in specimen. In this case only those grains are bright in images that have corresponding orientations. Bright and dark field images are complementary to each other and much better than aperture less image. In aperture less image bright and dark field images superimpose and contrast decreases.

(b) Diffraction Mode

Selected Area Diffraction (SAD)

In selected area diffraction (SAD) intermediate lens is focused in the back focal plane of objective lens. A second aperture called intermediate aperture is positioned in the image plane of objective lens as is shown in fig (2.23), to obtain the diffraction from the selected areas of the specimen. The specimen is first examined in image mode until a region of interest is found. The intermediate aperture is then inserted and positioned around this feature. The microscope is then switched into diffraction mode. The SAD pattern that appears on the viewing screen originates from the area selected in the image mode. SAD can be performed on regions of 10^{-6} meter

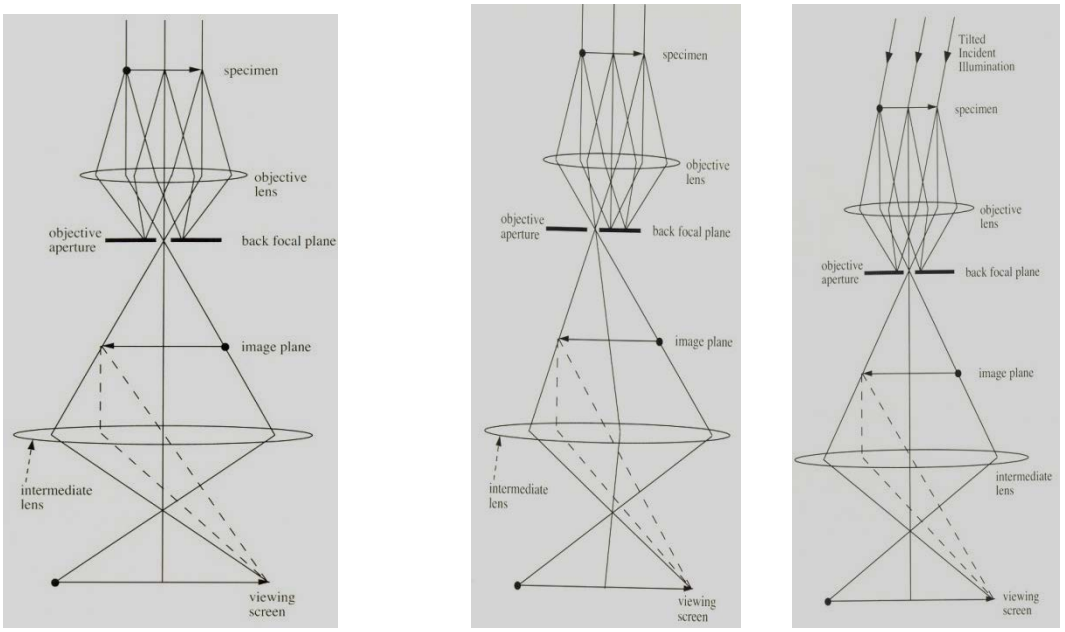

Bright Field **Dirty dark field** **Axial dark field**

(a) (b)

*Fig 2.22 Schematic diagram of a conventional TEM in **(a)** Bright field mode and bright field image and **(b)** dark field mode and dark field image*

diameter. For nano diffraction it is needed to use a nano beam technique as convergent beam electron diffraction.

The obtained electron diffraction pattern of Fe/Si multilayer is shown in Fig (2.24a). We can use the separation of the diffraction spots to determine interplanary spacing in crystals. Fig (2.24b) shows the geometry of the diffraction. From Braggs law

$$2d\sin\theta = \lambda$$

$\theta \sim 1^0$, and $\lambda = .037$ Å (for 100 keV electrons)

$$\sin\theta \sim \tan\theta \sim \tfrac{1}{2}(\tan 2\theta) \sim r/L$$

$$rd = \lambda L$$

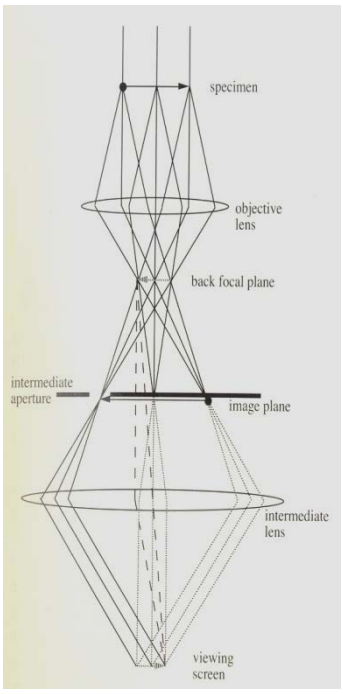

Fig 2.23 Schematic diagram of a conventional TEM in selected area diffraction mode.

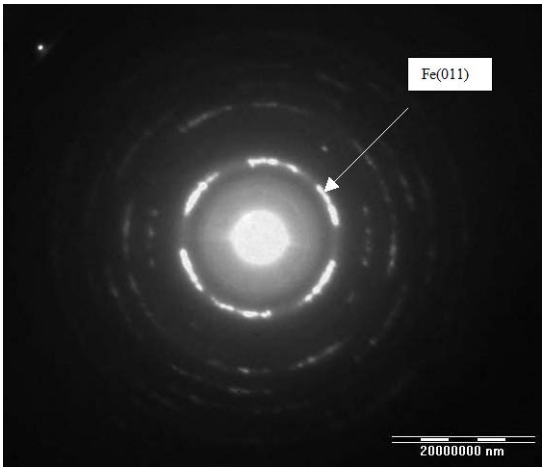

(a)

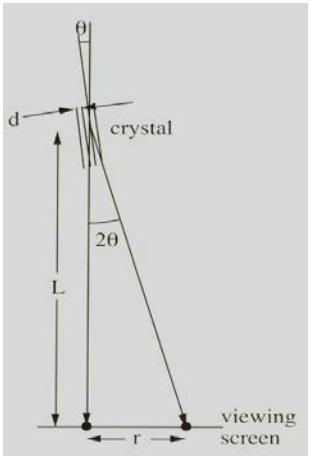

(b)

Fig 2.24 ***(a)*** *Obtained electron diffraction of Fe/Si multilsayer.* ***(b)*** *Diagram of geometry of electron diffraction and definition of camera length.*

Where L is characteristic of TEM called camera length[47] and r is the radius of diffraction ring. This equation is camera equation and λL is known as camera constant[47]. We measure r and calculate crystal spacing d. In small angle diffraction pattern, we see the small angle diffracted electrons, which gives the information about crystalline/amorphous structure of layers in thin films.

In TEM high-energy electron beam also inelastically scatter from specimen and gives rise to characteristic x ray emission. These characteristic x rays from each element are used to determine the concentration of different elements in the specimen. This is called energy despersive x-ray spectroscopy (EDS)[47]. High-energy electrons also loose their energy in specimen by plasmon excitations and other processes. By measuring this energy loss in transmitted beam information about these processes in specimen can be extracted. This is called electron energy loss spectrometry (EELS)[47].

We carried electron diffraction and cross-sectional measurements of multilayer samples. Samples for cross-sectional TEM, were prepared by standard sample preparation procedure including mechanical polishing, dimpling and ion mealing. Mechanical polishing was done by polishing the sample on emery paper, down to the thickness of 0.5 mm. Then sample was inserted into slotted bross rod and finally inserted into the brass tube of outer diameter 3 mm. This brass tube is cut into many slices of 1 mm thickness. Slice was again polished by emery paper down to 100 μm. Dimpling of mechanical polished sample was carried out, down to 20 μm thickness. Dimpled sample was ion mealed to get large electron transparent area. This sample was used for TEM characterization. TEM measurements were carried out using 200KV TECNAI 20 G2 TEM.

2.5.1 Soft X-ray reflectivity

Photograph of the experimental station for reflectivity measurement in soft x-ray-VUV region of SR beam from Indus-1[29] is shown in Fig 2.25. This experimental station is developed at Indus-1 reflectivity beamline[30] on this source. We have carried out the normal incidence soft x-ray/EUV reflectivity measurements to characterize our NbC/Si samples. The beamline delivers radiation in the range of 4-100 nm with high flux and moderate spectral resolution using a toroidal grating monochromator. Various absorption edge filters are provided in the beamline to suppress the higher order contamination from monochromator. The present reflectance measurements are carried out in the s-polarized geometry. The wavelength resolution $(\lambda/\Delta\lambda)$ of beam line in this spectral region is 200-500. The detector used is EUV/Soft x-ray photo diode. Reflectivity measurements can be carried out by a vacuum compatible two-axis reflectometer which has angular resolution < 0.01°, in large angular range of 0-90°, operates in 5×10^{-7} mbar

pressure range. Various types of scan i.e. θ-2θ scan, detector scan, rocking curve scan; offset scan are possible.

Fig 2.25 Photograph of the reflectivity experimental station on CAT-TGM beamline at SRS Indus-1.

References

1 "'High-Resolution X-ray Scattering from Thin flims and Multilayer", V. Holy, U. Pietsch, T. Baumbach, , Springer Heidelberg Germany (1999).

2 "Morden X-ray Physics", Jens Als-Nielsen, Des McMorrow, John Wiley & sons, Ltd, 2000.

3 Chason E. and Mayer T: M., Critical Reviews in Solid State And Materials Sciences, 22, (1997),1.

4 M. H. Modi, G. S. Lodha, S. R. Naik, A. K. Srivastava, R. V. Nandedkar, Thin Solid Films, 503, (2006), 115.

5 M. K. Tiwari, S. R. Naik, G. S. Lodha, R. V. Nandedkar, Analytical Science, 21,(2005), 757.

6 Archna Jaiswal, Sanjay Rai, MK Tiwari, V R Reddy, G S Lodha, R V Nandedkar, J. Phys.: Condens. Matter, 19, (2007), 01600 .

7 M. Nayak, M.H. Modi, G.S. Lodha, A.K. Shrivastava, P. Tripathi, A.K. Sinha, K.J.S. Sawhney, R.V. Nandedkar, Nucl. Instrum. Methods Phys. Res. B, 199, (2003),128.

8 S. R. Naik, S. Rai, G. S. Lodha, R. Brajpuriya, J. Appl. Phys. 100, (2006), 013514.

9 "X-ray Scattering from Soft Matter Thin Films", Metin Tolan, Springer, Germany, (1999).

10" Principles of Optics", Max Born, Email Wolf, Cambridge University Press,1975

11 L. G. Parratt, Phys. Rev., 95 , (1954), 359.
12 L.Nevot and P Croce. Rev.Phys.Appl. 15, (1980) ,761.
13 Roger Pynn, Phys. Rev, B, 45(2), (1992), 602.
14 D.L.Windt " IMD: software for modeling the optical properties of multilayer films" Computer in Physics 12, (1998) 360.
15 "Hand Book of Thin Deposition Processes and Technology", Klaus K. Schuegraf, Noyes Publishers, 1988.
16 T. W. Barbee, Opt. Eng. 25, (1987), 893.
17 S. V. Gapanov, F. V. Grain, S. A. Gusev, A. V. Kochemasov, Y. Y. Platonov, N. N. salashenko, E. S. Gluskin, Nucl. Instrum. Methods, 208, (1983), 227.
18 Eberhard Spiller, Armin Segmüller, Jack Rife, Rolf-Peter Haelbich, Appl. Phys. Lett. 37, (1980), 1048.
19 E. Spiller, Opt. Eng, 29, (1990), 609.
20 A. Kloidt, H. J. Stock, U. Kleineberg, T. Döhring, M. Pröpper, B. Schmiedeskamp and U. Heinzmann, Thin Solid Films, 228, (1993), 154.
21 S. Ogura, M. Niibe, Y. Watanabe, T. Iijuka, Proc. SPIE, 984, (1988), 140.
22 "Operation of Broad Beam Sources", Harold R. Kaufman, Raymond S. Robinson, Commonwealth Scientific Corporation Alexandria, Virginia.
23 "The Stopping and Range of Ions in Solids", by J. F. Ziegler, J. P. Biersack and M. D. Ziegler SRIM 2008.
24 S.M.Rossangel J. Vac. Sci and Tech. (A) 7, (1989), 1025.
25 D.M.Mattox J. Vac. Sci and Tech. (A) 7, (1989), 1105.
26 "Hand book of sputter deposition Principles, Technology and Applications". Wasa Kiyotaka, Hayakawa Shigeru.Westwood,Noyes publications 1992.
27 "Transmission Electron Microscopy and diffractometery of materials", Bernt Flutz, James Howe, Springer (1998).
28 N. D. Telling, C. A. Faunce, M. J. Bonder, P. J. Grundy, D. G. Lord, J. A. Van den Berg, S. Langridge, J. Appl. Phys., 89, (2001), 7074.
29 Indus-1 Activity Report, Centre for Advanced Technology, Indore, (2005).
30 R. V. Nandedkar, K. J. S. Sawhney, G. S. Lodha, A. Verma, V. K. Raghuvanshi, A. K. Sinha, M. H. Modi and M. Nayak, Current Science, 82, (2002),153 .

Chapter 3

Case Studies carried out using developed reflectometer

3.1 Introduction

As explained in the last chapter, x-ray reflectivity (XRR) is one of the standard techniques for the analysis of surfaces and interfaces. In order to calibrate the reflectometer various case studies were performed (using XRR as prime technique) and are covered in the present chapter. Examples includes studies done on bi-layers, tri-layers, multilayers , alloy thin films , gold coated foil mirror for x-ray space telescope

As discussed earlier Fresnel reflectivity from a sharp interface can be expressed as $R_F(q)$

$$R_F(q) = |r_{12}|^2 = \left| \frac{q_1 - q_2}{q_1 + q_2} \right|^2$$

In kinematical approximation away from critical angle, ratio of measured reflectivity R(q) to Fresnel reflectivity $R_F(q)$ from ideal sharp interface is related by[1]

$$R(q) / R_F(q) = \left| \int_{-\infty}^{\infty} \frac{d\rho(z)}{dz} \exp(iqz) dz \right|^2$$

Where ρ(z) is the electron density profile. Thus, provided that deviations from a kinematical approximation are negligible, x-ray reflectivity is a classical phase problem in one dimension. This arises from the fact that only the intensity and not the phase of the reflectance are measured. The analysis of reflectivity measurements is not simple and a plethora of analysis methods has been developed. These techniques include phase less inverse scattering methods[2,3,4] , Fourier analysis related methods[5 6,7] , moments analysis method[8], groove tracking method[9,10], wavelet analysis methods[11],[12] method based on distorted Born approximation[13], maximum entropy method[14,15] , methods using parametric B–splines [16,17] and the technique mixing different methods[18] . The above mentioned methods are fast and are able to produce electron density/scattering length density profile without any starting model assumption but sometimes they lead to unphysical models. All these methods are less accurate than the analysis based on Parratt's formalism [19] with roughness approximations[20] . In this approach, a theoretical curve is fitted to the measurement using techniques such as simulated annealing[21,22], the simplex

method[23] or least square refinement. For analysis of our data we have used analysis based on Parratt's formalism with roughness approximation by Nevot Croce factor[24] and least-squares refinement. Simulation of suitable model starts with a box-like scattering-length-density profile models and that requires a suitable initial model. It is important to note that if the initial model is not close to real, refinement techniques may converge to a wrong solution. In addition, it is also very difficult to find out a unique solution by fitting the reflectivity data. Examples given below explain the problems associated with fitting of x-ray reflectivity data.

3.1.1 How to arrive at a reasonable solution from x-ray reflectivity data fitting

Below is the example of the fitting of x-ray reflectivity data obtained from a NbC thin film of nominal thickness 20 nm deposited on Si(100) substrate with a surface roughness 0.4 nm. Figure (3.1) shows the reflectivity data (Open Square) measured upto $q_z = 0.15$ Å^{-1} with the simulation using a fitting model. Details of the model used for simulation are given in the table.

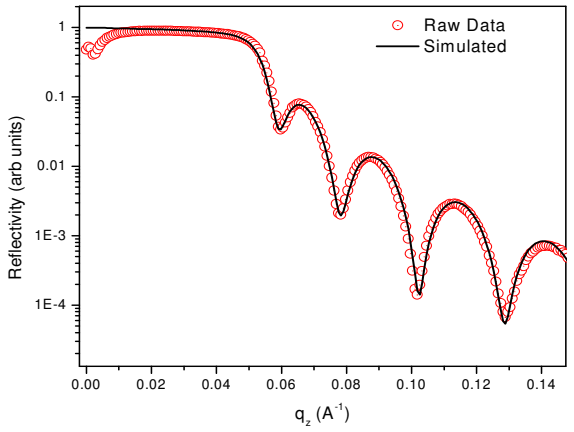

Fig 3.1 Reflectivity data (open square) measured upto 0.15 Å^{-1} q_z along with the simulation for a

Layer	Density (g/cc)	Thickness (nm)	Roughness (nm)
NbC	6.8 ±0.21	21.5± 0.15	0.9±0.1

The quality of fit looks good as simulated line is following all the data points. Error estimation of the thickness and density was done by changing the simulation parameter such that the graph shifted by more than double of the minimum step used for the measurement of the data and error in roughness was estimated by observing the change in chi^2 value of the fit. In present case accuracy of thickness estimation is 1.4 %, density estimation is 6.2% and roughness is estimated

with 22% accuracy. As explained by Holy et.al.[25] in their book the uncertainty in density of films can be estimated by dividing the minimum step size used for measurements with the critical angle θ_c. From this method it appears that for high density films it would be possible to measure density with higher accuracy, but due to higher absorption in high density films it becomes difficult to define θ_c accurately. In practice we cannot get density values with accuracy better than 4-5 %. Similarly available intensity of the source puts a limit on highest measurable q_z, due to which it is not possible to records features with length scales less than 0.5-0.8 nm and estimate thickness with accuracy better than 1%. From the present fitting we cannot say if there is any other layer present in the structure. To get more details about the structure one should measure data for larger q_z values.

We further acquired data for larger q_z values of the same sample. Figure (3.2) shows the fitting of reflectivity data measured upto q_z =0.25 $Å^{-1}$ q_z along with the two fitting models. In this figure two models have been used for simulation. First model is the same single layer model used in previous data fitting and extended to 0.25 $Å^{-1}$ q_z shown as blue line in the figure. Second model is a two layer model used for simulation shown as red line in figure (3.2). As can be seen in the figure (3.2) that simulated data using single layer model is not analogous with the measured data at high q values. In the attempt to match the oscillations observed at high q_z values, thickness of NbC layer was reduced to 20.9 nm but this spoiled the quality of fit at low q_z also.

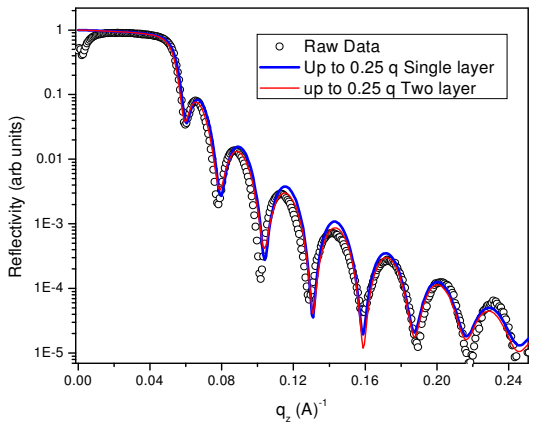

Fig 3.2 Reflectivity data (open square) measured upto 0.25 $Å^{-1}$ q_z along with simulated line with single layer (blue line) and two layer model (red line)

Single layer model			
Layer	Density (g/cc)	Thickness (nm)	Roughness (nm)
NbC	6.8 ±0.21	20.9 ±0.13	0.88 ±0.08

Two layer model			
Layer	Density (g/cc)	Thickness (nm)	Roughness (nm)
NbC	6.8 ±0.2	20.85 ±0.13	0.90 ±0.07
SiO_2	2.0 ±0.25	2.9 ±0.8	0.34 ±0.10

To improve the fitting we attempted a different two layer model. This model contains an NbC

layer and low density layer of SiO_2 on top of Si substrate which appears physically correct. The parameters used for simulation of both models are given in the adjacent tables. It is clear from figure (3.2) that none of the model is able to represent data completely and disagreement increases at high q_z values in both cases. Two layer model seems to fit the data slightly better than single layer model. Looking at the fitted values of the single layer and double layer model one can see that uncertainty in estimated thickness and roughness have reduced slightly due to availability of large q_z range for fitting. Also, in case of two layer model inserting a 2.9 nm low density SiO_2 layer seems to improve the fit quality but error in estimation of both thickness and roughness of SiO_2 layer used for fitting is very high compared to NbC layer. Form this fitting nothing more can be said other than that there may be one more layer in the structure. Largest q_z range measured puts a limit on the lowest spatial resolution which can be observed by reflectivity data. In this case this number comes out to be ~ 2.5 nm calculated using $2\pi/q_{max}$. This answers why parameters of the second layer could not be estimated with better accuracy as the lowest thickness which can be resolved with this q_z range is comparable with the thickness of SiO_2 layer. Our data is able to sense the presence of one more layer but it is not possible to accurately determine its thickness roughness etc. Extending the q_z range in measurement from 0.15 $Å^{-1}$ to 0.25 $Å^{-1}$ has given a confirmation that single layer model is not the correct model for fitting the reflectivity data and one more layer is required to improve the fit with data.

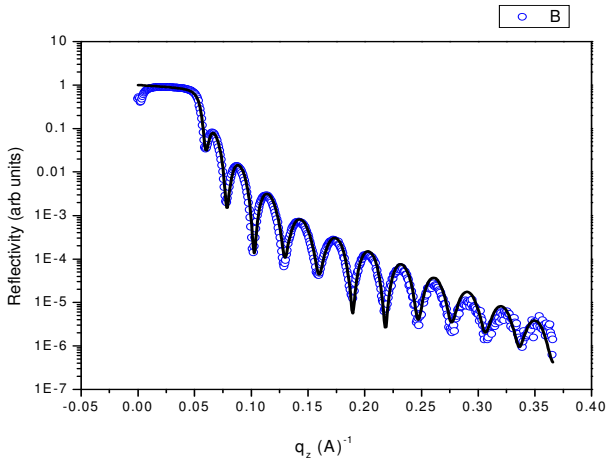

Fig 3.3 Reflectivity data (open square) measured upto 0.36 $Å^{-1}$ q_z along with the thre layer model simulation NbC film.

Three layer model			
Layer	Density (g/cc)	Thickness (nm)	Roughness (nm)
Low Density Layer	1.9 ±0.25	2.6 ±0.2	0.8 ±0.15
NbC	6.8 ±0.2	20.89 ±0.1	0.65 ±0.05
SiO_2	2.0 ±0.25	2.9 ±0.5	0.34 ±0.10

The experiment was thus further extended to reach the highest q range achievable. We could go up to 0.36 $Å^{-1}$ for the same sample with reasonable intensity. Figure (3.3) shows the reflectivity data (Open Square) measured upto q_z =0.36 $Å^{-1}$ q_z along with the simulation using a two layer fitting model. The parameters used for simulation of the fit are given in the table adjacent to the figure. The most interesting thing which has been revealed in fitting of this data is that the low density layer whose presence in the structure was suspected in the previous simulation for data up to q_z =0.25 $Å^{-1}$ q_z was confirmed in the present simulation. Additionally, placing a 2.6 nm low density layer at the top of the NbC film makes the simulated data fit with the measured reflectivity data fully. Indicating that the three layer model used for fitting is close to the actual structure of the film. Additionally error in the estimation of thickness and roughness of NbC layer has reduced to 1 % and 15% respectively which is better than achieved with single layer fit of data measured up to a q_z =0.15 $Å^{-1}$ (1.6 % for thickness and 22 % for roughness). Fitting of this data reveals that there is a density gradient at the top of the film. Density of the layer observed at the top matches closely with that of C layer which is possible. These details were not discernible when data was being simulated for the first case of q_z =0.15 $Å^{-1}$.

From above discussion we can conclude that one should try to get as high as q_z possible. This helps in resolving the density variation in the structure more precisely. While modeling the data, we should keep in mind the limit posed on the smallest layer thickness distinguishable by the maximum q_z measured. Inserting a layer with thickness lower than the distinguishable by the measurement would not lead to a physically correct model. The accuracy with which one can determine thickness and roughness of the films also depends on instrument resolution function which includes monochromaticity of the x-ray used and the divergence of the beam and minimum step size used for the measurement. Presence of larger q range further improves this limit. In the example discussed above, thickness accuracy in first case was ± 0.15 nm and it was reduced to ±0.1nm in last case. Insertion of more layers should be done only when fitting is not possible with single layer, one should always try to fit the data with minimum number of layers.

Because of phase problem of reflectivity there could be more than one models to describe the structure. Using the methods discussed we have tried to ensure the reliability of the model used for fitting. A good practical guess about the number of layers and their expected thickness from the available information helps in converging to the final values faster. Leaving the program to freely move and converge may end in unphysical results. As density and roughens of

layers have inter dependence, one should be careful in varying those parameters for a good fit. In case of multilayer fitting, similar approach can be used. Making a series of samples in case of multilayer helps in deciding the model to be used for fitting the reflectivity data. To improve the correctness of the model used for simulation either of the following methods were used: (1) Number of samples are prepared with the same preparation conditions and a single model was used for fitting the reflectivity data for all samples (2) Series of samples with different thicknesses were deposited and fitted with a similar basic model for the whole series, considering different thicknesses of the films. The example discussed below will explain this argument in more detail.

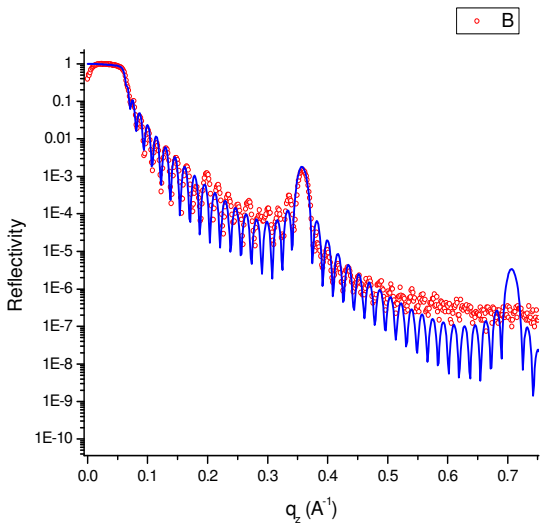

Fig3.4 Fitting of W Si Ml with Model1 details of the model are given in the adjacent table

Model 1			
layer	Thickness (nm)	Density (g/cc)	Roughness (nm)
Si	1.06 ±0.02	5.0 ±0.15	0.7 ±0.05
W	0.72 ±0.01	16.4 ±0.4	0.38 ±0.03

In this example it is demonstrated how to fit reflectivity data obtained from a multilayer and confirm which model is physically correct. The sample used for this study was prepared with expected nominal thickness of 1.2 nm for Si and 1 nm for W Layer. These numbers were estimated from the single layers of different thickness deposited for both W and Si. This sample was one of the series of samples prepared by changing the multilayer period. Fig. (3.4) and (3.5) show fitting of W/Si multilayer using two different models. Both simulations appear reasonably good up to first Bragg peak. Fitting is not so good beyond the first Bragg peak due to limitation

of dynamic range in our data. The difference between these two models is thickness of the W and Si layer. In model 1, we have kept thickness of the Si layer close to nominal thickness and reduced the thickness of W layer. To match the critical angle of multilayer, it was required to increase the density of Si layer (from 2.2 to 5.0 g/cc) as can be seen in the table. The starting roughness of both Si and W was kept equal to the values obtained from samples of higher thickness and was varied further to improve the fit. Fitting with model 1 looks better till q_z = 0.6 $Å^{-1}$ but at higher q_z it become clear that this model is not correct since second Bragg peak

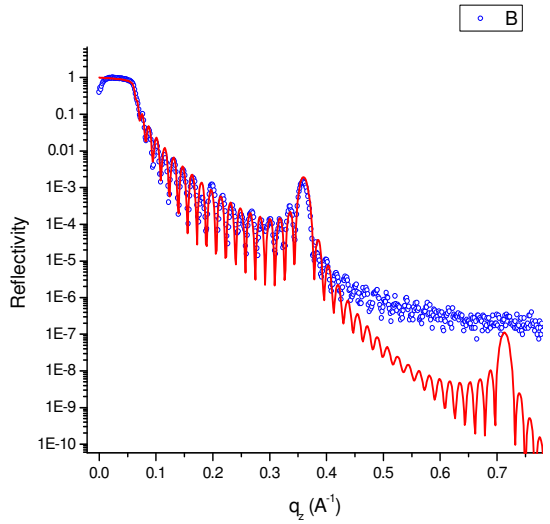

Fig3.5 Fitting of W Si Ml with Model 2 details of the model are given in the adjacent table

Model 2			
layer	Thickness (nm)	Density (g/cc)	Roughness (nm)
Si	0.65 ±0.01	3.0 ±0.15	0.7 ±0.05
W	1.12 ±0.02	16.75 ±0.5	0.43 ±0.03

observed in simulation is not visible in our data. In model 2, we simulated data by swapping the thickness of W and Si layer. In this case density of W layer was kept the same as before and density of Si layer was also reduced to 3.0 g/cc. This model appeared consistent with previous samples in which loss of Si layer during deposition was observed. In this model the density of Si layer was higher than the bulk and for W it was lower than the bulk. High roughness values of Si layer (0.7 nm) comparable to its thickness (0.65 nm) indicate that layer must be discontinuous. To confirm the density values, we simulated the data again keeping the bulk density values for both layers and modified the thickness and roughness values to match the simulation with measured data. As can be seen in fig. (3.6) the fit appears tolerable but still it is not matching

well with kiessig oscillations around $q_z = 0.25$ Å^{-1}. Also the roughness (1nm) of Si layer is higher than its thickness (0.65). This model than appeares unphysical. We further carried out cross-sectional TEM of the sample and found out that thickness of both W and Si layer appeared close to each other and the density contrast between W and Si layer has reduced compared to samples made with larger period thickness. This observation confirms that model 3 is not correct as in this model thickness of W layer (1.12 nm) is approximately double to Si layer (0.65 nm). Simulation was carried out again in which thickness of both W and Si layer was kept close to each other. To match the critical angle density of W layer was reduced little bit and of Si layer was increased as last step. Finally model 4 was arrived, as shown in fig. (3.7). This fitting is best among the considered models and is consistent with the series of samples made prior to this sample. This model also substantiates the observation of intermixing from cross-sectional TEM image. This example confirms that by making a series of samples it is possible to understand changes happening at the interface by x-ray reflectivity analysis. If in case we had only this one sample with us, it would not have been possible to decide which of the four models is correct for our sample. In the methodology used above a model was arrived at using XRR data analysis, which correctly depicts the structure of the multilayer analyzed. This will be demonstrated further in the case studies discussed ahead.

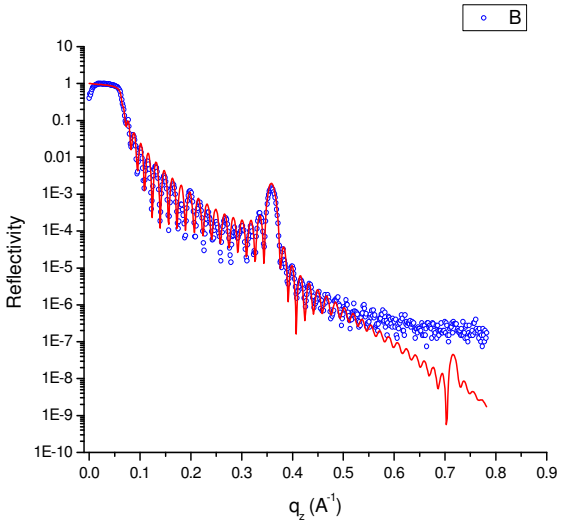

Fig3.6 Fitting of W Si Ml with Model 3 details of the model are given in the adjacent table

Model 3			
layer	Thickness (nm)	Density (g/cc)	Roughness (nm)
Si	0.65 ±0.01	2.2 ±0.1	1.0 ±0.05
W	1.12 ±0.02	17.0 ±0.4	0.47 ±0.03

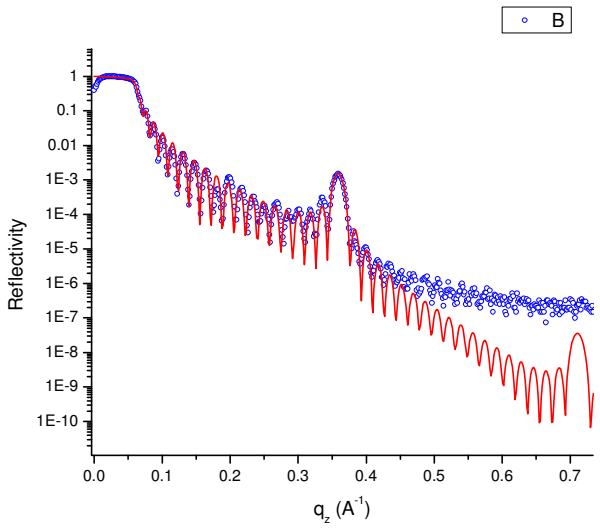

Fig3.7 Fitting of W Si Ml with Model 4 details of the model are given in the adjacent table

Model 4			
layer	Thickness (nm)	Density (g/cc)	Roughness (nm)
Si	0.81 ±0.01	4.6 ±0.2	0.8 ±0.04
W	0.96 ±0.01	16.7 ±0.4	0.45 ±0.02

3.2 Reflectivity study of pulsed laser deposited NiMnSb (alloy) thin films on Si (100) substrate

The half-Heusler compound NiMnSb is considered to be a half-metallic ferromagnet[26] and a potential candidate as a spin-injector in spintronics devices[27]. For this reason this system has been a subject of current interest and thin-films of NiMnSb have been successfully deposited on various semiconductor substrates[28,29]. Studies of electrical resistivity, magnetoresistance and Hall effect on off-stoichiometric NiMnSb films grown on Si substrate have revealed various interesting features[30,31]. A low temperature upturn is observed in the temperature dependence of resistivity for film thickness 130 nm and below along with large positive magnetoresistance. As the film thickness decreases, the magnitude of both the resistivity upturn and the magnetoresistance increase. The low temperature resistivity upturn in the 5 nm sample is more dramatic than in the thicker samples, and the question arises whether another mechanism is

operating in the thinnest sample[30]. In fact the nonlinearity in the *I-V* curve of the 5 nm film below the upturn is indicative of percolative behavior in that film. Hall effect measurements indicate that the room temperature electrical transport in these thin films becomes increasingly electron dominated with decreasing thickness, in marked contrast to the spin-polarized holes predicted for the bulk [29].

All these interesting features in transport properties raise the important question whether the nature of the films changes with the decrease in the film thickness and points towards the increasing significance of surface and interface of these films i.e. free surface electronic states. This motivates for a thorough investigation of the surface and interface characteristics of these films. A detailed investigation of surface and interface properties of these off-stoichiometric NiMnSb thin films grown on Si(100) substrate was done using grazing incidence x-ray reflectometry (XRR). We also used grazing incidence x-ray fluorescence (GIXRF) spectrometry to find out the depth dependent composition of the film along thickness direction. Also magnetization measurements of some samples have been done to see the effect of thickness on magnetic behavior. It has indeed been observed that the character of these films changes markedly below 35 nm thickness.

Four thin film samples of NiMnSb with nominal thickness 6, 34, 70 and 100 nm (estimated based on the number of laser pulses), were grown on Si(100) substrates with pulsed laser deposition (PLD) at 200 ^{0}C from a slightly manganese- poor $NiMn_{0.95\pm0.01}Sb$ target. These samples will be referred to as A, B, C and D in the discussion of the experimental results below. The details of sample preparations are given elsewhere[28]. The films were found to be polycrystalline and no significant change in texture was observed with thickness. To explore the change happening in the structure of thin films with thickness reduction XRR measurements were carried out on all samples. Before the measurements were carried out various standard alignment procedure were done to align both theta and two theta axes within 0.005°. All the measurements were performed with a step size of 0.005° in theta axes which is sufficient to observe any small changes in thin films. Some complementary magnetization measurements have also been performed using a commercial SQUID magnetometer (Quantum Design-MPMS5).

X-ray reflectivity Measurements

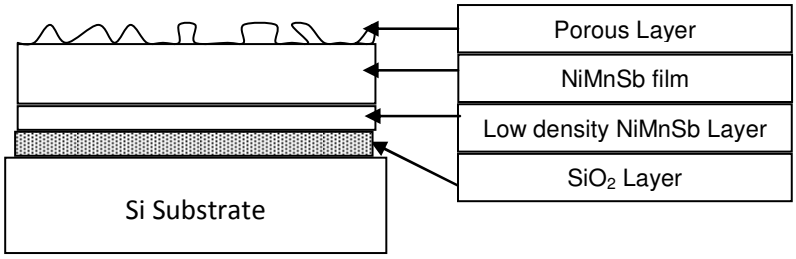

Fig 3.8. The model used for fitting the reflectivity data

The blank Si substrate roughness of 0.3 nm was independently estimated using XRR measurement. The XRR data are analyzed using the Parratt formalism[8] to derive the electron density profile (EDP) across the depth of the film, thickness and interfacial roughness. In the fitting procedure, one starts with a model structure consisting of layers with different thicknesses, roughness and densities. In this case if one starts with a simple single layer model on Si substrate, the fit quality is not good.

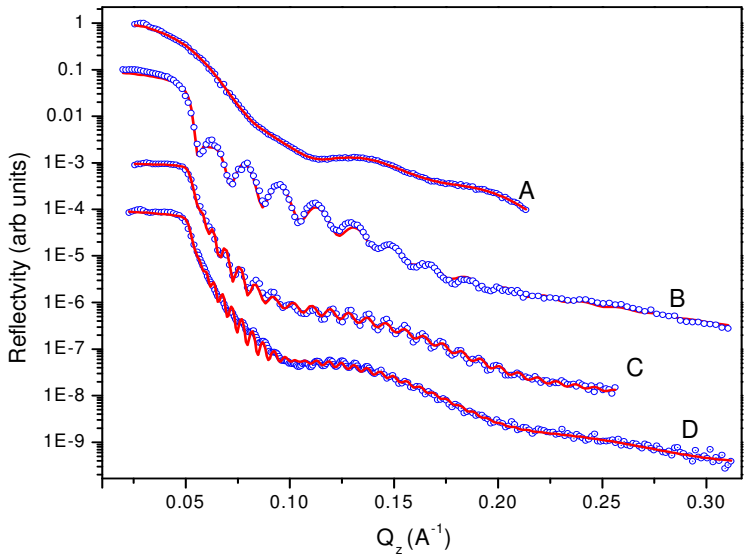

Fig. 3.9: X-ray reflectivity profile data (circular points) of samples A, B, C and D along with best fit line. The curves are vertically shifted for clarity vertically shifted for clarity.

To improve the quality of fit more layers were introduced in a systematic manner. The guide line of inserting new layers was the same as discussed in the beginning of this chapter. Finally, best fit model was derived which yielded excellent fit with the measured reflectivity data. Figure (3.8) shows the best fit model extracted by fitting the reflectivity data. In this model, there are four layers comprising of (1) native oxide layer on the silicon substrate, (2) low density NiMnSb layer, (3) NiMnSb layer with density near the bulk density and at the top, (4) a low density porous layer. The fit parameters, i.e. thickness, roughness and density of each layer, are allowed to vary in a controlled manner. The best fit gives the thickness, roughness and density of each layer and roughness convoluted electron density profile (EDP) of the structure can be calculated using this information.

A non- linear least square-fitting algorithm was used to refine the thickness, roughness and density values by the χ^2-minimization technique. The best fits obtained are plotted in Fig.(3.9)

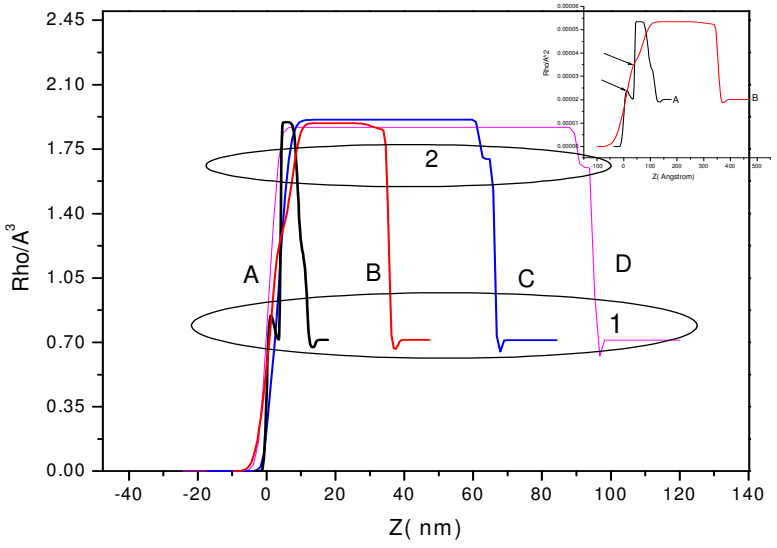

Fig. 3.10 Scattering length density profile of structure as a function of thickness for samples A, B, C, and D. Inset: SLDP of samples A and B is shown magnified for clarity.

for each sample. Figure (3.10) shows roughness convoluted electron density profile (EDP) of the structure as a function of thickness for samples A to D obtained by fitting the measured reflectivity profile. Thickness of SiO_2 (native oxide) layer for all samples is 2-3 nm, which

shows up as a dip in EDP, marked as region 1 in Fig. (3.10). This layer is usually present due to oxidation of the top surface. Thickness of second layer i.e low-density NiMnSb layer is 3-5 nm for all samples, and density of this layer is 15-22 % less than the bulk density, marked as region 2 in fig (3.10). This low-density layer might have formed due to poor ordering of the film leading to a less dense structure during initial growth process. This observation is in agreement with the observation of Schlomka et.al.[32]. Above this low density layer there is NiMnSb film with density close to bulk density. Estimated thicknesses of NiMnSb film on samples A, B, C and D are 7.6, 33.2, 67.5 and 96 nm respectively. Note that these thickness values are not the same as those based on the number of pulses (nominal thickness values). The roughness values are within 1.2 to 1.8 nm. For samples A and B, a reliable fit could not be obtained unless a porous layer (very low density layer) is incorporated in the model. This layer was not needed for sample C and D. The EDP for sample A and B show (inset in figure 3.10) a fluctuating behavior at vacuum film interface side. In sample A, the thickness of porous layer is 3 nm with roughness 0.8 nm. In case of sample B roughness of the porous layer increases to 2.1 nm which shows itself as a slow density gradient in EDP profile. The porosity of this layer for sample A is estimated to be 56 % and porosity seems to decrease in sample B to 43 %. This porosity disappears in sample C and D. This means that morphology of the film is changing with

Sample Name	Layer Name	Thickness(nm)	Roughness (nm)	Density
Sample A	SiO_2 Layer	3.8 ± 0.3	0.7 ± 0.1	Bulk (2.2 g/cc)
	Low density NiMnSb Layer	2.5 ± 0.22	1.0 ± 0.1	22 % less than Bulk
	NiMnSb Layer	4.9± 0.22	1.2 ± 0.1	Bulk
	Porous Layer	2.9 ± 0.25	0.8 ± 0.1	56 % less than bulk
Sample B	SiO_2 Layer	3.0 ± 0.2	0.5 ± 0.08	Bulk (2.2 g/cc)
	Low density NiMnSb Layer	4.5 ± 0.2	1.9± 0.1	15 % less than Bulk
	NiMnSb Layer	28.7± 0.14	1.6 ± 0.1	Bulk
	Porous Layer	3.0 ± 0.2	2.1 ± 0.15	43 % less than bulk
Sample C	SiO_2 Layer	2.2 ± 0.2	0.4 ± 0.08	Bulk (2.2 g/cc)
	Low density NiMnSb Layer	4.4 ± 0.22	0.5± 0.05	15 % less than Bulk

	NiMnSb Layer	63± 0.3	1.0 ± 0.1	Bulk
	Porous Layer			Not Detected
Sample D	SiO_2 Layer	2.1 ± 0.2	0.4 ± 0.08	Bulk (2.2 g/cc)
	Low density NiMnSb Layer	5.0 ± 0.22	0.8± 0.08	15 % less than Bulk
	NiMnSb Layer	90± 0.35	1.3 ± 0.1	Bulk
	Porous Layer			Not Detected

Table 3.1 : Details of thickness, roughness, and density of various layers of all NiMnSb/Si(100) films (samples A–D). Densities of low-density NiMnSb and porous layers are gives as percent change of NiMnSb layer.

thickness. Fitted thickness roughness and density values of various layer are given in the table above. The error in estimation of density of each layer was not more than 15% of the reported value and errors in thickness and roughness estimation are given in table (3.1). To confirm that the change in density observed is not due to segregation of alloying elements. We carried out grazing incidence angle dependent X-ray fluorescence (GIXRF) variation of Sb-Lα and Mn-Kα fluorescence intensities in the samples as a function of incident angle. The ratio of fluorescence of Sb-Lα and Mn-Kα was found to constant through thickness confirming that no segregation of elements is happening in thickness direction. So the change in density is happening due to porosity getting generated on thickness reduction.

To check whether this difference in morphology / density profile caused any influence on the physical properties of these thin films, resistivity and magnetization measurements have been performed on the thickest sample D and thinnest sample A. As in the earlier study[29] the resistivity measurements show a distinct difference between these two samples. The thinnest sample A shows a negative coefficient of resistance in the temperature regime down to 30 K, clearly indicating non metallic character of the sample. While indication exists for non-metallic behavior in the sample D also in the low T regime, at higher T (> 200K) it definitely shows metallic behavior. Magnetization measurements on sample-D show saturation behavior in M-H curve at 5K this indicates that sample D is ferromagnetic in nature. In contrast the M-H curve at 5K for sample A is almost linear this clearly indicates that this sample is not ferromagnetic in

nature. These results strongly suggest that the morphology indeed influences the behavior of these films.

In this study the structure of NiMnSb thin films was examined with XRR studies and it was explored how it is changing with thickness. It is concluded that formation of a very low-density layer at the top in 7.6 and 33.2 nm thick films is happening. GIXRF measurements indicate absence of any segregation of alloying elements. Hence this layer must be a highly porous layer, which is appearing as a very low-density layer in reflectivity data. The porosity of this layer decreased with the increase in the film thickness, and in thicker 67.5 and 97 nm films, no porous layer is observed. The present study clearly demonstrates that morphology of ultra thin films of NiMnSb is markedly different from the films with thickness greater than 60 nm as seen by scattering length density variation at vacuum film interface. The distinctly different magnetic and transport properties observed for thickest (D) and thinnest (A) samples show that this morphological disorder influences the physical properties of these films. The XRF studies rule out any compositional anomaly and the influence of surface/interface roughness as the source of the interesting magnetic and transport properties.

3.3 Oxidation studies of Niobium thin films at room temperature by x-ray reflectivity

In this case study we have carried out analysis of growth kinetics of oxidation process on Niobium thin film surfaces exposed to air at room temperature in a non destructive manner using x-ray reflectivity.

Nb thin film coated on copper (Cu) radio frequency (RF) cavities (Nb/Cu) can be an effective alternative to superconducting (SC) particle accelerator cavities based on bulk Nb technology[33]. Surface roughness of the film greatly influences its usefulness. Also formation of a few nanometer of an insulating oxide-Nb_2O_5 on the surface of the thin film is expected to be affecting the surface conductivity of the cavity directly. Knowledge of thin films structure along with oxide layer thickness and roughness is required to design the cavity properly. This understanding can help in evolving and optimizing a process to grow a protective layer on Nb/Cu cavities.

For this study, Nb thin films of nominal thicknesses 10nm (Sample A), 20nm (Sample B), 30nm (Sample C), 75 nm (Sample D) and 120 nm (Sample E) were prepared on Si (100) substrates kept at room temperature by Ion beam sputtering. Silicon dioxide layer present on the Si-substrate was not removed and its thickness and rms-roughness was measured with XRR method. The flow rate of Ar gas was kept at 3.5 standard cubic centimeters per minute while total pressure in the chamber was maintained at ~ 5 x 10^{-4} Torr during deposition. The deposition rate was kept ~ 6 Å/min for all samples. The XRR and grazing incidence X-ray diffraction (GIXRD) measurements were carried out on a reflectometer developed in-house. GIXRD of these samples showed single phase polycrystalline Nb film. In this report result of time dependent studies of oxidation performed on thin film Nb samples A and B are reported. Assessment of oxide layer growth was done by XRR measurements while these samples were exposed to air at room temperature for prolonged periods of time.

Results of XRR measurements as a function of wave vector transfer $q_z=4\pi \sin(\theta)/\lambda$ performed on sample A at time intervals of t_1 (7.2 x 10^3 sec), t_2 (2.59 x 10^5 sec), t_3 (5.95 x 10^7 sec), and t_4 (9.02 x 10^7 sec) are shown in fig (3.11). The moment at which the films were exposed to air was considered as starting time i.e. t = 0 sec. The 't_i' (i=1, 2, 3, 4) is time for which the sample was exposed to atmospheric ambient at room temperature (T) before XRR measurements were performed. In the fitting procedure, χ^2-minimization technique along with non-linear least square fitting was used to refine the thickness, roughness and density values. During the refinement, it became clear that if we start fitting the data with single layer of Nb on Si substrate, it is not possible to fit the experimental data. Thus to improve fitting quality systematic addition of more layers was done. The best-fit model extracted by fitting the reflectivity data suggests that all films have three layer structures (see inset of fig 3.11). These layers are defined as top oxide layer corresponding to NbOx (usually present due to oxidation of top surface of the film), middle layer corresponding to Nb and bottom layer which is SiO_2 i.e. native oxide layer on Si substrate. It should be noted that fitting of reflectivity data was not possible if we remove any of the layer from the model. The obtained parameters using the recursive formalism are tabulated in table (3.2). Continues lines show a fit to reflected data plotted with different symbols. The extracted values of thicknesses of Nb (d_{Nb}), Nb_2O_5 (d_{Nb2O5}), and its roughness (σ_{Nb2O5}) are given in table (3.2). Similar measurements were performed on

sample B at t_1 (7.2 x 10^3 sec), t_2 (2.59 x 10^5 sec), t_3 (3.89 x 10^7 sec), and t_4 (6.22 x 10^7 sec). The corresponding extracted values of X_{Nb}, X_{Nb2O5}, and σ_{Nb2O5} are given in table (3.2).

Above measurements show that an oxide layer of ~2 nm gets formed immediately after deposition which grows at a slow rate even at room temperature. The thickness variation of Nb_2O_5 with time for samples A and B shows that oxide thicknesses reach a saturation value of ~4.2 nm after 1045 to 720 days. Slight reduction in top surface roughness is seen with oxidation time. Detailed analysis of oxide layer thickness variation with time showed that the oxidation process follows a modified Cabrera-Mott model of thin films. In conclusion we have demonstrated that non destructive surface sensitive XRR technique is very effective to study the

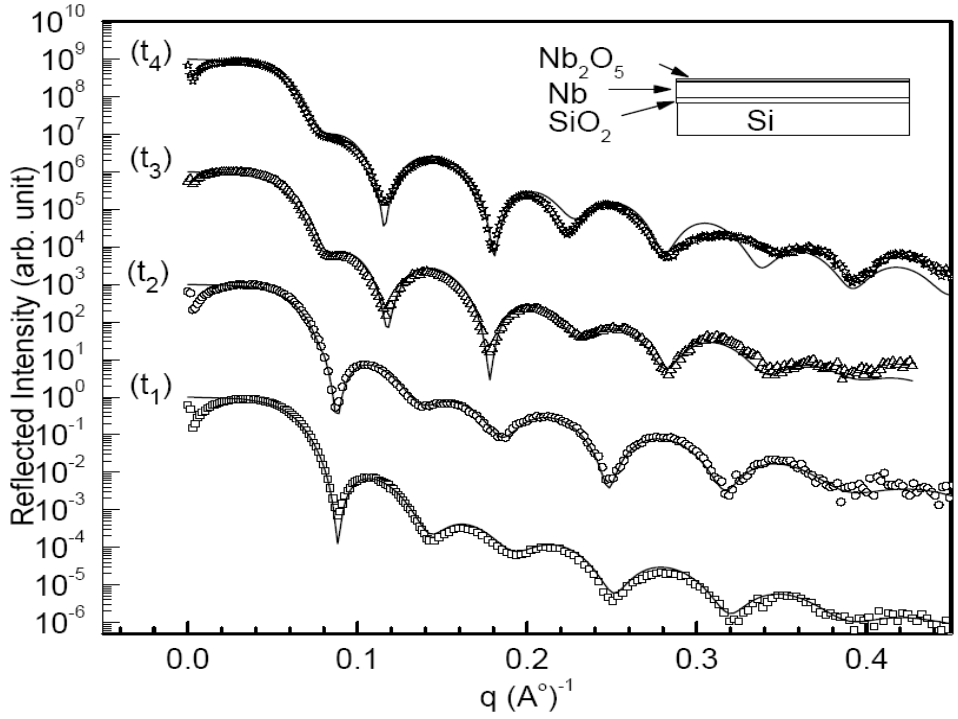

Fig 3.11 The plot of XRR measurements as a function of momentum transfer vector $q=4\pi \sin(\theta)/\lambda$ for sample A done at time intervals of t_1 (7.2 x 10^3 sec), t_2 (2.59 x 10^5 sec), t_3 (5.95 x 10^7 sec), and t_4 (9.02 x 10^7 sec). Continues lines show a fit to reflected data. The y-axis for t_2, t_3, and t_4 plots is shifted

	t (Sec.)	X_{Nb2O5} (nm)	σ_{Nb2O5} (nm)	X_{Nb} (nm)
Sample A (10nm)	7.20E3	1.8± 0.2	0.7± 0.1	8.1± 0.1
	2.59E5	2.2± 0.15	0.5± 0.1	7.9± 0.1
	5.95E7	4.0± 0.15	0.5± 0.1	7.17± 0.1
	9.02E7	4.2± 0.15	0.45± 0.1	6.95± 0.1
Sample B (23nm)	7.20E3	2.2± 0.15	0.5± 0.1	21.5± 0.12
	2.59E5	2.7± 0.1	0.5± 0.1	21.1± 0.12
	3.89E7	4.1± 0.1	0.5± 0.1	20.5± 0.12
	6.22E7	4.3± 0.1	0.45± 0.1	20.4± 0.12

Table 3.2 Fitting parameters where; 't' is time, after which the XRR measurements were performed; X_{Nb2O5} is thickness of top oxide layer; σ_{Nb2O5} is roughness of the top oxide layer; X_{Nb} is thickness of

growth kinetics of oxidation process on Nb thin film surfaces exposed to the field conditions of room temperature and air at atmospheric pressure. Further we conclude on the basis of our studies that a protective layer should be grown in-situ to avoid oxidation of Nb thin film surface of Nb/Cu cavities

3.4 Characterization of Co/ Si biayers and multilayers

Over the last few years, metal–metal multilayers (MLs) have been extensively studied due to their potential application in electronics. Co/Si is one such system that shows interesting magnetic behaviour. This system is reported to show superparamagnetic behaviour [34] for low thickness of the Co layer (~2.2nm), whereas for Co layer thickness of the order of 100 nm, it shows an oscillatory magnetic behaviour between different Co layers as a function of Si layer thickness[35,36,37]. This type of coupling is well established and understood in the case of metal/metal multilayers [38]. However, the picture is not clear for an insulating or semiconducting spacer layer.

In this context, the Fe/Si system, which shows similar behaviour, has been well studied[39]. Reports have suggested that the formation of an iron silicide layer at the interface might be responsible for such oscillatory behaviour in the Fe/Si system[40,41]. Our group has also carried out

investigations on Fe/Si interface and found out the changes happening at the interface. In that study on Fe/ Si trilayer and multilayers we carried out interface studies using x-ray reflectivity, cross-sectional TEM and depth resolved x-ray photo electron spectroscopy. It was found that Fe and Si interdiffuse into each other at both (Fe/Si and Si/Fe) interfaces of Fe/Si thin films. Interdiffusion of Fe and Si is clearly visible in results of cross sectional TEM measurements. Interdiffusion of Fe and Si into each other leads to formation of silicide interlayers at interfaces. Interlayers Si_Fe (at Si/Fe intetrface) and Fe_Si (at Fe/Si interfaces) were observed in the XRR and confirmed in XPS measurement results. Interlayer formation is independent of the thicknesses of Fe and Si layers and deposition techniques. Thickness of Si_Fe and Fe_Si interlayers are found to be ~1.3nm and ~0.7nm respectively[42]. After the formation of these interlayers at room temperature, further interdiffusion stops at interfaces. Interdiffusion of Fe and Si are different at both interfaces and hence the interfaces are asymmetric in nature[43]. After the analysis of the electron diffraction pattern, it was found that FeSi phase is the main phase forming at the interface. In the similar way, there is a finite possibility that the origin of this type of interesting magnetic behaviour of the Co/Si system might also depend on a characteristic of the interface i.e. on the formation of a cobalt silicide layer at the interface. This is because Co and Si are also known to have negative heat of mixing, which encourages mutual solubility at the interface and the formation of intermetallic alloys of varying composition[44,45,46]. It has also been shown that both evaporated[47] and sputtered[48] Co/Si multilayers have amorphous interlayers. High resolution cross sectional electron microscopy results of Co and Si show that for a small thickness of Co (~3.0nm), the metal is converted to an amorphous silicide layer whereas thicker Co layers can retain an unalloyed part. For thin Co and Si layers *(*~5 nm*)*, elemental Co or Si may not be present, but instead intermetallic alloy gets formed with an average composition. Thus, all these studies suggest that Co and Si have a strong tendency of forming alloys at the interface. However, this system has not been studied extensively and information is still lacking which explains the interfacial characteristics and the structure of the Co/Si multilayer system. Hence, it is still not clear whether the Si layer thickness or the formation of silicide is playing the dominant role in governing the magnetic behavior of the system. For this reason, we carried out present investigation and prepared Co/Si MLs of varying thickness to study the interlayer coupling in the as-deposited samples. X-ray reflectivity (XRR), x-ray standing wave (XSW) measurements and x-ray diffraction (XRD) measurements on the as-deposited Co/Si MLs have

been performed. Some preliminary magnetic characterization of samples at room temperature has also been done by magneto-optical Kerr effect measurements (MOKE).

On Si (100) substrates 6 multilayers, designated as A, B, C, D, E & F, of Co and Si with 10 bilayers having varying thickness of Co (~ 4.5-8.0nm) and Si (~2.0-7.5nm) were deposited by Ion Beam Sputtering (IBS) deposition technique. Bilayers having same thickness of Co and Si were also deposited on both Si(100) as well as float glass substrate, designated as BL1 and BL2 respectively. The substrates were cleaned by chemical cleaning using nitric acid and ultrasonic cleaning using acetone. Before deposition the r.m.s roughness of the substrate was measured by XRR measurement. Total pressure in the chamber during the deposition was maintained at ~10^{-4} Torr. To calibrate the thickness of Co and Si layers, a number of samples were deposited. Deposition rate was kept ~0.05nm/sec.

To get the information about the thickness of the individual layers, surface and interface roughness, interdiffusion and the formation of silicide layer, XRR measurements were performed in our laboratory. To check the formation of silicide layer and also to check

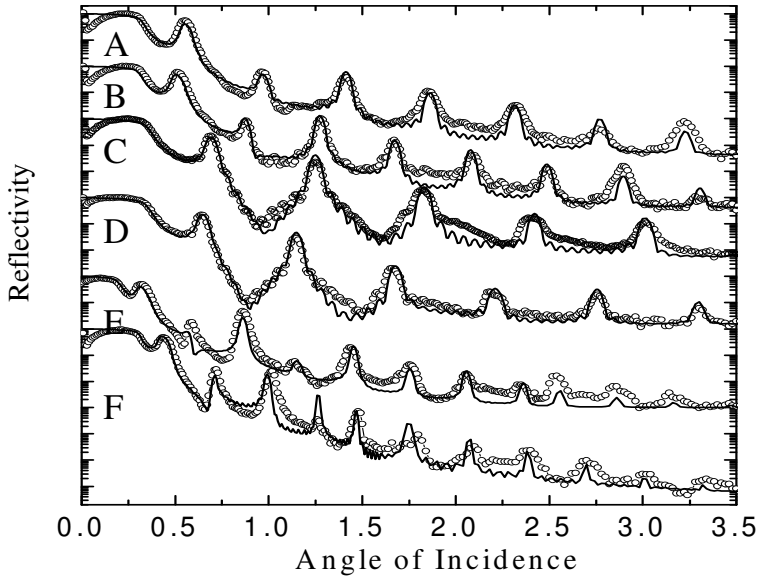

Fig 3.12. XRR pattern of the all Co/Si MLs. Circles are experimental data. For the sake of clarity the data have been shifted in y-axis; Continuous lines show fit to the data.

whether the Co and Si layer that is being deposited are in the crystalline or amorphous form, we

have performed wide-angle x-ray diffraction (XRD), using rotating anode x-ray generator from Rigaku equipped with Cu target operated at 50KV and 200mA.

Fig. (3.12) shows the x-ray reflectivity patterns for all the six as-deposited ML samples. Bragg peaks arising due to ML periodicity are distinctly visible upto 8th order. For the theoretical fit to the experimental data Parratt recursion formalism is used.

X-ray reflectivity technique was used to study the details of the nature of surfaces and interfaces involved. Fallon *et al.*[44] have fitted the x-ray reflectivity data considering the formation of silicide layer at the interface. The quality of fitting shown in the report is not so good, indicating that the model they have chosen might not be correct. Since our aim was to study the nature of interface in Co/Si ML system, we have done the detailed analysis of the XRR data. Allowing the variation of various parameters like, electron density, layer thickness and surface and interface roughness of the layers, the experimental data were fitted. We found that the fitting is quite good when no silicide layer formation at the interface is considered as shown

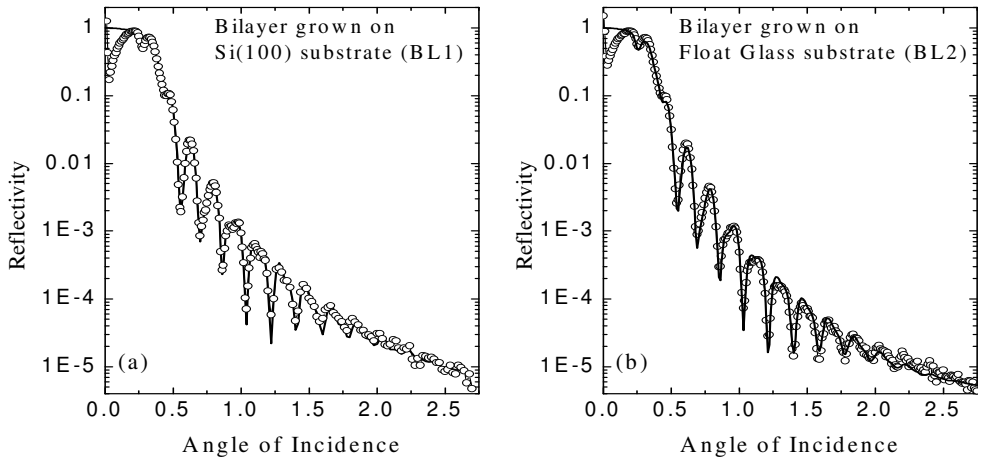

Fig *3.13. XRR pattern of the Co/Si bilayer samples (a) on Si(100) Substrate, BL1 (b) on float glass substrate, BL2 . Circles are experimental data. Continuous lines show fit to the data.*

in Fig. (3.12). The slight difference in the fitted and the experimental data, seen in Fig. (3.12) might be due to the thickness inhomogenity in various layers of Co and Si.

In multilayer structures since a large number of layers are involved, a slight error in parameters like thickness, roughness, electron density etc of the individual layers affects the reflectivity pattern. To avoid this, two bilayers of Co and Si of same thickness on both Si(100)

and float glass substrate were prepared. Here in these bilayer samples Co is deposited first on both the substrates.

We have done x-ray reflectivity measurements on both these bilayers. The pattern is shown in Fig.[3.13 (a) and (b)], for the bilayers deposited on Si(100) (BL1) and float glass (BL2) substrate respectively. It can be seen that there is no difference in the x-ray reflectivity pattern of both these bilayers grown on Si(100) and float glass substrates. We have fitted these patterns assuming no silicide layer at the interface. It can be seen that it gives an excellent fit with this model. The quality of fit confirms that our model is correct and hence no silicide layer is distinctly visible at the interface. The fitted values of the thickness and roughness of Co and Si for all the multilayers as well as the bilayer samples are given in Table (3.3) and the parameters are found to be physical.

However, Petford-Long *et al.* [49] and Ruterana *et al.*[50] have shown that both evaporated as well as sputtered Co/Si multilayers show amorphous interlayer. High-resolution electron micrographs have suggested that for small, nominal Co thicknesses (~3nm) the metal is converted to an amorphous silicide layer. Thicker Co layers can retain a part that is unalloyed. For relatively thin Co and Si layers (≤5nm) elemental Co and Si may not be present and instead, an alloy forms with an average composition. Moreover, Naik *et al* [43] have also demonstrated using XRR data, even the formation of ~1.2-1.5 nm thick silicide layer in Fe/Si system, could be detected. This suggests that in our Co/Si MLs also, silicide layer if present, its thickness or the volume fraction is very low that it could not be detected distinctly as a layer by XRR measurements. This may also mean that it might be present as a discontinuous layer, which in turn is giving a large roughness (as given in Table-3.3).

Samples	Co Layer		Si layer	
	Thickness (nm)	Roughness (nm)	Thickness (nm)	Roughness (nm)
A	4.8± 0.06	1.0± 0.1	4.85± 0.05	0.36± 0.1
B	5.1± 0.06	0.9± 0.1	5.6± 0.06	0.4± 0.05
C	5.35± 0.05	0.4± 0.08	2.0± 0.03	0.8± 0.1

D	5.95± 0.05	0.4 ± 0.07	2.2± 0.03	0.7± 0.1
E	7.38± 0.07	0.77± 0.1	7.05± 0.07	0.4± 0.1
F	8.0± 0.09	1.1± 0.1	6.0± 0.08	0.55± 0.04
BL1	23.1± 0.15	0.83± 0.1	21.9± 0.15	0.76± 0.1
BL2	22.8± 0.15	0.85± 0.1	22.1± 0.15	0.83± 0.1

Table 3.3. Parameters obtained from the reflectivity fitting of multilayers and bilayers

We also performed wide angle XRD of all the 6 samples. Fig (3.10) shows the XRD pattern of the as-deposited Co/Si MLs and the bare Si (100) substrate. A strong peak around $2\theta=33^{o}$ corresponds to the Si substrate. Other very small and fine peaks which are observed are due to the substrate. It can also be observed that XRD pattern of as-deposited Co/Si multilayers A, B, C and D shows a broad and well defined peak at around 44^{o}. This intense and broad peak corresponds to the (002) hcp planes of Co. The presence of this peak indicates that the cobalt in these MLs is crystalline in nature and is highly oriented in (002) direction. This result is consistent with reports by Fallon *et al.*[44,45,46]. However, it can also be noted from the figure that the intensity of this peak decreases for samples E & F, which have high thickness of Co as well as Si layers. It is almost seen as a flat background in the figure. However, if we magnify only the portion containing this peak for samples E & F (as shown in Fig. 3.14), we will find that instead of one peak there are three different peaks. These three peaks are identified as reflections from the hcp (100), (002) and (101) planes at d spacing close to those of hcp cobalt. This indicates that the films, which were otherwise strongly textured for low thickness of Co and Si layers lose their texture for higher thickness of Co and Si layers. Since in these two samples E and F, thickness of both Co and Si layer is rather high, it is difficult to say if Co or Si layer is forcing Co layer to lose its texture. To check this we performed x-ray diffraction measurements on pure Co films of various thickness grown on Si(100) substrate. The XRD patterns for Co films having different thickness showed that upto the thickness of 12nm Co layer remains textured. It is therefore clear that Co is losing its texture in the multilayer not due to increase in its thickness beyond a certain

limit. To further confirm it we performed x-ray diffraction measurements on the both the bilayer

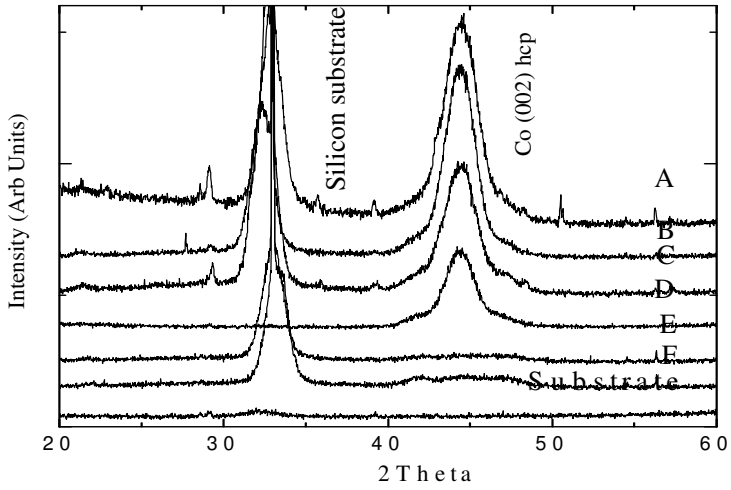

Fig 3.14 Wide angle XRD pattern of all the MLs along with the Si (100) substrate. For the sake of clarity the data have been shifted in y-axis. Presence of a broad peak at $2\theta \sim 44^{o}$ for samples A, B, C & D, indicates that Co is crystalline in nature and the films are highly textured.

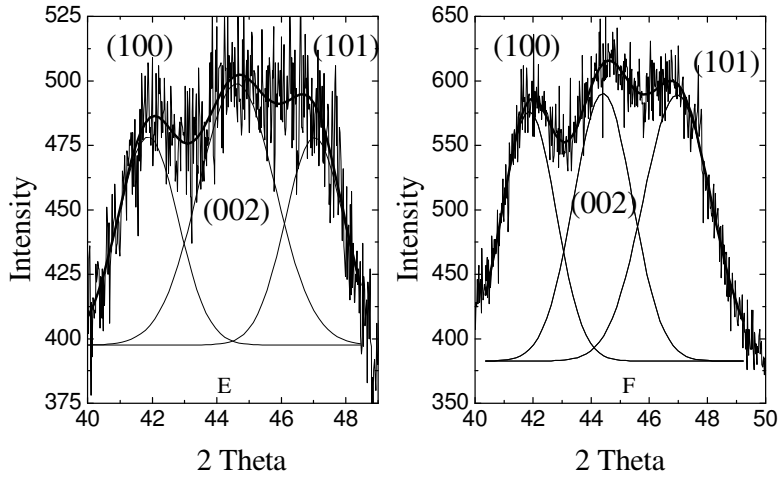

Fig 3.15 Magnified wide angle XRD pattern for samples E & F. Single peak corresponding to (002) plane of Co, as seen in Fig (3.14), has been broken into three different peaks. These three peaks correspond to (100), (002) & (101) planes of Co.

samples BL1 and BL2, where Si layer is 22 nm thick and Co layer is 23 nm thick. We have chosen such high thicknesses since we needed thicknesses more than what we have in the ML samples E and F. X-ray diffraction data of the bilayer grown on Si(100) substrate showed that Co layer has lost its texture. This is evident from the three peaks that are distinctly present. Similar effect is seen for the bilayer sample grown on float glass substrate. But in this sample it can be seen that although the texture of Co layer is lost but the three peaks are also not distinctly visible. This might be due to the reason that in this particular case the Co layer is grown on an amorphous substrate i.e. the float glass, due to which it might initially not be textured and the deposition of Si layer above the Co layer must have enhanced this effect.

The crystalline correlation length "ξ", can be estimated from the full width at half maximum (FWHM) of the Co (002) diffraction peak. Correlation length for the samples A, B, C, D, E & F calculated using the Scherrers formula is given in Table-3.4. Absence of Si peaks in the XRD pattern suggests that Si, a spacer layer, in all these multilayers is amorphous in nature. Thus, we have found that in all the multilayers Co is crystalline in nature whereas Si is amorphous. Fallon *et al.* [46] have shown that Co in Co/Si Multilayer system is highly oriented and the correlation length increases as we increase the thickness of the Co layer. Fallon *et al.*[45] have also a reported that Co-Si alloy films shows (002) hcp texture for low concentration of

Samples	Correlation Length (ξ)
A	3.8± 0.5
B	3.9± 0.5
C	4.0± 0.5
D	4.1± 0.5
E	3.2± 0.5
F	3.4± 0.5

Table 3.4. Correlation length calculated using Scherrer's formula for all the as-deposited ML samples.

Si and this texture is lost when the concentration of Si is increased. But none of them have shown the effect of increase in the thickness of Si layer in the Co/Si ML system. Thus, we have found that the Co layer in Co/Si multilayer system is highly oriented only for the multilayer containing low thickness of Si layers and this texture is lost as we increase the thickness of the Si layer, this thickness is ~5.6 nm. No peak due to silicide phase formation in the as-deposited Co/Si ML is seen in the XRD pattern, suggests that silicide phase is not present and even if it is present its volume fraction is so low that is presence is not seen in the XRD pattern.

Magnetic measurements carried out using MOKE showed only ferromagnetic coupling between the Co layers. The hardness or softness of this ferromagnetic behavior is highly governed by Si layer thickness. We have not observed any oscillatory behavior with respect to Si layer thickness in the interlayer coupling as observed by Lucinski *et al.*[37] and superparamagnetic behavior as observed by Grundy et al.[34] and Lucinski *et al.*[36], in the preliminary MOKE measurements at room temperature.

All these suggest that it is the texture of the Co layer, which depends on the thickness of the Si layer that affects the magnetic properties of Co/Si system. Since silicide layer is not visible distinctly at the interface, its possible effect on the magnetic behavior of the system is not clear**.** Thus, structural and in turn magnetic properties of Co/Si ML system are highly governed by thickness of the Si layer and not by silicide layer.

3.5 Characterization of thin foil gold mirror for soft x-ray telescope

X-ray telescopes based on grazing incidence provide the necessary high sensitivity for x-ray observations by virtue of their imaging capability and reduction of the background levels encountered in space. High efficiency x-ray reflectors with low scattering are very important to realise a good point spread function for a telescope. ASTROSAT is an Indian Multiwavelength Satellite designed to cover a very broad band of X-rays, UV and optical is planned to be launched by a Polar Satellite Launch Vehicle in 2014 into a near-Earth Equatorial orbit [51]. A Soft x-ray imaging telescope (SXT) [52] is among its five major payloads. Here, we present x-ray reflectivity measurements of the mirrors made for the SXT.

The Soft x-ray Telescope (SXT) for ASTROSAT[51] is designed based on Wolter type I configuration[53],[54] which involves a combination of confocal surfaces of paraboloid and hyperboloid mirrors reflecting x-rays at grazing incidence onto a small detector e.g., an x-ray CCD. All the mirrors for SXT have been made at TIFR. All gold mirrors were coated on aluminum foils of required curvature by replication technique. In this technique a smooth glass cylinder of outer diameter matching in size with the curvature of the rolled foil was coated with gold (thickness ~200nm) in a DC-Magnetron Sputtering machine and this gold film was transferred on Al foils[55].

Detailed x-ray reflectivity characterization of the mirrors at multiple energies is extremely important during the process of fabrication to qualify them and also to test their performance after subjecting them to various environmental tests. This telescope is designed to work in range of 0.2 to 8.0 keV. The present work describes hard x-ray measurements at 8.05 and 5.41 keV. These mirrors were of big size (~10^2 cm^2) and have high curvature; hence it was difficult to perform x-ray reflectivity measurements on a commercial x-ray reflectometer. Thus, we have carried out x-ray reflectivity measurements on a reflectometer developed in house at RRCAT using a sealed tube and shown in Fig. (2.8 in chapter 2) The size of the beam was 4 mm × 50 μm and the footprint of the beam on mirror was in the range of 2.3–6 mm. We have tested the quality of the surface of a large number of these mirrors. The quality is measured by studying the reflectance, roughness and density of the Au layer derived from x-ray reflectivity measurements using CuKα (8.05 keV), CrKα (5.4 keV) sealed x-ray tube sources.

We have examined the quality of the surface of a large number of these mirrors. X-ray reflectivity measurements have been performed on several mirrors selected randomly from the manufacturing process. Another sample of mirrors was also subjected to various types of hot, cold and thermovac cycles to simulate the effects of satellite environment and storage as part of the qualification procedure required by the Indian Space Research Organization. Here, we present results from a sample of 8 mirrors table below. Figure (3.13) shows a typical x-ray reflectivity pattern of the mirrors, obtained using CuKα radiation. All the other mirrors give a similar reflectivity pattern. These patterns were then fitted assuming various models, to calculate the thickness, roughness and density of the layers of all the replicated gold foil mirrors. In the present case we first considered a single layer model of pure gold with variable roughness and

thickness. This resulted in the thickness of a gold layer that is fairly large, and was thus treated as a substrate. However, we found that the quality of the fit to the data was very poor. To improve the quality of fit to the measured reflectivity data, we introduced one more layer on top of the gold film, treating the bottom thick gold layer as the substrate having bulk density of gold. We then tried to vary the thickness, roughness and density of this top layer and roughness of the bottom thick gold layer. The fit quality improved significantly and the best fits were obtained for such two-layer models, where the top surface layer has a thickness of a few tens of Angstroms and ~10% lower density compared to the bulk density of gold. Henceforth, we shall refer to this top layer of gold with less density as compared to the bulk density of the gold, as the top low density layer.

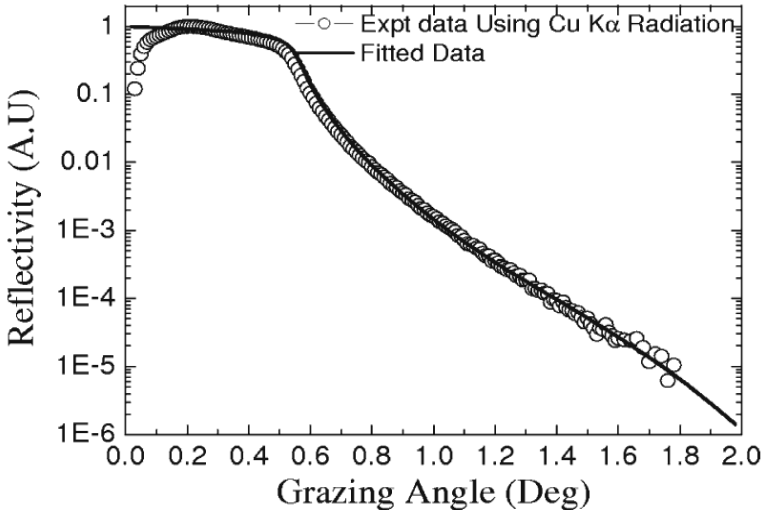

Fig 3.16 X-ray reflectivity pattern of a typical mirror measured at 8 keV

We have also subjected the few mirrors to reflectivity studies using Chromium target, i.e. Cr K_α radiation. All the other mirrors give similar reflectivity pattern. Fitted results and a comparison with respect to the results obtained from the fitting of the data obtained using Cu K_α and Cr $K_\alpha$radiation are given in Table 3.5. One observation which is clearly visible from the table is that top layer roughness values measured with Cr target are 0.5-0.9 nm and with Cu target they are 0.9-1.4 nm. This indicates that mirror appears smoother at longer wavelengths which is a beneficial feature as operating range for the telescope is 0.2-8 keV. Hence it would show higher reflectivity at longer wavelengths.

In this study we have demonstrated that even large size optics can be analyzed on developed reflectometer. Few of these measurements were also repeated at the x-ray beam line at U-lab in Nagoya University, using 1.5 keV and 8 keV X-rays and the rms roughness values obtained were in the range of 1.0–1.5 nm which confirmed our results. These measurement helped in developing the first Indian soft x-ray telescope. These measurements also helped in predicting the performance of the telescope.

Sample Name	CHROMIUM 5.41 keV		Copper 8.04 keV	
	Top Au Layer Thickness (nm)	Top Au Layer Roughness (nm)	Top Au Layer Thickness (nm)	Top Au Layer Roughness (nm)
S6	1.8±0.15	0.5±0.1	2.6±0.17	0.9±0.12
S7	1.8±0.15	0.6±0.1	3.1±0.2	1.0±0.14
S8	2.5±0.2	0.9±0.1	3.1±0.22	1.4±0.14
S9	2.2±0.18	0.62±0.08	3.0±0.2	1.17±0.12
S10	2.0±0.2	0.81±0.1	3.1±0.22	1.35±0.12
S11	2.7±0.21	0.9±0.13	2.7±0.2	1.2±0.1
S12	2.0±0.17	0.64±0.06	2.0±0.15	0.9±0.1
S13	1.7±0.15	0.6±0.06	2.1±0.2	0.95±0.1

Table 3.5 Parameters of gold coating obtained from comparative study of gold mirrors using Chromium and Copper Kα x-rays

3.6 Summary

From the case studies discussed in this chapter we have demonstrated the use of x-ray reflectivity in getting details of electron density profile of the thin film structure other than just estimating film thickness and roughness. Knowledge of density profile gives finer details about the structure like information about porous layer formation in NiMnSb thin films, oxide layer formation in Nb thin films and no interlayer formation in Co/Si multilayers. Also we have characterized ASTROSAT soft x-ray space telescope gold coated mirrors using our developed

reflectometer. In this chapter we have demonstrated that by systematic and watchful investigation of XRR data obtained from samples it is possible to get comprehensive structural details. This knowledge base developed in analysis of various systems would be used in further chapter in handling even more complicated situation in case of short period multilayers.

References

1 "Morden X-ray Physics", Jens Als-Nielsen, Des McMorrow, John Wiley & sons, Ltd, 2000

2 A. van der Lee, Eur. Phys. J. B 13, (2000) 755.

3 M. V. Klibanov and P. E. Sacks, J. Math. Phys. 33, (1992) 3813.

4 W. L. Clinton, Phys. Rev. B 48, (1993) 1.

5 M. K. Sanyal, S. K. Sinha, A. Gibaud, K. G. Huang, B. L. Carvalho,M. Rafailovich, J. Sokolov, X. Zhao and W. Zhao, Europhys. Lett. 21, (1993), 691.

6 E. M. Lee, J. E. Milnes and I. C. Wong, Physica B 221, (1996), 159.

7 H. J. Voorma, E. Louis, N. B. Koster, F. Bijkerk and E. Spiller, J. Appl.Phys. 81, (1997), 6112.

8 F. Rieutord, A. Braslau, R. Simon, H. J. Lauter and V. Pasyuk, Physica B221, (1996), 538.

9 X.-L. Zhou and S.-H. Chen, Phys. Rev. E 47, (1993), 3174.

10] C.-H. Chou, M. J. Regan, P. S. Pershan and X.-L. Zhou, Phys. Rev. E 55,(1997), 7212.

11 E. Smigiel and A. Cornet, J. Phys. D: Appl. Phys. 33, (2000), 1757.

12 O. Starykov and K. Sakurai, Appl. Surf. Sci. 244, (2005), 235.

13 P. Mikul´ık and T. Baumbach, Physica B 248, (1998), 381.

14 D. S. Sivia, W. A. Hamilton, and G. S. Smith, Physica B 173, (1991), 121.

15 D. S. Sivia, W. A. Hamilton, G. S. Smith, T. P. Rieker, and R. Pynn, J. Appl. Phys. 70, 1991, 732.

16 N. F. Berk and C. F. Majkrzak, Phys. Rev. B 51, (1995), 11296.

17 J. S. Pedersen, J. Appl. Crystallogr. 25,(1992),129.

18 M. K. Sanyal, J. K. Basu, A. Datta and S. Banerjee, Europhys. Lett. 36, (1996), 265.

19 L. G. Parratt, Phys. Rev. 95, (1954), 359.

20 K. Stoev and K. Sakurai, The Rigaku J. 14, (1997), 22 .

21 K. Kunz, J. Rieter, A. Gotzelmann, and M. Stamm, Macromolecules 26, (1993), 4316.

22 A. Ulyanenkov and S. Sobolewski, J. Phys. D: Appl. Phys. 38, (2005), 235.

23 N. F. Berk and C. F. Majkrzak, Phys. Rev. B 51, (1995), 11296.

24 L. Nevot and P Croce. Rev.Phys.Appl. 15, (1980) ,761.

25 "High-Resolution X-ray Scattering from Thin flims and Multilayer", V. Holy, U. Pietsch, T. Baumbach, , Springer Heidelberg Germany (1999).

26 R. A. de Groot, F. M. Mueller, P. G. v. Engen, and K. H. J. Buschow, Phys. Rev. Lett. 50 (1983), 2024.

27 S. A. Wolf, D. D. Awschalom, R. A. Buhrman, J. M. Daughton, S. von Molnár, M. L. Roukes, A. Y. Chtchelkanova, and D. M. Treger, Science 294 (2001), 1488.

28 J Giapintzakis et al Appl. Phys. Lett. 80 (2002), 2716.

29 S. Gardelis et al. Appl. Phys, Lett. 85, (2004), 3178.

30 W. R. Branford, S. K. Clowes, M. H. Syed, Y. V. Bugoslavsky, S. Gardelis, J. Androulakis, J. Giapintzakis, C. E. A. Grigorescu, A. V. Berenov, S. B. Roy, and L. F. Cohen, Appl. Phys. Lett. 84, (2004), 2358.

31 W. R. Branford, S. K. Clowes, Y. V. Bugoslavsky, S. Gardelis, J. Androulakis, J. Giapintzakis, C. E. A Grigorescu, S. A. Manea, R. S. Freitas, S. B. Roy, and L. F. Cohen, Phys. Rev. B69, (2004), 201305.

32 J.-P. Schlomka, W.Press, M. R. Fitzsimmons, M. Lutt, and I. Grigorov Physica B 248, (1998), 140.

33 J. Tueckmantel,IEEE Trans Appl. Supercond. 9, (1999), 270.

34 Grundy P J, Fallon J M and Blythe H J Phys. Rev. B 62, (2000), 9566.

35 Inomata K and Saito Y ,J. Appl. Phys. 8,(1997), 5334.

36 Lucinski T, Kopcewicz M, Hutten A, Bruckl H, Heitmann S, Hempel T and Reiss G Mater. Sci. 21, (2003),25.

37 Lucinski T, Wandziuk P, Stobiecki F, Andrzejewski B, Kopcewicz M, Hutten A, Reiss G and Szuszkiewicz W J. Magn. Magn. Mater. 282,(2004), 248.

38 Vega A, Rubio A, Balbas L C, Dorantes-Davila J, Bouarab S, Demangeat C, Mokrani A and Dreysse H, J. Appl. Phys. 69,(1991) ,4544.

39 Endo Y, Kitakami O and Shimada Y, Phys. Rev. B 59, (1999),4279.

40 de Vries J J, Kohlhepp J, de Broeder F J A, Jungblut R, Coehoorn R, Reinders A and de JongeWJM , Phys.Rev. Lett. 78,(1997), 3023.

41 Endo Y, Kitakami O and Shimada Y, IEEE Trans. Magn. 34, (1998),906.

42 S. R. Naik, S. Rai, M. K. Chattopadhyay, V. K. Sharma, S. Majumdar, and G.S. Lodha, Journal of Applied Physics 104, (2008) 1.

43 S R Naik, S Rai, M K Tiwari and G S Lodha, J. Phys. D: Appl. Phys. 41 (2008) 115307

44 Fallon J M, Faunce C A and Grundy P J , J. Phys.: Condens. Matter 12, (2000),4075.

45 Fallon J M, Faunce C A, Grundy P J and Blythe H J J. Appl. Phys. 87,(2000), 6833.

46 Fallon J M, Faunce C A and Grundy P J J. Appl. Phys. 88, (2000), 2400.

47 Petford-Long A K, Sterns M B, Lee C H, Nutt S R, Ceglio M and Hawryluk A M J. Appl. Phys. 61. (1987),1422.

48 Ruterana P, Haudy P and Boher P J. Appl. Phys. 68,(1990) 1033.

[49] Petford-Long A K, Sterns M B, Lee C H, Nutt S R, Ceglio M and Hawryluk A M J. Appl. Phys. 61, (1987)1422.

50 Ruterana P, Haudy P and Boher P J. Appl. Phys. 68, (1990), 1033.

51 Singh, K.P.: Science from ASTROSAT. BASI 30, (2002) 803

52 Singh, K.P.. BASI 30, (2002), 799.

53 Wolter, H.Ann. Phys. 10, (1952), 94.

54 Wolter, H.Ann. Phys. 10, (1952), 286.

55 Kunieda, H. Appl. Opt. 40, (2001), 553.

Chapter 4

Interface analysis of Short period Multilayers

4.1 Introduction

As discussed in chapter 1, with the improvement of the technology of multilayer growth and the increasing availability of high-brightness synchrotron x-ray sources along with next generation free electron laser sources[1], interest has grown in the use of multilayers of shorter periods. Most of the applications require high radiation and thermal stability, high spectral selectivity and, in particular, high reflectance. X-ray multilayers with small periods around ~ 2 nm are of great interest. This is related to their widespread use as radiation-stable dispersive optical elements [2], polarizers for synchrotron radiation, dispersive elements for x-ray diagnostics of high-temperature plasmas[3] , normal incidence reflectors for (soft-) x-ray microscopy in the water window (2 to 4 nm)[4] , for applications in x-ray astronomy and also for magneto- optical polarization spectroscopy[5]. Short period bilayers are also required for developing depth graded broadband reflectors. The lowest limit of the bilayer period in broad band reflector decides the highest energy radiation which can be reflected. In this chapter we have discussed our investigations on interface of W/Si, W/C and W/B_4C multilayers to find out the lowest limit of these multilayers which can be deposited without significant intermixing.

4.1.1 Studies on W/Si multilayers

In order to fabricate good quality short period multilayers, it is very important to select suitable material combination. W/C, W/B_4C and W/Si are promising material combination for fabricating short period multilayers in hard x-ray region. There are various reports on the performance of short period structures made of W/C, W/B_4C and W/Si as discussed below. It has been observed that reflectivity close to theoretical value of a multilayer structure can be obtained for multilayers with periods above 6.5 nm. For shorter periods it is not possible to get more than 50% of theoretical values[6]. Various investigations have been done to understand the cause for this reduction[7,8,9,10]. The performance of such structures depends primarily on the practically achievable interface perfection. Any deviation from atomically smooth and chemically abrupt interface reduces the reflectance of the multilayer stack. The requirement on interface quality becomes stringent in the case of short period multilayers (d ~2 nm) as the relative importance of the interface roughness increases at low thicknesses. Many studies have been carried out to comprehend the performance of such structures. Jankowaski *et.al.*[11] fabricated 60 periods of W/B_4C multilayers with period as low as 6.7 Å calling them “amorphous crystals” because

individual layers were amorphous but maintained a long range order like crystals. Multilayers made of W/Si having periods 1.6-2.8 nm have been examined by Hasan *et.al.*[12] using x-ray reflectivity and energy dispersive spectroscopy. They have found significant intermixing and re-sputtering of Si during W deposition but no evidence of re-sputtering of W during Si deposition was found. All the studies discussed above have concentrated on how to deposit good quality short period multilayer but none have examined the changes happening at the interface of the multilayer as one reduces the period thickness. Walton *et.al.* [6] have reported systematic investigation of W/B_4C multilayer of periods changing from 5nm to 0.5 nm. They have investigated the microstructure of the films by x-ray reflectivity and cross-sectional TEM. This study gives an insight of the microstructure changes occurring due to period reduction. But in there reflectivity fitting analysis they have not estimated the roughness of W and B_4C layer independently. Similar work has been done by Vidal *et.al.*[13] on W/Si and W/C multilayers, where they have compared the nature of interface and reflectivity of both multilayers with TEM and XRR. Analysis of multilayer structure using TEM gives very local information which may not represent the average behavior but x-ray reflectivity give much better average information. However, as they have examined multilayers with number of periods in range of 50 to 100, it would not have been possible to do a detailed fitting of the x-ray reflectivity (XRR) data including individual Kiessig oscillations. Complete fitting of XRR data reveals more complete information about the interface roughness variation, interface mixing, and change in density of individual layers with the multilayer period. If samples have less number of layer pairs performing a complete fitting and analysis becomes easier.

Most of these studies discussed above have examined multilayer prepared using magnetron sputtering. Not many reports are available on detailed investigations of short period multilayer prepared using ion beam sputtering method. Ion beam sputtering technique has advantage over other physical vapor deposition processes like e-beam evaporation and magnetron sputtering. In e-beam evaporation, the energy of adatoms reaching the substrate are below 1 eV hence it is difficult to deposit films with smooth morphology and mostly films grow with columnar structure. This problem of low adatom energy is not present in magnetron sputtering. However, in magnetron sputtering plasma has to be generated and sustained in the sputtering zone. Also, the deposition takes place at higher Ar partial pressure leading to contamination of Ar trapping inside the growing film surface. In ion beam sputtering technique

ions are generated inside an independent source which is kept away from sputtering zone and ions are made to hit on the target by using extraction mechanism. Hence deposition takes place at a lower working pressure of at least one order below than that in magnetron sputtering. Deposition by IBS technique produce films with better morphology and packing density[14].

In all sputtering deposition techniques it is known that large number of ions or neutrals get reflected from the target and hit the freshly growing film surface. This process of back scattering is equivalent to that of ion/neutral beam hitting the growing surface as if ion assisted deposition is happening. These neutrals and ions hitting the film have sufficient energy to modify the growth and interface of the film [15]. The energy and number density of reflected neutrals/ions is high when atomic mass of the target is higher than the atomic mass of the sputtering gas[16] . If the target atom mass is less than the sputtering gas, there will be a very small flux of neutrals getting reflected from the target. Rossangel *et.al*[16] has concluded that bombardment of depositing film during sputtering should be considered as an unavoidable artifact of sputtering deposition technique. Hasan *et.al*.[12] have observed while depositing W/ Si multilayers by magnetron sputtering that reflected neutrals from W target can have energies >80 eV which is sufficient for re-sputtering the atoms of growing Si film. Our simulation with TRIM[17] as discussed in chapter 2, also confirm that indeed the energy of reflected neutral can be more than 100 eV. They have found significant intermixing and re-sputtering of Si during W deposition but did not find any evidence of re-sputtering of W during Si deposition. They have shown that as long as W layer thickness is below 1.4 nm re-sputtering of Si keeps on happening and once W layer thickness reaches 1.4 nm re-sputtering of Si stops In case of short period multilayers and broadband reflectors it becomes very important to know what is the shortest period thickness which can be deposited with good density contrast. Re-sputtering can seriously limit the period of the shortest bilayer which can be fabricated without discontinuity. Deposition by ion beam sputtering can also suffer by re-sputtering due to back scattered ion/neutral. E.Franke *et al*.[18] have monitored the reflected particles using a mass spectrometer in an ion beam sputtering system. They found significant flux and energy of reflected ions and neutral particles. It would be interesting to see the influence of reflected neutrals on growth in ion beam sputtered multilayers.

In first part of our study we investigated W/Si multilayers with period in the range of 10.5 nm to 2.5 nm nominal thickness to understand how the structure and intermixing behavior of the stack changes as the period thickness is reduced. We also examined the influence of re-sputtering on the multilayer structure as the period thickness is reduced. Detailed analysis of structural changes along with period thickness has been carried out using XRR, and GIXRD measurement. This work has been motivated by the need for developing high reflectance hard x-ray multilayer monochromators and broad band super mirrors for beamlines on Indus-2. Development of short period multilayers is a pre-requisite for the above mentioned goals.

4.1.2 Experimental Details

W/Si multilayers on float glass substrate were deposited using the in-house developed ion beam sputter deposition system. Base pressure in chamber before gas flow was 6 X 10^{-7} mbar and during the deposition it was maintained at ~ 4 X 10^{-4} mbar. We used commercially available 4" sputtering targets of 99.95% purity for W and 99.99 % purity for Si. The target to substrate distance during deposition was 35 cm. All substrates were cleaned in nitric acid and ultrasonic cleaning in acetone. Before deposition, r.m.s. roughness of each substrate was measured by x-ray reflectivity (XRR) technique on a reflectometer developed in house. The measured roughness of all substrates was ~0.4 nm.

Before multilayer deposition, we optimized deposition process parameters so that films with low interface roughness could be produced. For optimization we deposited various bilayers of 10nm thick Si on 10nm W, on a float glass substrate with different deposition parameters. It was found that films deposited at 1000 V beam voltage and a gas flow rate of 3 standard cubic centimeter per minute (SCCM) were best from the interface roughness point of view. The roughness of W layer was estimated to be 0.3 nm and of Si layer was estimated to be 0.4nm. The deposition rate for different materials was determined by depositing various thin films of W and bilayers of Si on W on float glass substrates and their thicknesses were measured by XRR. It was found that the deposition rate of W layer was ~1.3-1.4 nm/min and of Si layer was ~1.2.nm/min for all samples. Deposition rate was kept low as very thin layer were to be deposited. The thickness values estimated by XRR were used to calibrate the difference between actual deposition thickness and thickness shown by the quartz crystal monitor to accurately estimate the nominal thickness.

After the optimization, seven samples of different period thickness (d) were deposited. The nominal thickness of multilayer period was varied from 10.5 nm to 2.4 nm marked as A-G. Details of the sample name and sample thickness and deposition time of individual layer are given in Table 4.1. Sample A-D had 10 layer pairs, Sample E had 15 layer pairs and sample F and G had 20 layer pairs deposited.

Characterization of all the samples was done using grazing incidence x-ray reflectivity (XRR) technique. Standard alignment procedures were done to align both theta and two theta axes within 0.002˚. All the measurements are performed with a step size of 0.005˚ in theta axes, which is sufficient to observe any small changes in thin films. Specular reflectivity was measured in over the range of Θ = 0˚ to 3 to 4˚ depending upon the sample.

Grazing incidence x-ray diffraction (GIXRD) was also performed on some the samples to find out amorphous or crystalline state of layers. GIXRD was done using Bruker D8-Discover system consisting of Θ - Θ goniometer. The incident beam has parabolic mirror to give parallel beam. The measurements were done for all samples at an incident angle of 0.5˚. Long soller slit along with LiF flat monochromator was used to collect data in diffraction beam arm. Cross sectional TEM (CSTEM) of sample G was carried out using CM 200 Philips microscope equipped with LaB_6 filament.

4.1.3 Results and Discussions

Figure (4.1) shows the plot of normalized reflectivity (experimental reflectivity divided by ideal value) with multilayer period. Ideal values were calculated using bulk density and 0.2 nm interface roughness values. Ideally this graph should have shown a horizontal line drawn at y ~1. But we see that that initially when the multilayer period is large, the plot is somewhat straight but after sample C (d= 2.9 nm) it starts to deviate from straight line and drops significantly away from the straight line as the multilayer period is reduced. This indicates that as the period thickness reduces, changes are happening in the microstructure of the films, which are not matching with our model of smooth and abrupt interface used for simulation of ideal value. Generally when the multilayer period is reduced in the range of 2 nm the percentage of interface roughness with respect to layer thickness becomes very important. To achieve good reflectivity, interface roughness should be much less than the layer thickness.

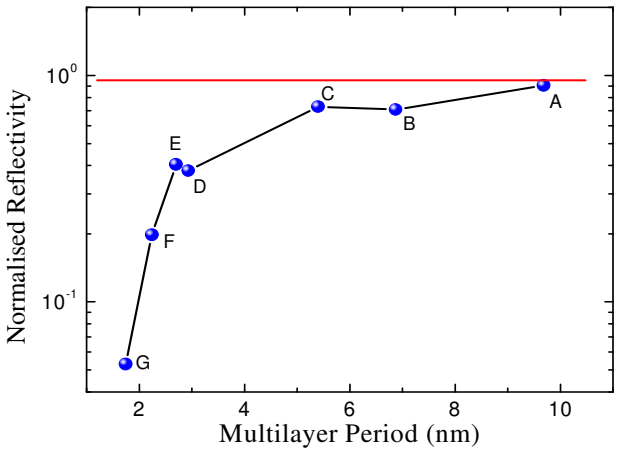

Figure 4.1 Variation of normalized reflectivity with multilayer period

To understand the difference in the microstructure of the samples at low period thickness detailed XRR fitting was carried out. For analysis of XRR measurements, Parrett recursive formalism was used to model reflectivity calculation. Roughness was taken into account using Nevot-Croce model. Various possible models were tried to fit the reflectivity data, for example layers composed of pure W and amorphous Si, or of Si and W layer as W_xSi_y, with either symmetric or asymmetric interface widths. Out of various models considered it was found that best match with the experimental data for all samples was obtained with two-layer model. In two-layer model, only layers of W and Si were considered for all samples. There was no need of an interlayer in any of the samples. Considering, top Si layer to be partially oxidized helped to improve the fit quality. This is expected due to exposure of sample to air. Figure (4.2) shows the GIXRR experimental profiles (open circles) along with fitted curves (solid red lines) as a function of wave vector transfer $q=4\pi\sin\theta/\lambda$ for all A-G samples. One can see that Kiessig oscillation in all samples are clearly visible and are matching well with the simulated profile. Simulations show that in samples with shorter period (e.g. F- G) even a thickness error of less than 0.05nm would spoil the regularity of Kiessig oscillation due to the uncertainty in total period thickness[13]. The observation of well defined Kiessig oscillation indicates that bilayer periodicity is maintained in all samples for all layer pairs.

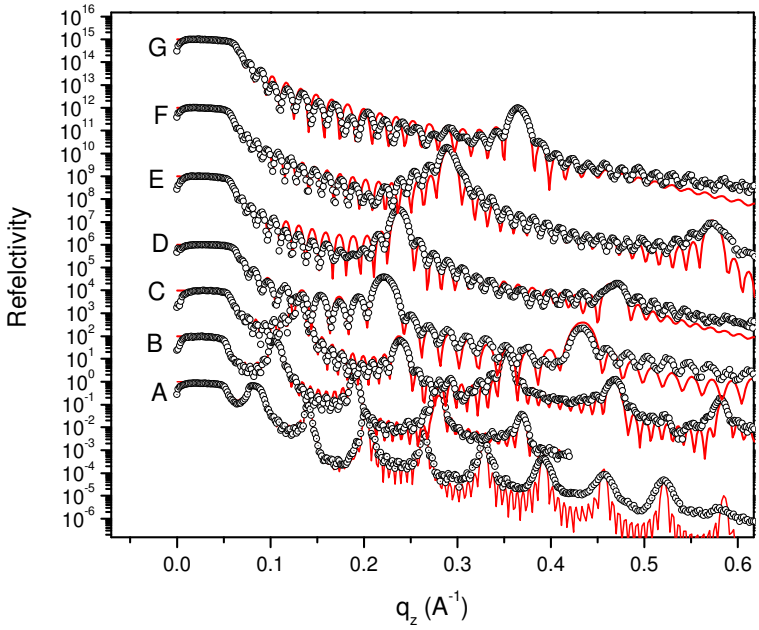

Fig 4.2 X-ray reflectivity curves both experimental (open circles) and fitted (solid lines) as a function of wave vector transfer 'q_z ($Å^{-1}$) for all samples (A-G)

Results of XRR analysis are given in Table (4.1) and (4.2). Table (4.1) contains details of nominal thickness as per the calibrations of each layer, estimated thickness and estimated thickness of W and Si layers. The difference in the estimated thickness and expected thickness W and Si layers for all samples are also listed in Table 4.1. It can be seen from Table 4.1 that the estimated period thickness is less than the nominal thickness. The difference in the estimated thickness and the expected thickness for W layer is negligible. But in case of Si layers, it can be seen that the difference for samples A-D it is constant around 0.8nm, but for samples E-G it reduces linearly with W layer thickness as can be seen in Figure (4.3). Loss in Si thickness matches with difference in the estimated period thickness and the nominal period thickness.

Sample Name	Nominal Period (nm)	Estimated Period Thickness (nm)	Expected W Layer Thickness (nm)	Estimated W Layer Thickness (nm)	Difference in expected and estimated W thickness (nm)	Expected Si Layer Thickness (nm)	Estimated Si Layer Thickness (nm)	Difference in expected and estimated Si thickness (nm)
A	10.5	9.68±0.12	4.2	4.22±0.04	0.02	6.25	5.46±0.08	-0.79
B	7.8	6.87±0.11	2.8	2.7±0.04	-0.1	5.0	4.17±0.07	-0.83
C	6.6	5.4±0.11	2.8	2.52±0.04	-0.28	3.75	2.88±0.07	-0.87
D	4.0	2.93±0.06	1.96	1.68±0.03	-0.28	2.0	1.23±0.03	-0.77
E	3.4	2.7±0.05	1.4	1.4±0.02	-0.0	2.0	1.3±0.03	-0.7
F	2.9	2.24±0.05	1.12	1.05±0.02	-0.07	1.75	1.19±0.03	-0.56
G	2.4	1.74±0.05	1.12	1.01±0.02	-0.11	1.25	0.7±0.03	-0.52

Table 4.1. Details of nominal thickness, estimated thickness and loss of material due to re-sputtering for each layer in all samples

Sample Name	Estimated Period Thickness (nm)	Estimated W Layer Thickness (nm)	Density of W Layer (gm/cc^3)	Roughness of W Layer (nm)	Estimated Si Layer Thickness (nm)	Density of Si Layer (gm/cc^3)	Roughness of Si Layer (nm)
A	9.68±0.12	4.22±0.04	17.46±0.61	0.55±0.03	5.46±0.08	2.13±0.07	0.98±0.05
B	6.87±0.11	2.7±0.04	17.46±0.61	0.49±0.03	4.17±0.07	2.16±0.07	1.15±0.05
C	5.4±0.11	2.52±0.04	17.46±0.61	0.35±0.03	2.88±0.07	2.20±0.07	0.79±0.05
D	2.93±0.06	1.68±0.03	17.41±0.61	0.35±0.03	1.23±0.03	2.83±0.1	0.85±0.05
E	2.7±0.05	1.4±0.02	17.39±0.61	0.35±0.03	1.3±0.03	3.15±0.1	0.85±0.05
F	2.24±0.05	1.05±0.02	15.95±0.58	0.45±0.03	1.19±0.03	4.17±0.12	0.75±0.05
G	1.74±0.05	1.01±0.02	15.68±0.57	0.45±0.03	0.7±0.03	6.45±0.18	0.7±0.05

Table 4.2. Details of estimated density of W and Si layer along with interface roughness for all samples

This indicates that only Si is getting lost during deposition and no loss of W is observed. Similar loss of Si has been observed by Hasan *et.al.*[12] , in samples made by magnetron sputtering. They attributed this to high-energy neutrals and ions getting reflected from the target during W deposition and hitting the Si layer. They have explained loss of Si as a two step process in which Si atoms are first transported through the growing W layer and then removed by collision with reflected high-energy particles bombarding the growing surface. They proposed that the maximum distance, which Si atoms can travel through W, is 1.4 nm, so once W layer thickness reaches 1.4 nm re-sputtering of Si stops. No loss of W is observed as when Si deposition goes on, at that time the energy of the reflected neutrals and ion is not high enough to cause re-sputtering of freshly deposited W layer.

From table (4.1) it is clear that maximum thickness of Si which is getting lost due to re-sputtering is ~0.8 nm. To understand the relationship between Si loss and W layer thickness we plotted amount of Si lost and W layer thickness in figure (4.3). In figure (4.3), It can be observed that (1) Maximum thickness of Si which gets re-sputtered is ~0.8 nm, (2) Si keeps on getting re-sputtered as long as W layer thickness is less than 1.4 nm and (3) For W layer thickness is less than 1.4 nm loss of Si is proportional to the thickness of W layer. Observation (2) appears to confirm the prediction of Hasan *et.al*. that maximum distance which Si atoms can travel through W is 1.4 nm. But if removal of Si is by transport of Si thorough W layer (as explained by Hassan) than one should observe an intermixed transition layer of 1.4 nm at W on Si interface and no intermixing at Si on W interface. To see the strength of these inferences we revisited our fitting models to fit the data including an interlayer. However, no improvement in the fitting quality was observed. In most of the samples attempts to insert an interlayer spoiled the quality of fit. Also, if such a thick interlayer (1.4 nm) was there in our samples it should have been certainly detected by XRR. There are many reports in which W on Si interface was found to be very smooth and no evidence of intermixing/interlayer has been found by them [13,19,20], as observed by us. In this situation the two stage process as explained by Hasan *et.al*. for re-sputtering of Si during deposition may not be a correct picture. Most of the re-sputtering might be happening due to direct impact of high energy neutrals hitting the freshly deposited Si layer

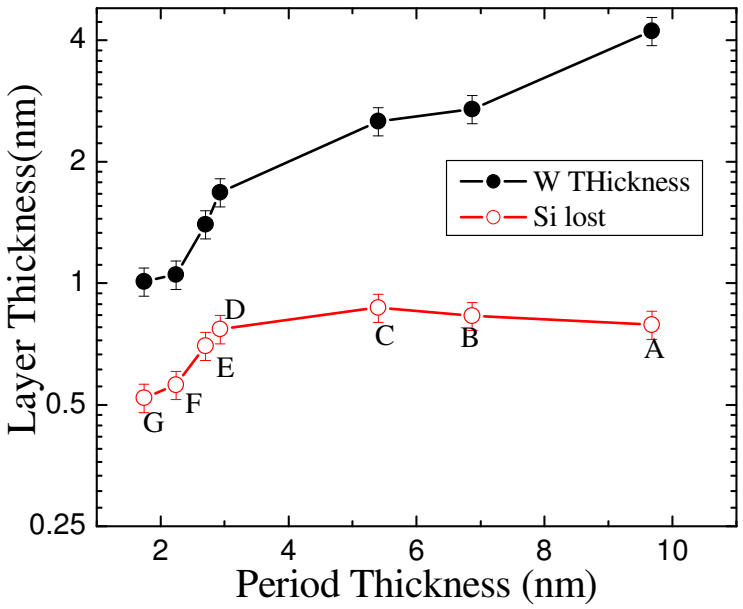

Figure 4.3 Plot amount of Si lost (red open circle) and W layer thickness (black square) with period thickness (along with highest error bar observed in data analysis)

and not by transporting the Si through W layers and then being removed, as explained by Hasan et.al. When W layer becomes thicker than 1.4 nm it becomes continuous and covers the whole surface hence, it is not possible to remove Si below it by high-energy neutrals hitting at the top surface.

To understand the intermixing and diffusion behavior it is important to examine the densities and roughness of individual layers. The estimated densities of W and Si layer along with r.m.s. roughness are given in the Table (4.2). One thing must be noted here that in simulation of XRR curve with to fit experimental data, density of layers was changed as a last step when it was not possible to fit the data further by gamma or interface roughness variation. The guide lines for changing the density was fix the density and thickness of W layer using the deposition parameters and do minimum variation in density of Si layer which was minimum required for improving the goodness of fit and estimate the final density of Si layer. Interface roughness of Si layer is around 0.75-1 nm and of W layer is around 0.35 to 0.45 nm. The roughness of Si layer is much higher than the roughness estimated in case of bilayers (0.4nm). It

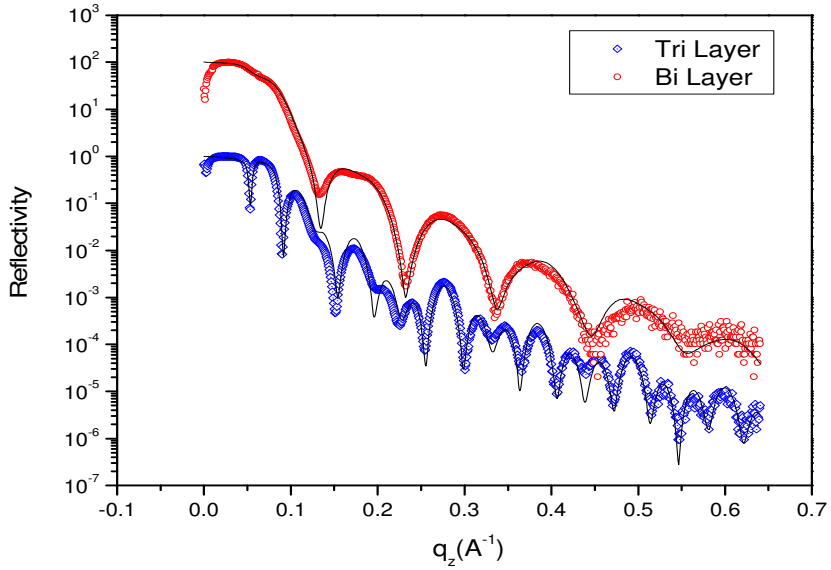

Fig 4.4 Typical XRR pattern of Bi layer of W/Si and tri layer of W/Si/W deposited at 1000 V beam voltage along with best fit line

must be getting increased due to bombardment of high energy neutrals hitting Si layer during deposition of W. Whereas, W deposits smoother as neutrals hitting during Si layer deposition are not of high energy. To confirm this fact we again deposited few bilyers and trilayer of W/ Si and W/Si /W at beam voltage of 800, 1000 and 1200 V. Typical XRR pattern of Bi layer of W/Si and tri layer of W/Si/W deposited at 1000 V beam voltage along with best fit line is shown in fig.(4.4). XRR of all samples showed that in bilayer the roughness of Si was 0.4 nm and in trilayer when W layer was deposited on top of Si it was increasing to 0.9 nm. This observation confirms that hitting of reflected neutrals is modifying the interface and generating an asymmetry in the roughness of W on Si interface to Si on W interface. The influence of beam voltage on the interface roughness was not observable. Interface asymmetry of similar nature was observed by Kessels *et.al*. in W/Si multilayers deposited using Ion assisted e-beam deposition[19] confirming that ion were damaging the Si layer. When they increased the assisted ion energy to 250 eV, the W on Si interface roughness increased to 0.9 nm and Si on W interface was having roughness of 0.5 nm, similar as in our case. In Table (4.2) one can see that as the period of the samples go down, densities of W and Si layer start to change. Figure (4.5) shows variation in the density contrast (Difference between densities of W layer to Si layer) as a function multilayer period. It can be observed that when period is above 5.4 nm (above sample

D) the densities of W and Si layer are within normal range. The density of W layer is 9.5% less then bulk W density. Similarly density of Si layer is 8.5 % less than bulk, which is expected as by sputtering method one does not get densities equal to bulk density due to porosities getting developed in the film during deposition. In case of sample D, where thickness of W and Si is 2.52 nm and 1.23 nm respectively, density of Si layer has increased to 2.83 g/cc from 2.13 g/cc. This indicates that some amount of W has diffused into Si layer. This can be explained with relative increase in roughness of the Si layer. The thickness of Si layer is only 1.23 nm and roughness is 0.85 nm, this high percentage of interface roughness compared to the layer thickness indicates that Si layer must be discontinuous at the interface. The discontinuity should enhance the diffusion of W into Si and increase the density of Si layer. In sample E, where thickness of W and Si is 1.4 nm and 1.3 nm respectively, the density of Si layer has further increased and density of W layer has also reduced suggesting that the now Si has also diffused into W layer. This confirms the observation made in re-sputtering analysis above that when W layer when goes below 1.4 nm it becomes partially discontinuous which promotes mixing of Si into W layer. Increase in the roughness of W layer when its thickness is 1.4 nm or below also confirms that film is getting discontinuous. Hence, diffusion of Si gets enhanced and density of W layer begins to fall. In following samples (F and G) as thickness of both W and Si are

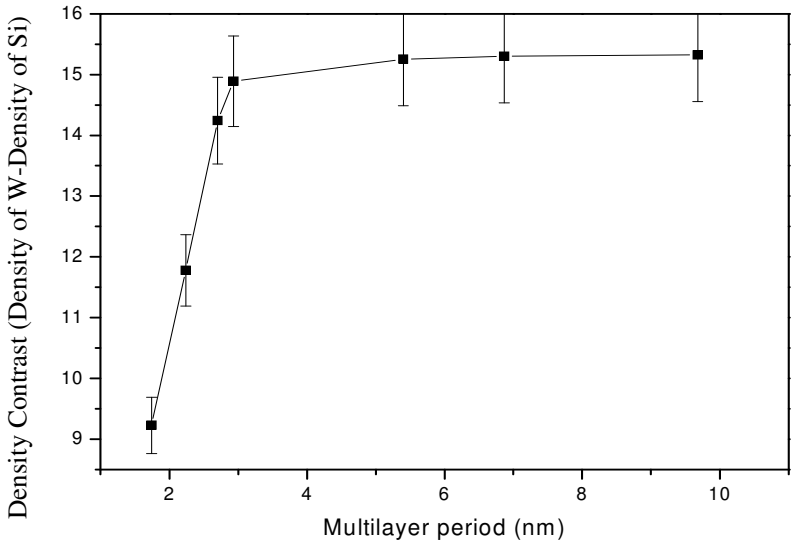

Figure 4.5: Variation of density contrast (density of W –density of Si) with period

low and these layers become discontinuous hence intermixing gets enhanced and density of Si layer keeps on increasing and reaches to 6.45g/cc and density of W layer keeps on reducing and reaches to 15.68g/cc in sample G. Analysis of re-sputtering and density data indicates that when thickness of W goes below 1.4 nm and thickness of Si layer goes below 1.3 nm diffusion of W and Si layers into each other starts and density contrast between two layers starts to drop at a rapid rate as can be seen in figure (4.5). This means that in W/Si x-ray multilayer the shortest period multilayer which can be deposited without intermixing should be more than 2.7 nm. If we have to reduce this period thickness some method needs to be adopted to stop intermixing and make the interface smoother.

Cross sectional TEM (CSTEM) of sample G was carried to see the layer structure of the shortest period sample. As can be seen in figure (4.6) that layer structure are maintained and all the layers in the multilayer are visible as separate layers. A closer look at the image shows that at some places layers appear very thin or discontinuous. Also, the contrast between W and Si layer is very poor it confirms that huge intermixing has happened as observed by GIXRR data analysis. Electron energy loss measurements (EELS) were also done on same sample which showed that both W and Si are present though out the multilayer stack confirming the diffusion of W and Si into each other. Another interesting observation is that in spite of huge intermixing overall multilayer periodicity is maintained. The thickness of the bilayer period estimated from the image is 1.7 nm and the total stack thickness is 34.5 nm which matches well with the XRR.

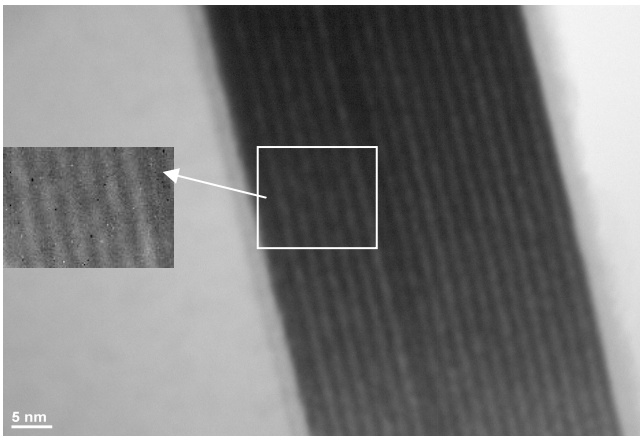

Figure 4.6 : Cross section TEM image of sample G. Inset shows discontinuity in the layers at some locations.

Grazing Incidence X-ray Diffraction (GIXRD) was carried out on all the samples to examine the crystalline nature of the samples. Figure (4.7) shows GIXRD pattern of samples B,D,E and G. For samples B,D and E (110) and (211) peaks of W are clearly visible indicating W is polycrystalline in nature in these samples. Peak widths for samples B,D and E are of the same order indicating that the grain sizes in these samples are same. In case of sample G (110) peak is very broad and (211) peak is not at all visible implying that W layers are either very fine grained nanocrystalline or amorphous in these thin layers. W layer becoming amorphous is unexpected but it can be explained as some amorphous phase of W_xSi_y might be formed due to heavy diffusion of Si into W. Similar observation was made by Windt and Vidal *et.al* [13,20] for thin W /Si multilayers. GIXRD data also confirms of large intermixing of W and Si.

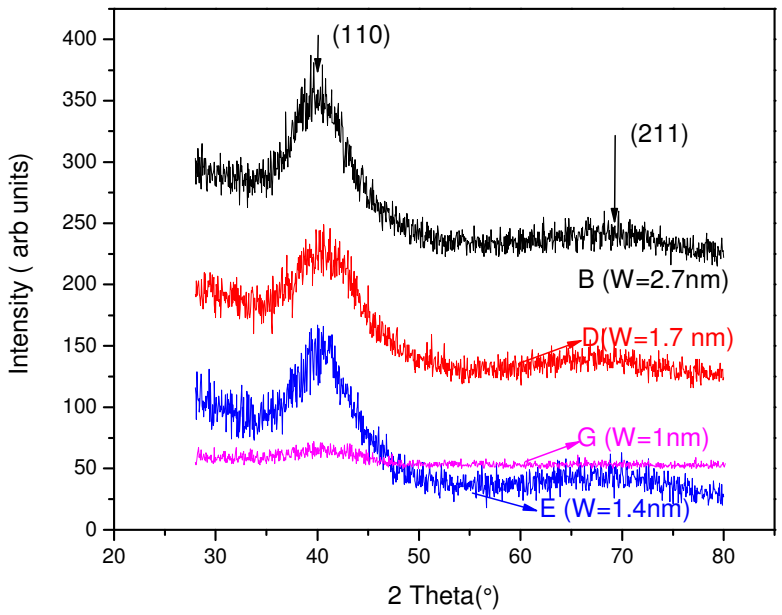

Figure 4.7 : GIXRD pattern of samples B,D,E and G measured at incidence angle of 0.5 deg.

4.1.4 Conclusion on W/Si

The analysis of XRR, data indicates that re-sputtering of Si layer happens during deposition and no re-sputtering of W layer occurs. Maximum thickness of Si which gets removed during deposition is ~ 0.8nm. This information about maximum thickness of Si getting lost is very useful for designing the short period multilayers and super-mirrors. Resputtering of Si layer stops once thickness of W layer reaches 1.4 nm. Absence of interlayer in thicker samples (A-D) indicates that re-sputtering is not a two stage process as predicted by Hassan et.al. When W layer thickness becomes greater than 1.4 nm it becomes continuous and covers the whole surface hence it is not possible to remove Si below it by high-energy neutrals hitting at the top surface. This is observed that re-sputtering is modifying the interface and generating an asymmetry in the roughness of W on Si interface to Si on W interface. There is no means by which this asymmetry can be removed in present setup. In the case of thinner samples (D-G) density of W and Si layer begin to change indicating that inter-diffusion/mixing has started. When thickness of W goes below 1.4 nm and thickness of Si layer goes below 1.3 nm inter-diffusion/mixing of W and Si layers into each other starts due to cascade produced from reflected neutrals hitting the surface. This observation points out that shortest period multilayer which can be deposited without intermixing should have W more than 1.4nm and Si more than 1.3nm. This means that shortest period of W Si layer which can be deposited is 2.8 nm.

One question has still remained that is Si diffusing into W is possible as Si is a smaller atom and it can diffuse into W layer. But what is driving W to move into Si. To understand this we did TRIM[17] simulations to find out the influence of back reflected ions and neutral hitting the Si surface. We further did simulations to understand the influence of these ion/neutrals hitting the freshly grown Si film when W deposition begins. Calculations were done to find out recoil distribution of W due to hitting of 100 eV ion/neutrals. Simulations were done for two cases in first case we had 1.5 nm of Si layer on the top of 1.5 nm thick W layer and in other cases thickness of Si layer was reduced to 1 nm. All the simulations were done for hitting by just 20000 particles having 100 eV energy. Figure (4.8) shows the recoil distribution of W atoms

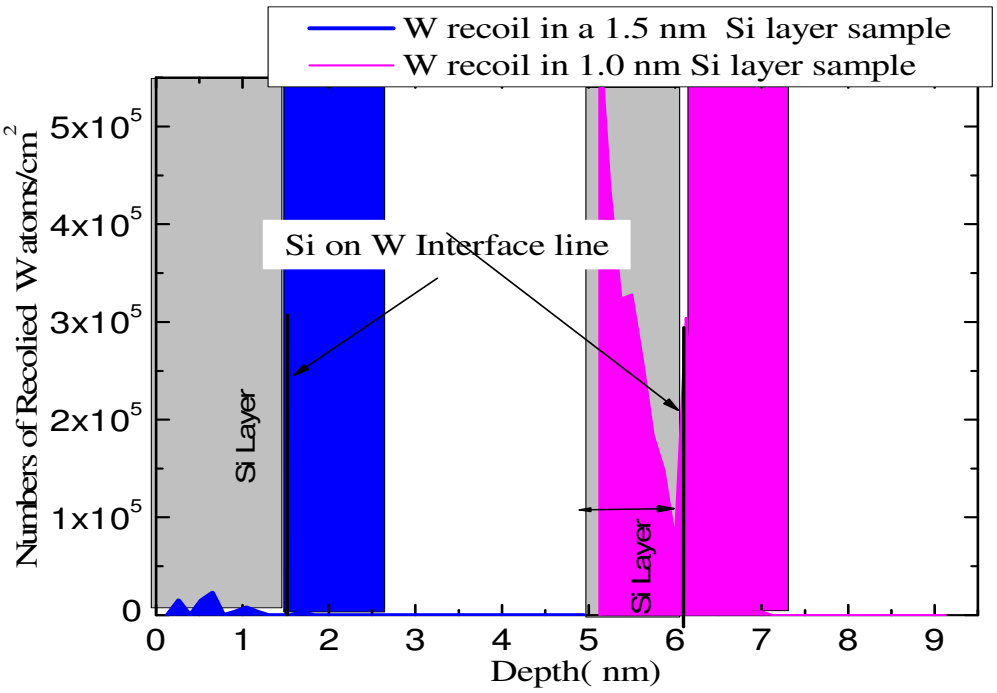

Fig. 4.8 Distribution of recoiled W atoms on W/Si interface due to bombardment of 100 eV Ar ion hitting the Si on W layer. The recoil distribution graph has been shifted on X-axis (depth direction) for clarity, Left side show W distribution when top Si layer is 1.5 nm thick and right side when Si is 1 nm thick. W/Si interface has been marked as black line in the graph.

when the top layer of Si of 1.5 and 1 nm thickness is bombarded with 100 eV ions/neutrals. Si layer is on the left side of the interface line and W is on the other side. The recoil distribution graph has been shifted on X-axis (depth direction) for clarity. It can be clearly seen than when Si layer is 1.5 nm thick little amount of W is diffusing towards Si layer but when Si layer thickness was reduced to 1.0 nm large recoil movement of W on Si side of the interface. These simulations support the observations made above from XRR fitting that when thickness of Si layer is less than 1.5nm more intermixing is expected. This analysis points out that the reflected neutral not only re-sputter the Si layer but also produce intermixing at the buried interface of Si and W if thickness of Si layer is below 1.5 nm. This implies that the real limiting factor for making sharper interface at shorter periods is controlled by hitting of reflected neutrals and ions.

Walton et.al.[6] had observed that shortest period multilayer of W/ B_4C which can be deposited without appreciable loss in reflectivity is 1.5 nm while in W/Si case it is 2.7 nm. Common explanation for this observation is that difference must be due to the fact that B_4C

being a compound is more resistant to diffusion compared to Si. But the observed interface mixing is bombardment induced and from our studies the answer for sharper interface should be that either B_4C must be resistant to bombardment induced intermixing or energy of the reflected neutrals should be low in Walton's case of magnetron sputtering. As we know that energy of reflected neutrals is of same order in both ion beam sputtering and magnetron sputtering. Hence, B_4C must be resistant to damage due to neutrals.

4.1.5 Comparison of damage resistance for different combinations

To compare the damage resistance of Si compared to B_4C and C which are popular choices of spacer layer for fabricating hard x-ray mirrors we did TRIM simulations in which all these layer were bombarded with 100 eV Ar ions. From figure (4.9) it is clear

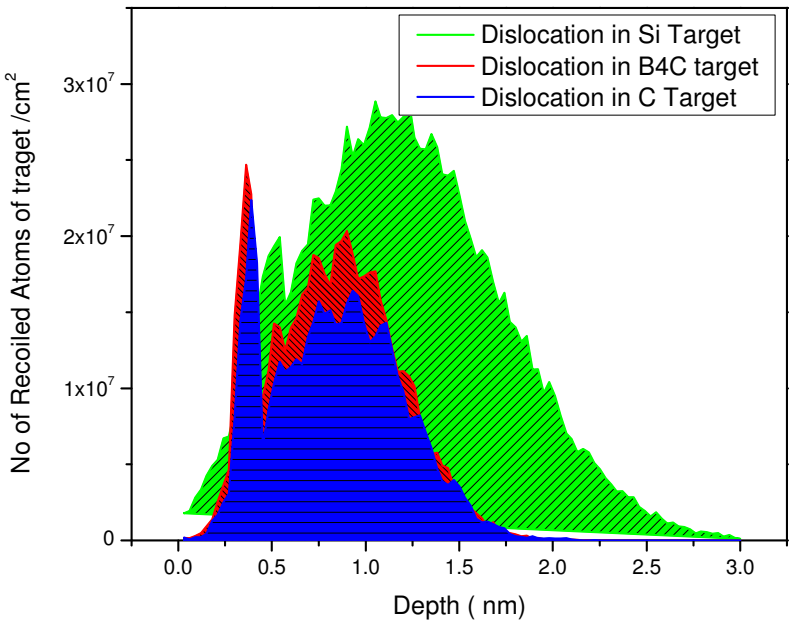

Fig 4.9 Damage profile produced due to hitting of 100 eV ions/neutrals on 3 nm layer of Si B_4C and C layer.

that damage extends much deeper up to ~ 2.2 nm in case of Si and in case of both B_4C and C it extends up to 1.5 nm. This proves that indeed both B_4C and C have larger damage resistance from reflected neutrals compared to Si. This is happening due to large lattice binding energy, surface binding energy and displacement energy of B_4C and C compared to Si. This seems a major reason why we are able to produce multilayers with sharper interface with C and B_4C. To confirm this observation we fabricated few bi layers of W/C and W/B_4C and tri layers of W/C/W and W/B_4C/W and analyzed the interface with XRR. The observations were following; the interface roughness of C layer in bilayer was 0.5 nm and in tri layer increased to 0.55nm. This indicates that depositing W on top of C does not change the interface roughness much. In case of B_4C in bilayer samples its roughness was 0.65nm and in trilayer it increased to 0.7nm. In this case also, not much change of interface roughness was observed due to W layer deposition but the intrinsic roughness on B_4C layer was high in bilayer. This might be due to charging of B_4C target during deposition. Because B_4C is highly insulating Ar ions hitting the target may not have got neutralized and charging of target surface must have reduced the energy of incident ion because of surface charging. This in turn has reduced the energy of sputtered atom which has manifested in terms of increased roughness of B_4C layer in the bilayer sample. Depositing B_4C with rf source should produce favorable results. Further we fabricated few multilayer of W/C and W/ B_4C and compared the reflectivity performance at 8 keV. Figure (4.10) show that comparison of reflectivity of 3nm sample and 1.74 nm samples. It is clearly visible that in 3 nm sample there is not much difference in the first Bragg peak reflectivity of all W/Si W/C and W/ B_4C multilayers. But in case of 1.74 nm sample reflectivity of W/C is way ahead of W/Si. The difference in reflectivity is even more significant because the W/Si sample had 20 layer pairs and W/C sample had only 10 layer pairs. The reason for this difference is that intermixing is high in W/Si sample compared to W/C sample in 1.7 nm sample. In 3 nm samples as the thickness of spacer layer is large enough to stop intermixing that is why not much difference in the reflectivity is seen. These observations guided us to fabricate some more samples of W/B_4C in a magnetron sputtering system in which B_4C could be deposited with rf source and carry out a detailed investigation of the interface on this combination.

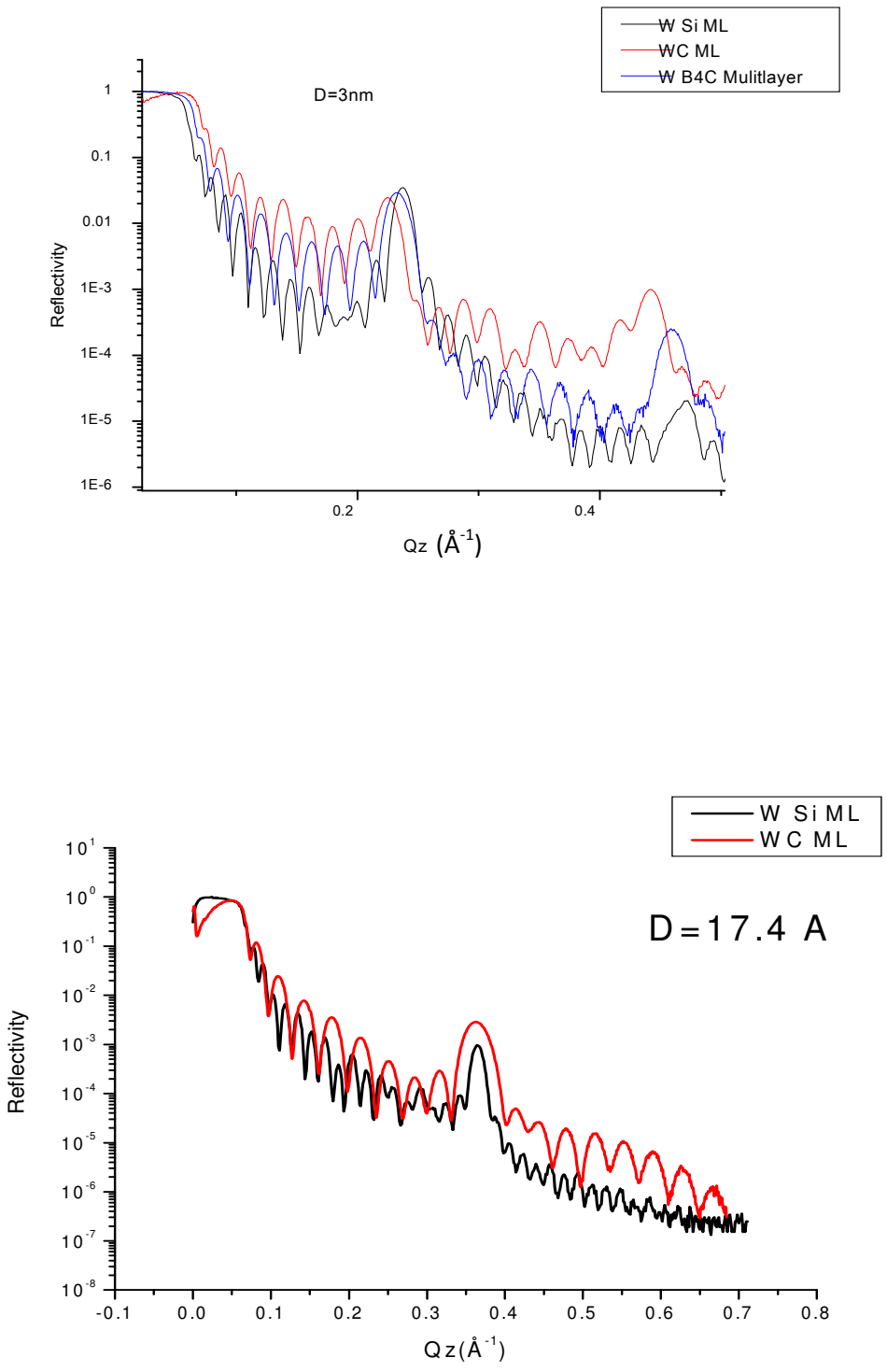

Fig. 4.10 Comparison of reflectivities of 3 nm (top) period W/Si, W/C and W/B_4C multilayer. (bottom) comparisons of 1. 74 nm period multilayer of W/Si and W/C.

4.2 Studies on W/B_4C multilayers

As explained in previous section that if W/ B_4C is deposited with magnetron sputtering it should be possible to get much lower interface roughness compared to W/Si. To check this possibility we decided to carry out a study on W/B_4C system. Walton et.al.[6] have reported systematic investigation of W/B_4C multilayer of periods changing from 5nm to 0.5 nm. They have investigated the microstructure of the films by x-ray reflectivity and cross-sectional TEM. They have found that that interface width reduces with period thickness and individual layers become discontinuous when period thickness goes below 1.5 nm. They also observed expansion of W rich layers by 60-80 % from their nominal value. This study gives an insight of changes in microstructure occurring due to period reduction. In their reflectivity fitting analysis they have not estimated the density and roughness of W and B_4C layer independently. They have found that the interface width reduces with period thickness and individual layers become discontinues when period thickness goes below 1.5 nm. According to our analysis of W/Si samples, interface roughness should increase on period reduction due to bombardment induced intermixing. Also, in their reflectivity fitting analysis they have not estimated the roughness of W and B_4C layer independently. We decided to make sample of W/B_4C with varying periods and carry out a detailed fitting of XRR data to get complete information about roughness, thickness, and density of individual layers in the multilayer. If samples have less number of layer pairs doing a detailed fitting and analysis becomes easier and it would be possible to deduce more information for example the minimum thickness of each layer thickness at which they remain continuous in ultra short period samples. Multilayer samples with periods in the range of 1.3- 4.0 nm and 20 layer pairs were used in this study. The structures of as deposited and vacuum annealed samples were studied using hard x-ray reflectivity (XRR), x-ray diffraction (XRD) and Transmission electron microscopy (TEM).

4.2.1 Experimental Details

The multilayer samples were deposited using magnetron sputtering system as discussed in chapter 2. Si (100) wafers, after ultrasonically cleaning first in acetone and then in methanol were used as substrate. Native silicon oxide layer was not removed from substrate. The base pressure in the process chamber was of the order of 10^{-8} mbar, and Ar pressure during the

deposition was $5x10^{-3}$ mbar. The power of W target was varied from 80-130 W and rf power of B_4C target was 700 W. To deposit the shorter period W/ B_4C multilayers, lesser power was applied on W target to reduce the deposition rate. Eight samples marked as A-H were made.

Sample Name	W layer Thickness (nm)	B_4C layer Nominal Thickness (nm)	B_4C layer Thickness (nm)	W Layer Roughness (nm)	B_4C Layer Roughness (nm)	W density g/cc	B_4C density g/cc	Total Period	First Bragg Peak reflectivity (%)
A	1.60 ±0.02	2.6	2.43 ±0.02	0.25 ±0.03	0.28 ±0.03	16.4 ±0.3	2.2 ±0.15	4.03 ±0.04	63
B	1.72 ±0.02	2.2	2.05 ±0.02	0.24 ±0.03	0.29 ±0.03	16.4 ±0.3	2.2 ±0.15	3.77 ±0.04	58
C	1.69 ±0.02	2.0	1.85 ±0.02	0.29 ±0.03	0.37 ±0.03	16.4 ±0.3	2.2 ±0.15	3.55 ±0.04	47.9
D	1.0 ±0.01	1.6	1.42 ±0.02	0.30 ±0.03	0.35 ±0.03	16.4 ±0.3	2.2 ±0.15	2.42 ±0.03	13.8
E	0.97 ±0.01	1.2	1.05 ±0.02	0.22 ±0.03	0.35 ±0.03	16.4 ±0.3	2.2 ±0.15	2.02 ±0.03	5.7
F	0.85 ±0.01	1.1	0.95 ±0.02	0.30 ±0.03	0.45 ±0.04	16.2 ±0.3	2.4 ±0.15	1.8 ±0.03	2.1
G	0.8 ±0.01	0.9	0.72 ±0.01	0.28 ±0.03	0.42 ±0.04	16.2 ±0.3	3.0 ±0.2	1.52 ±0.02	0.8
H	0.8 ±0.01	0.8	0.5.2 ±0.01	0.31 ±0.03	0.5 ±0.04	15.7 ±0.3	5.6 ±0.3	1.32 ±0.02	0.07

Table 4.3 Details of nominal thickness, estimated thickness, density, roughness, for each layer and total period along with first order Bragg peak reflectivity all deposited samples.

In our samples nominal thickness of B_4C layer was continuously reduced from 2.6 to 0.8 nm and the nominal thickness W layer was kept around 1.7 nm in samples A-C and around 0.9 nm in samples D-H as given in Table (4.3). Thickness of W was not reduced below 0.9 nm as there is a possibility that it may become discontinuous below this thickness. By systematically reducing the B_4C layer thickness it would be possible to find out minimum thickness of B_4C, at which it remains continuous.

4.2.2 Results and Discussion

All the measurements were performed with a step size of 0.005˚ in theta axes, which is sufficient to observe any small changes in thin films. Specular reflectivity was measured with 100 micron slits in θ /2 θ geometry over the range of θ = 0˚ to 3 to 5˚ depending upon the sample. Successive scans of same sample after removing and replacing on the diffractometer produced changes in peak position by less than 1 % and in peak reflectivity by less than 3 % of measured value. Grazing incidence x-ray diffraction (GIXRD) was also done on some samples to find out amorphous or crystalline state of layers. Figure (4.11) shows the XRR experimental

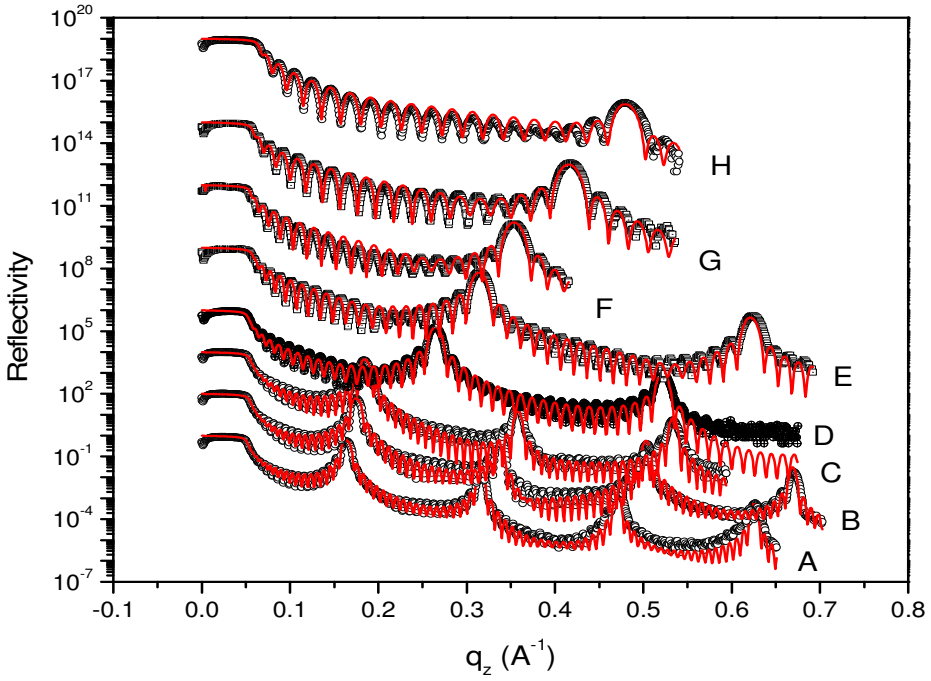

Fig. 4.11 X-ray reflectivity curves both experimental (open circles) and fitted (solid lines) as a function of wave vector transfer 'q_z ($Å^{-1}$) for all the as deposited samples (A-H)

profiles (open circles) along with fitted curves (solid red lines) as a function of wave vector transfer q = 4πsinθ/λ for all the as deposited samples (A-H). One can see that Kiessig oscillation

in all as deposited samples are clearly visible and are matching well with the simulated profile. Simulations show that in samples with shorter period (e.g. F- H) even a thickness error of less than 0.05nm would spoil the regularity of Kiessig oscillation due to the uncertainty in total period thickness. Estimated values of the average thickness, roughness and density of W and B_4C layer along with first Bragg peak reflectivity for all the as-deposited samples are listed in Table (4.3). As mentioned earlier we wanted to keep W thickness around ~ 0.9 nm in samples D-H and around ~ 1.7 nm in samples A-C and reduce the B_4C thickness continuously. From table (4.3) it can be seen that in as deposited samples estimated thicknesses of W and B_4C layers are close (within 0.2 nm) to the nominal values. This observation of estimated W layer thickness emerging same as nominal is differing with the observation made by Walton *et.al*. where they have observed swelling of W layer as high as 80% more than nominal thickness due to intermixing of W into B_4C and producing a W rich layer. In our samples no such W rich inter layer was observed. In XRR analysis we tried to examine the presence of such a layer by inserting the interlayer in the model. In most of the samples attempts to insert an interlayer spoiled the quality of fit indicating absence of such a layer. If any interlayer thicker than the interface roughness was there in our samples it should have been certainly detected by XRR measurements.

In the as deposited samples density of W layer was estimated to be 16.4 g/cc which is 15 % less than the bulk value and density of B_4C layer is 2.2 g/cc which is 12 % less than bulk. The reduction is expected as by sputtering method one does not get density equal to bulk density because of porosities getting developed due to extremely high quench rate in the film during growth. Density of W layer has remained constant in samples A to E whereas in sample F and G slight reduction to 16.2 g/cc is observed and in sample H density has reduced to 15.7 g/cc indicating that some intermixing of B_4C has happened in samples F,G and H. Density of B_4C layer has changed in as deposited layer for sample F to 2.4 g/cc (10 % more than samples A - E) and further increased in samples G and H to 36%, and 154% more respectively. This increase in density is signifying that W is getting mixed in B_4C layer in these samples. High density of B_4C layer in the as deposited sample H suggests severe intermixing. Additionally it is interesting to note that highest density of W layer obtained by Ion beam sputtering was 7 % more than that observed in these samples. This indicates that ion beam sputtering is producing metal films with better packing density.

Looking at the variation in roughness of layers we find roughness of W layer has remained constant between 0.22-0.3 nm for all periods as shown in figure (4.12). In case of B_4C layer roughness is showing a non linear increasing trend with thickness reduction. The ratio of magnitude of roughness to layer thickness is increasing very rapidly as the period is reduced and

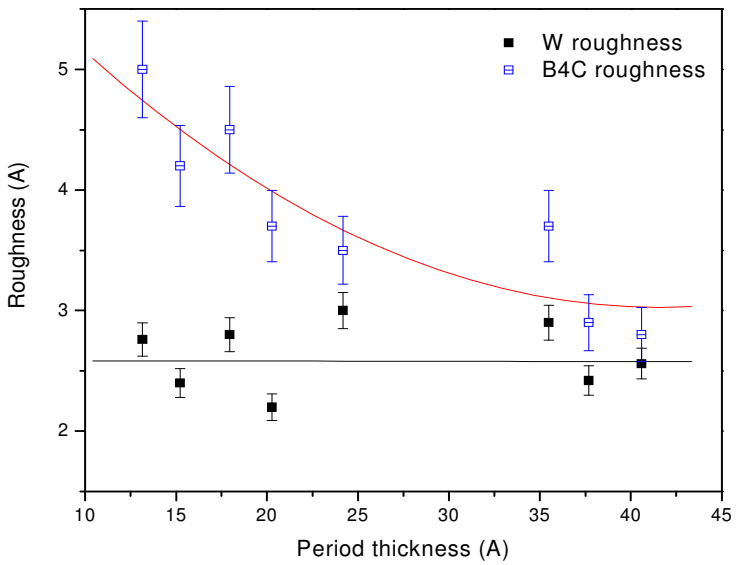

Fig. 4.12 Variation of roughness of W and B_4C layer with multilayer period

reaches 50 % of the film thickness for samples F, G & H. This high relative roughness ratio indicates that coverage of B_4C layer may not be complete in these samples. Tabulated density values of B_4C gives a clear picture of this variation in density with film thickness. It can be seen from Table 4.3 that when B_4C layer thickness goes below 1.0 nm its density begins to increase indicating presence of W in the B_4C layer. When, B_4C layer thickness goes below 0.7 nm, its density increases more rapidly suggesting increased intermixing and loss of density contrast along with fall in peak reflectivity. Simultaneous increase in roughness of B_4C layer along with increase in density of B_4C in the as deposited samples F-H confirms that W is intermixing and interface roughness is increasing. This increase in roughness must be due to enhancement in chemical roughness because of intermixing. One can draw following inference from these observations (1) when B_4C layer thickness is above 1.0 nm no mixing of W in B_4C happens,(2) when B_4C thickness goes below 1.0 nm some amount of W gets implanted in B_4C layer, (3)

when B_4C layer thickness goes below 0.7 nm severe intermixing of W takes place and (4) increased intermixing is the cause of reduction in Bragg peak reflectivity of multilayers. This kind of intermixing can have influence on the long term stability and performance of the multilayer mirror.

To understand the degradation in the interface character of low thickness samples, simulation of damage produced through hitting of B_4C layer by reflected Ar ion/ neutral from the W target was carried out. It was found using TRIM that 30% of Ar ions hitting the W target can get reflected and 25% of the reflected ions can have very high energies nearing 100 eV or more. This estimate matches with reference[21]. Calculations were done to find out recoil distribution of W and B_4C due to hitting of 100 eV ion/neutrals. Simulations were done for three cases in first case we had 1.1 nm of B_4C layer on the top of 1.0 nm W layer and in other cases thickness of B_4C layer was reduced to 0.9 and 0.5 nm. All the simulations were done for hitting by just 20000 particles of 100 eV energy. Figure (4.13) shows the recoil distribution of B_4C and W atoms when the top layer of B_4C of 0.5, 0.9 and 1.1 nm thickness is bombarded with 100 eV ions/neutrals. The recoil distribution graph has been shifted on X-axis (depth direction) for clarity. It can be clearly seen than when B_4C layer is 1.1 nm thick little amount of B_4C is recoiling towards W layer and no event of W recoil towards B_4C layer was recorded. However, when B_4C layer thickness was reduced to 0.9 nm more recoil of both W and B_4C was seen on each side of the interface and in case of B_4C being 0.5 nm large movements of both species was seen on either side. These simulations support the observations made above from XRR analysis that when thickness of B_4C layer is less than 1.0 nm more intermixing is expected and B_4C layer becomes nearly discontinuous at 0.5 nm thickness. This analysis again points out that the cause for making sharper interface at shorter periods is controlled by hitting of reflected neutrals and ions. From these observations we can conclude that when B_4C layer thickness goes below 1.0 nm intermixing of W starts in the B_4C layer. The intermixing is happening due to bombardment of high energy reflected ion/neutrals as confirmed by simulations. Lowest continues thickness of B_4C have been estimated to be 1.0 nm. By no other method than adopted in this study we could have deduced lowest continuous film thickness of the insulating B_4C layer. From these observations it can be concluded that multilayer with W around 0.8 nm and B_4C around 1.0 nm can be deposited with lowest interface roughness and intermixing. Our observations are in contrast with earlier work done by Walton et. al. We have observed increase in B_4C layer

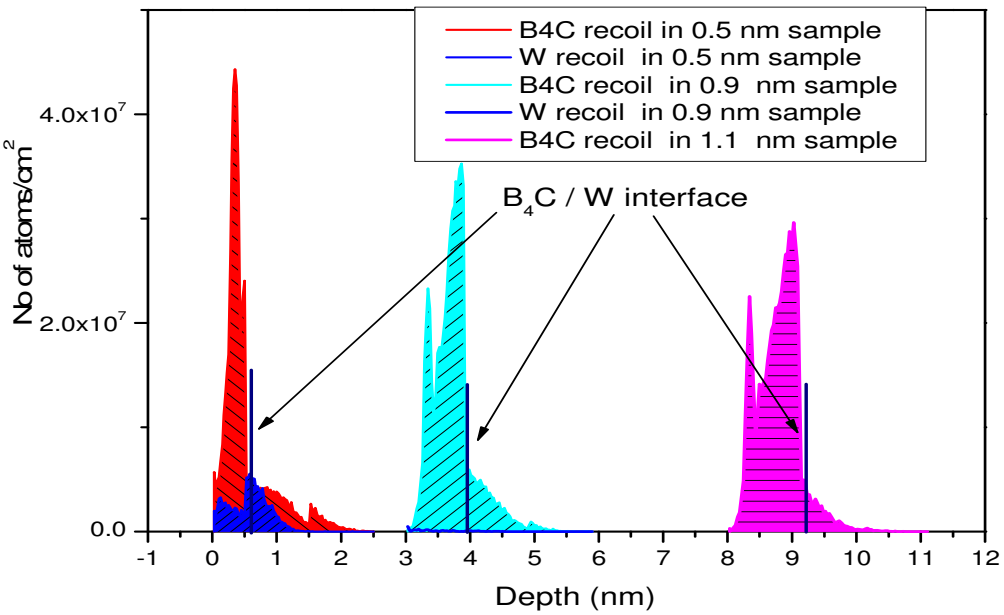

Fig. 4.13 Recoil distribution of B_4C and W atoms when samples having top layer B_4C of 0.5, 0.9 and 1.1 nm thickness above 1.0 nm W layer is bombarded with 100 eV ions/neutrals. The recoil distribution graph has been shifted on X-axis (depth direction) for clarity.

roughness with period reduction and no increase in W layer thickness which is differing with observations by Walton et.al. Present study reveals that 1.8 nm period is the smallest period which should shows sharp and stable interface.

4.2.3 Annealing Studies

To check the thermal stability of these multilayer samples some of the samples were annealed. The annealing treatments of multilayer samples were carried out as follows. The multilayer samples were placed in aluminum boat inside the quartz tube. The quartz tube is turbo molecularly pumped down to a base pressure of the order of 10^{-6} mbar using a turbo molecular pump. All the multilayer samples were heated at 500^0C for duration of 4 h. The furnace was capable of reaching the set temperature within 25 min. The samples cooled down to room temperature over several hours.

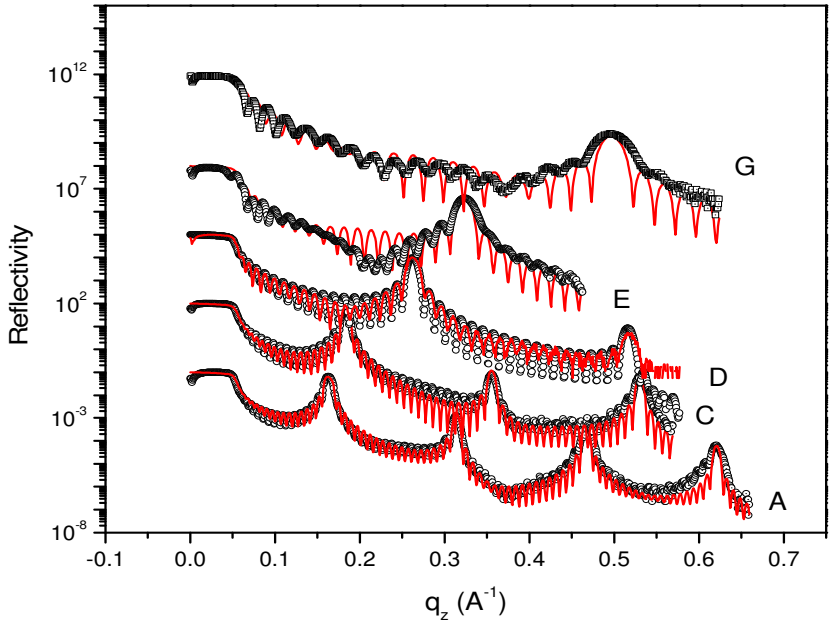

Fig. 4.14 X-ray reflectivity curves both experimental (open circles) and fitted (solid lines) as a function of wave vector transfer 'q_z ($Å^{-1}$) for samples annealed at 500 ^{0}C for duration of 4 hours

Figure (4.14) shows XRR data with fitted curve for annealed samples. In case of annealed samples loss in regularity of Kiessig oscillations can be seen for samples E and G indicating thickness changes are happening in the structure of the films due to annealing, where as in samples A,C and D no changes in regularity of Kiessig oscillations are seen demonstrating that large period thickness samples are stable after annealing. It can be seen form table (4.4) that all the multilayers have shown changes in period and peak intensity due to annealing. Results of changes due to annealing are listed in Table (4.4). It is clearly visible from the table that samples of 2.4 nm and larger period show expansion of ~ 0.03 nm after annealing and samples below this period show variable compaction which increases with reduction in the period thickness. This kind of expansion and contraction due to annealing has been observed earlier by Jankowaski et.al.[22]. They observed ~ 5% (0.2 nm) expansion in 4.0 nm W/B_4C sample and 6% (0.12 nm) contraction in 2.0 nm samples. They argued that all structures relax upon vacuum annealing hence contraction of period is obvious but expansion in 4.0 nm sample is attributed to probable crystallization of thicker W layer present in 4.0 nm sample. But they did not show proof of such

Sample Name	W layer Thickness (nm)	B_4C Thickness layer (nm)	W Layer Roughness (nm)	B_4C Layer Roughness (nm)	W density g/cc	B_4C density g/cc	Total Period / (Period before annealing)	First Bragg Peak reflectivity / (Reflectivity before annealing)
A	1.60 ±0.01	2.46 ±0.02	0.25 ±0.02	0.27±0.03	16.4	2.2	4.06/ (4.03)	65.5/(63)
C	1.7 ±0.01	1.88±0.01	0.29±0.02	0.37±0.03	16.4	2.2	3.57/ (3.77)	49.5 /(47)
D	1.0 ±0.01	1.44±0.01	0.35±0.02	0.45±0.03	16.4	2.2	2.44/ (2.42)	10/ (13.8)
E	0.94±0.01	1.02±0.02	0.31±0.02	0.43±0.03	16.4	2.9	1.96 /(2.02)	3.9 / (5.7)
G	0.7±0.01	0.57±0.02	0.27±0.02	0.48±0.03	15.0	3.7	1.27/ (1.52)	0.06 (0.8)

Table 4.4 Details of estimated thickness, density, roughness, for each layer and total period along with first order Bragg peak reflectivity all annealed samples.

a change occurring in the structure by diffraction. Also, they had analyzed only two period thicknesses in the study. Our observation is different; they observed much larger Expansion and contraction than what is observed in present study. Expansion changes observed by us were so small (0.03 nm) that we repeated our measurement and confirmed that indeed it was repeatable and not measurement error. Our explanation to the observed expansion in present study is based on following points. Magnetron sputtered W films grows with high compressive residual stress and magnitude of stress increases with thickness[23] , hence samples with larger period must be growing with high amount of residual stress. Windt *et.al.* [24] also observed that W/B_4C multilayers grown with magnetron sputtering grow with high residual stresses. This indicates that on annealing the compressive stress locked in the film must be getting relaxed leading to slight increase in period. The change in period thickness should accompany change in density but XRR can detect change in density with ~ 5% accuracy only and change in thickness with better than ~ 1% accuracy. That is why we do not see any major change in density of layers in large thickness samples. In case of samples below 2.4 nm stresses in the films are not very high hence these samples show compaction due to porosities getting annihilated on annealing and contraction is mainly observed in the B_4C layer. More compaction is seen in sample G where B_4C thickness is low (0.72 nm) and discontinuity is high.

Another observation from annealed samples is that estimated density value of W layer is comparable to as deposited samples A to E. In case of sample G some reduction of density was

noticed (8.5 % less than as deposited value). This shows that due to annealing, further diffusion of boron has happened in W layer. In case of B_4C layer only E and G samples have shown increase in density confirming both W and B_4C are diffusing and intermixing into each other due to annealing in these samples. These observations show that samples G is more susceptible to damage due to annealing whereas samples A and B have not shown any influence of annealing on their interface character and samples D and E have shown moderate change in the interface roughness. Multilayers with larger period thickness are more stable whereas smaller period thicknesses have shown sensitivity to annealing. It can be seen in table 4.4 that in samples A and C gain in reflectivity is seen due to period expansion, moderate drop is seen in samples D (72 % of as deposited value), E (68% of as deposited value) and very large drop for sample G (7.5 % of as deposited value). It can be concluded that samples with period 2.0 nm (E) and above show good thermal stability and samples below this value show sensitivity to annealing and drop in Bragg peak reflectivity due to annealing. This indicates that as deposited samples with unmixed interface show good thermal stability also.

To corroborate if change in period of multilayers due to annealing has any relationship with change in crystalline state of films grazing incidence x-ray diffraction was carried out on these samples. GIXRD pattern did not show much change in structure due to annealing. Figure (4.15) shows GIXRD pattern of sample A and sample E before and after annealing. In sample A broad peaks of W (110) and (211) plane are clearly visible indicating that W layer is polycrystalline with very small grain size. The grain size of sample A estimated from peak width comes about 2.0-2.5 nm. In case of sample E (110) peak is very broad and (211) peak is not visible implying that W layers are either very fine grained nano-crystalline or amorphous in these thin layers. One sharp peak in the center of the graph is from the Si substrate. No change in the width of the peaks is visible after annealing of samples. This confirms that annealing is not changing the crystal structure of layer in these samples. Hence, this cannot be the cause of variation in period thickness due to annealing as explained by Jankowaski et.al[22]. No observation of any new phase in the multilayer due to annealing is similar with the measurement done by Siffalovic *et.al*[25] . In their study they examined influence of rapid thermal annealing for 120 second on W/B_4C sample of 1.37 nm period with 80 layer pair and found that at 500 ˚C there was no new phase formation found and at 900 ˚C only some indication of chemical reaction between W and B was found.

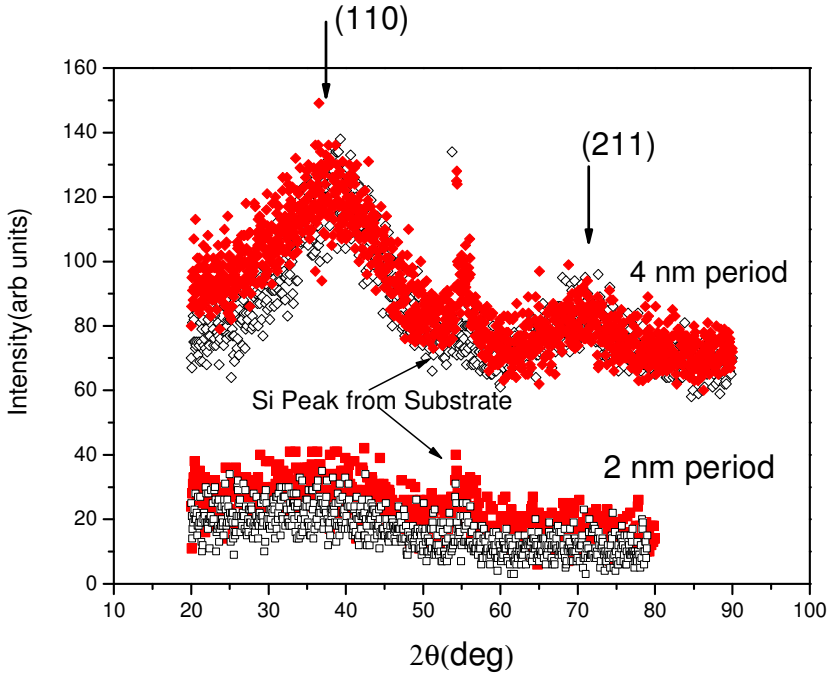

Figure 4.15: GIXRD pattern before and after annealing of samples A (open diamond before annealing, filled diamond after annealing) and E (open rectangle before annealing, filled rectangle after annealing) measured at incidence angle of 0.6 deg.

Examination of the interface structure was carried out by cross sectional TEM (CSTEM) of as deposited samples E (D= 2.02 nm) and G (D=1.52 nm).The layer structure of the shorter period samples is shown in figure (4.16). In this figure black layer represents W and white layer represents B_4C. It is visible that layer structure is maintained and layers in the multilayer are visible as separate layers in both samples. But contrast between W and B_4C layer is much better in sample D compared to sample G. This also confirms that intermixing is high in sample G. Multilayer layer period thickness estimated from the TEM image is 2.0 nm for sample E and 1.5 nm for sample G which matches with the thickness estimated by XRR. No swelling of W layer is seen as observed by Walton *et. al*. A closer look at the image in sample G it can be clearly seen that at many places the W layers are connected across few B_4C layers (some of such locations are encircled in the figure). Another interesting observation is that in spite of intermixing overall multilayer periodicity is maintained. It can be concluded that W layer is continuous in both samples and B_4C layers is significantly discontinuous in sample G and B_4C

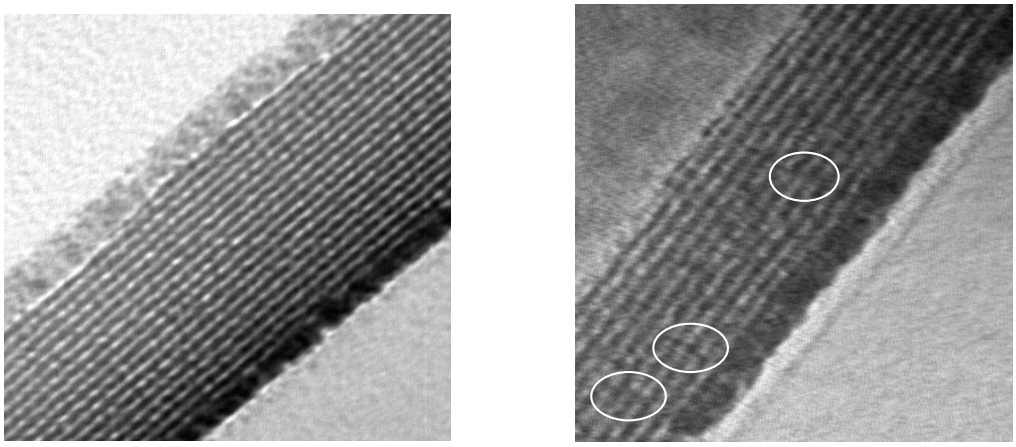

sample E sample G

Fig.4.16 : Cross sectional TEM of sample E (D= 2.02nm) and G(D=1.52nm)

layer is slightly irregular at some places in sample E. These images substantiate the structural analysis done on the basis of XRR data.

4.2.4 Development of Large layer pair samples

After all the optimization and annealing studies we carried out deposition of large layer pair multilayer samples of W/B_4C. Since, it was concluded that the minimum thickness of W and B_4C which can be deposited as continuous layer were 0.9nm and 1 nm. To check the evolution of interface roughness with increasing bi-layer number, N we fabricated multilayer with period 2 nm and bi-layer numbers 20, 40, 100, 200 and 300. It was observed that intefaces were becoming smoother with increasing N and diffused component was reducing with increase in number of layer pairs. Reflectivity of first Bragg peak for sample with 100,200 ad 300 layer pair sample is shown in figure (4.17). The 300 layer pair, 2 nm period sample has shown 1.2% energy resolution at 8 keV and 59% reflectivity. The achieved reflectivity and resolution are comparable with the best multilayers deposited by magnetron sputtering [26]. The high refelctivity and high resolution proves that devloped multilayer mirrors are suitable to be used as a monochromater or grazing incidence mirror in hard x-ray region.

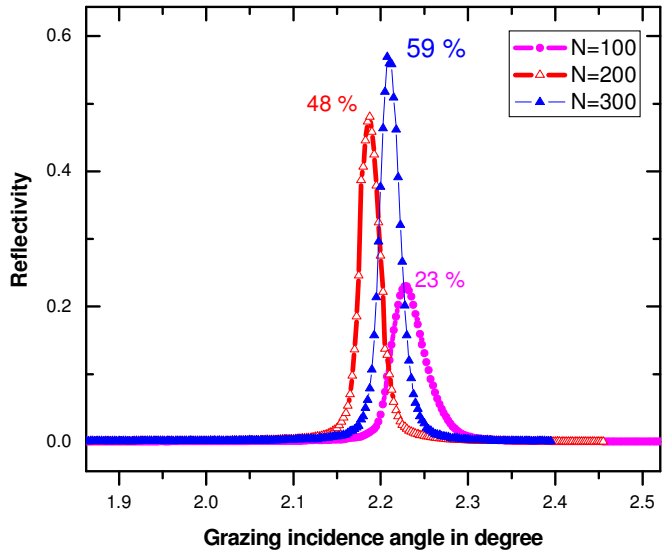

Fig. 4.17 Measured x-ray reflectivities of W/B_4C multilayers with variable bi-layer numbers 100,200 and 300 at Cu-K_α radiation (8.05 keV).

To further characterize our mirrors we have measured the reflectivity of these samples at BESSY. Normal incidence reflectivity near the C-K edge was measured at the BESSY-II optics beamline. Wavelength versus reflectivity measurement was carried out at 85° incidence angle. The results with simulations are shown in shown in figure (4.18) red line in figure shows the simulated pattern. The soft x-ray reflectivity pattern showed reflectivity of 1.85% at 40.24 Å. This reflectivity is comparable with that obtained by Seely *et.al*.[27]

Hard x-ray reflectivity fitting of reflectivity data revealed that the sample had W thickness of 9.2 Å with 2.8 Å roughness and B_4C layer of 11.15 Å with 3.5 Å roughness. Fitting of soft x-ray normal incidence reflectivity could be done, using IMD[28], with same parameters as obtained by hard x-ray reflectivity except that roughness had to be increased to 3.2 Å for W layer and 3.7 Å for B_4C layer. The optical constants used for fitting were not required to change; this confirms layers have not got intermixed.

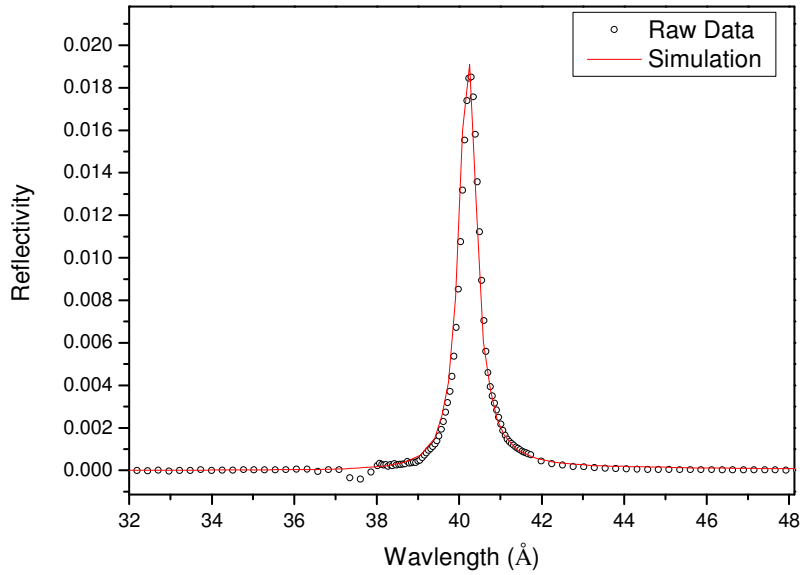

Fig. 4.18 Wavelength versus reflectivity pattern measured at 85° incidence angle along with simulation (red line)

4.2.5 Stresses in Multilayers

One more comment about stress in our multilayers. In our explanation of annealing studies on W/B_4C we have presumed that the cause of expansion of multilayer period was relaxation of stress but we have not given any proof of that. The proof of high stress in 4 nm period multilayer we got when we tried to deposit larger layer pair samples of 4 nm period. We could deposit 50 layer pair samples without any problem but when we deposited 100 layer pair samples of 4nm period. Multilayer started peeling off few hours after deposition confirming that

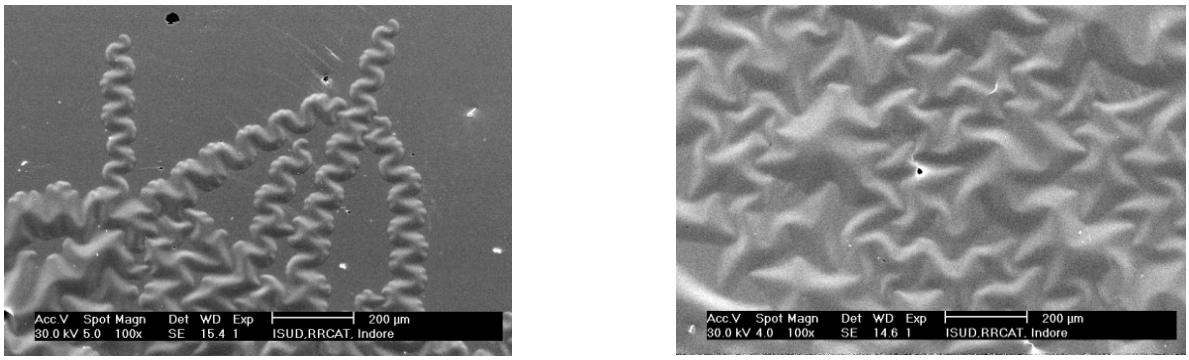

Fig. 4.19 SEM image of peeled off samples of 4 nm period of 100 layer pair

these samples are under very high stress. Figure (4.19) shows the SEM image of peeled off samples. Crimpling of the film can be clearly seen the picture. This confirms that 4nm period sample do have huge amount of compressive stress which increase with increasing number of layer pairs.

4.2.6 Summary

SRIM simulations were done for damage calculations when Si, C and B_4C layers were bombarded with 100 eV Ar ions. It is observed from the calculations that both B_4C and C have much larger damage resistance compared to Si. This is happening due to large lattice binding energy, surface binding energy and displacement energy of B_4C and C compared to Si. This seems a major reason why we are able to produce multilayers with sharper interface with C and B_4C. These results were confirmed by depositing bilyers and trilayers of W/Si, W/C and W/B_4C. It was observed that in W/Si/W trilayers the interface roughness of Si layer was increasing from 0.4 in bilayer to 0.9nm in trilayer, whereas in case of W/C/W and W/B_4C/W trilayers not much increase in the interface roughness of C or B_4C was observed. This confirmed that C and B_4C being more resistant to damage by reflected neutrals should produce sharper interface.

Major observations of our study on W/B_4C multilayers between 1.2 to 4 nm periods are the following. It is observed that when B_4C layer thickness goes below 1.0 nm intermixing of W starts in the B_4C layer. The intermixing is happening due to bombardment of high energy reflected ion/neutrals as confirmed by SRIM simulations. Lowest continues thickness of B_4C have been estimated to be 1.0 nm. From these observations it can be concluded that multilayer with W around 0.9 nm and B_4C around 1.0 nm can be deposited with lowest interface roughness

and without intermixing. Our observations are in contrast with earlier work done by Walton *et. al*.[10] and Jankowski *et. al*. We have observed increase in B_4C layer roughness with period reduction and no increase in W layer thickness which is opposite of observations by Walton et.al. The measured Bragg peak reflectivity after annealing of different samples show that samples of 2.0 nm period or above do not show much degradation in the reflectivity of first Bragg peak. Also, density of W and B_4C layers has remained unchanged after annealing in these samples indicating their stability. Present study reveals that 1.9 nm period is the smallest period which should shows sharp interface and good thermal stability for W/B_4C combinations. Our studies on large layer pair samples have confirmed these conclusions. This is very useful information for developing high heat load short period multilayer mirrors. We could fabricate 2 nm period 300 layer pair samples with best reflectivity and good resolution for hard x-ray applications.

Our study carried out on W/Si system had concluded that minimum thickness W/Si multilayer which could be deposited without intermixing was ~2.8 nm. It was suggested that using a compound spacer layer would reduce the probability of chemical reaction between W and the spacer layer. Hence it would be possible to produce a multilayer with even lower periods without intermixing. Present study has demonstrated that indeed it is the case. But the reason for achieving lower roughness and lower thickness continuous layer is resistance to damage due to bombardment of reflected neutrals. Simulations with SRIM have shown that Si layer shows two times larger damage due to reflected Ar neutral of around 100 eV energy than B_4C layer.

On the basis of this study we can conclude that reflected neutrals play a important role in growth of multilayer mirrors. They influence the growth in two ways (1) re-sputter the low Z layer and make it rough (2) If thickness of low Z layer is less than 1.5 nm for Si layer and 1 nm for B_4C layer than reflected neutrals produces intermixing at the buried interface below low Z layer by creating a collision cascade. It this way these neutrals reduce the contrast between low Z and high Z layers. To further extend the period to shorter lengths it would be required to reduce the damage from reflected ions /neutrals of low Z layer. Simulations using SRIM have shown that using Xe in place of Ar would reduce the number of reflected ion/neutrals to 25% of what is expected with Ar with slightly reduced energies. But use of Xe would reduce the sputter yields of B_4C by half. The thermal stability shown by these multilayers and lack of chemical reaction

between W and B_4C give an idea that depositing multilayer at higher temperatures than room temperature might help us in achieving even shorter periods with lower roughness.

References

1 Stefan P. Hau-Riege, Henry N. Chapman, Jacek Krzywinski, Ryszard Sobierajski, Sasˇa Bajt, Richard A. London, Magnus Bergh, Carl Caleman, Robert Nietubyc, Libor Juha,Jaroslav Kuba, Eberhard Spiller, Sherry Baker,Richard Bionta, K. Sokolowski Tinten, Nikola Stojanovic, Benjawan Kjornrattanawanich,7 Eric Gullikson, Elke Plo¨njes,9 Sven Toleikis,9 and Thomas Tschentscher , Physical Review Letters 98, 145502 (2007)

2 E. Spiller, Soft X-Ray Optics 1994 SPIE, Optical Engineering Press.

3 S.V. Bobashev, A.V. Golubev, Yu.Ya. Platonov, L.A. Shmaenok, G.S. Volkov, N.N. Salashchenko, V.I. Zayzev, Phys. Scripta 43, (1991) 356.

4 J. Kirz, C. Jacobsen, M. Howells, Quart. Rev. Biophys. 28, (1995) 33.

5 J.B. Kortright, M. Rice, S.-K. Kim, C.C. Walton, T. Warwick, J. Magn. Magn. Mater. 191, (1999) 79.

6 Walton C.C., Thomas G. and Kortright J.B. Acta mater. 46,(1998) 3767,

7 Windt, D. L. and Kortright, J. B., SPIE Press, Bellingham, WA, (1989), 246.

8 Phang, Y. H., Kariotis, R., Savage, D. E. and Lagally, M. G., J. appl. Phys., 72, (1992), 4627.

9 Christensen, F. E., Shou-hua, Z., Hornstrup, A., Schnopper, H. W., Flag, P. and Wood, J., J. X-ray Sci. Tech., 3, (1991), 1.

10 Stearns, D. G., J. appl. Phys., 71, (1992), 4286.

11 Jankowski, A. F., Makowiecki, D. M., Wall, M. A. and McKernan, M. A., J. appl. Phys., 65, (1989), 4450.

12 Hasan, M. M., Highmore, R. J. and Somekh, R. E., Vacuum, 43,(1992), 55.

13 B.A.Vidal, J.C.Marfaing, J.Appl.Phys., 65, (1989),3453.

14 A.Paul, J.Winghermuhle, Appl. Surface Science 252, (2006) 8151.

15 R. Balu, A.R.Raju , V.Lakshminayranan,S.Mohan, Mater.Sci. Eng(b) 123, (2005) 7.

16 S.M.Rossangel J. Vac. Sci and Tech. (A) 7, (1989), 1025.

17 "The Stopping and Range of Ions in Solids", by J. F. Ziegler, J. P. Biersack and M. D. Ziegler, SRIM 2008.

18 E.Franke . H.Neumann, M.Zeuner,W.Frank, F.Bigl, Surf. Coat. Technol. 97, (1997) 90.

19 M.J.H.Kessels, J.Verhoven, F.D.Tichelaar and F.Bijkerk , Surface Science 582, (2005) 227.

20 D.L.Windt, F.E.Chrisenten, W.W.Craig, C.Hailey,F.A.Harrison, M.Jimenez-Garete, R.Kayanaraman and P.H.Mao, J.Appl.Phys., 460, (1988)2000.

21 D.B.Bergstrom, F.Tian, I.Petrov, and J.E.Greene, Appl. Phys. Lett.,67 , (1995), 3102.

22 A. F. Jankowski, L. R. Schrawyer, and M. A. Wall, J. Appl. Phys. 68, (1990), 5162.

23 Shen Y.G. and Mai Y.W. Q. C. Zhang, D. R. McKenzie, W. D. McFall, and W. E. McBride Journal of App. Phys. 87(1), (2000), 177.

24 David L. Windt Proc. SPIE, (2007), 6688.

25 Peter Siffalovic, Matej Jergel, Livia Chitu, Eva Majkova, Igor Matko, Stefan Luby, Andreas Timmann, Stephan Volker Roth, Jozef Keckes, Guenter Alois Maier, Alexandra Hembd, Frank Hertlein and Joerg Wiesmann J. Appl. Cryst. 43, (2010), 1431.

26 http://henke.lbl.gov/multilayer/survey.html

27 J.F. Seely, G. Gutman, J. Wood, G.S. Herman, M.P. Kowaski, J. C. Rife, and W. R. Hunter, "Normal incidence reflectance of W/B4C multilayer mirrors in the 34-50 Å wavelength region," Appl. Opt. 32, (1992), 3541.

28 D.L.Windt " IMD: software for modeling the optical properties of multilayer films" Computer in Physics 12, (1998), 360.

Chapter 5

Development of Soft X-ray Normal Incidence Mirror

5.1.1 Introduction

Silicon-based multilayer systems have been developed in last two decades that have high normal incidence reflectance at photon wavelengths longer than the Si-L edge near 124 Å. This is a wavelength region where the absorption of silicon is low, as can be inferred from the optical constants for silicon, shown in Figure (5.1). The Mo/Si multilayer system is perhaps the most famous of all, providing normal-incidence reflectance approaching 70% just below the Si Ledge. The experimental performance of Mo/Si in the range from about 125-200 Å is roughly 85% of the theoretical maximum that would be obtained if it were possible to fabricate these films with perfectly smooth and sharp interfaces.

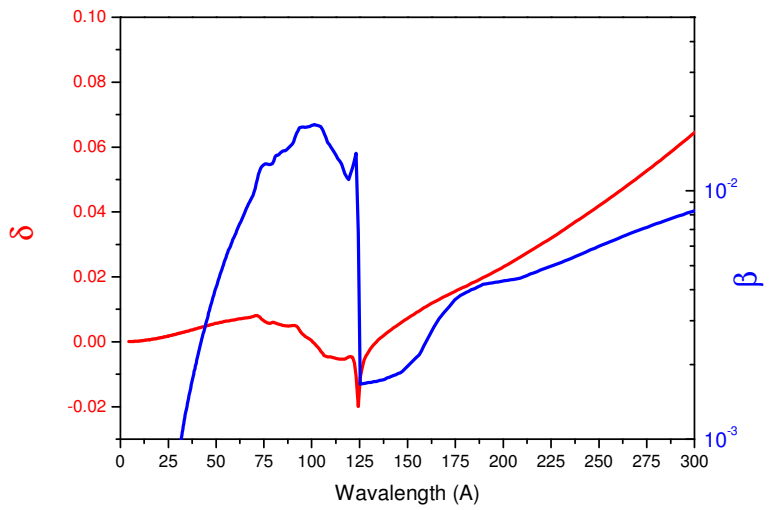

Fig. 5.1 Optical constant of Si

Due high normal incidence reflectivity Mo/Si multilayers are currently the most promising reflective coating for extreme ultraviolet (EUV) lithography activity operating at 13.6 nm wavelength. However, it has a severe drawback of poor thermal stability caused by negative heat of mixing between Mo and Si. The reflective properties of Mo/Si multilayers are directly correlated to the structure of the interface; broadening of the interface due to interdiffusion processes and roughness development significantly reduces the reflectivity [1,2]. Resultantly this structure undergoes interface degradation right after the deposition process. A number of studies have been performed to investigate the origin of Mo/Si intermixing and its dependence on the deposition parameters [3,4,5]. Our group has also carried out extensive analysis of Mo/Si multilayer and examined the Mo/Si interface using soft x-ray reflectivity[6],

and also used soft x-ray resonant reflectivity to investigate the chemical reaction happening at the interface[7]. This has resulted, in minimizing the intermixing but not totally eliminating it. This suggests that interlayer formation is an intrinsic property of the Mo/Si material pair and could present a fundamental barrier to achieve maximum optical performance [8]. Different approaches have been adopted in the past to overcome the interdiffusion and structural degradation problem by inserting a barrier layer of boron carbide or pure carbon between the Mo and the Si to prevent their intermixing [9]. However, all these efforts lead to significant compromise in reflectivity performance.

Rapid development of free electron laser (FEL) sources [10,11] generating ultra short EUV pulses have posed new challenges for the optics. X-ray pulses of very high intensity from these sources induce radiation damage [12,13]. The emerging technology requires improved optical components and therefore numerous research work is being carried out to find high stability and high reflecting multilayer mirrors [14,15].

Carbides of refractory metals (Mo, Nb) are known to exhibit excellent physical properties like high melting point, good electrical conductivity and extreme hardness. In the 10-20 nm wavelength region, the refractive index properties of these metal carbides are almost identical to their metallic constituents. Therefore, it is expected that a multilayer comprised of a refracting layer of metal carbide with a spacer layer of Si should exhibit a similar high reflectivity performance. Previous studies on carbide layers suggest that these carbides are non-stoichiometric and contain vacancies in the carbon lattice sites [16,17]. From multilayer point of view, the presence of unsaturated carbon in near vicinity of the metal species (Nb, Mo) may act as a barrier for direct chemical mixing with Si. Earlier attempts of putting a barrier layer of B_4C between Mo and Si was to prevent the chemical mixing of two species. However inserting an extra layer leads to phase variation in the waves reflecting from different interfaces at Bragg condition and thereby resultant phase mismatch reduces the overall reflectivity. Moreover, the barrier layer should be ultra-thin in order to minimize such phase mismatch which ultimately requires a stringent deposition control.

In order to find a stable arrangement for the wavelength range of interest we tried a compound layer of NbC instead of either pure Mo or Nb. Using the atomic scattering database of Henke *et al.* [18] it become clear that NbC compound gives similar refractive index contrast with silicon as shown in figure (5.2). It suggests that the optical constants of Mo and NbC are similar in the 10-20 nm wavelength region.

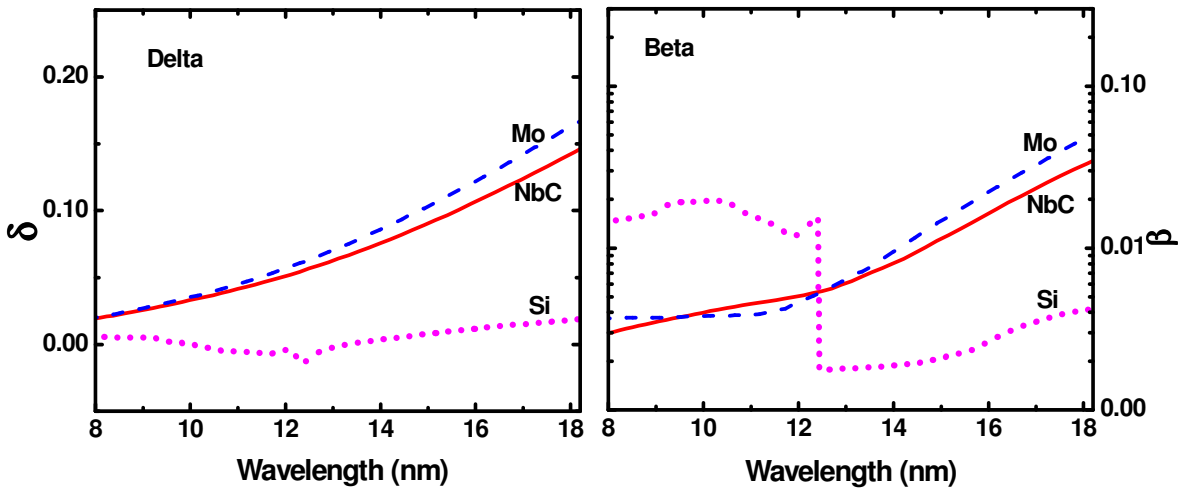

Fig. 5.2 A comparison of the optical constants of NbC, Mo and Si in the10-20 nm wavelength region [18].

The simulation carried out for NbC/Si and Mo/Si for identical structural parameters (*d- 6.3 nm, N= 51 Layer Pairs, Γ= 0.428, roughness σ = 0.3 nm for all interfaces*) shows that the theoretical reflectivity of Mo/Si (73.1%) and NbC/Si (70.6%) are almost identical. The results of calculations are plotted in Fig. (5.3). For any other identical structure of Mo/Si and NbC/Si, the reflectivity was found to be close with each other.

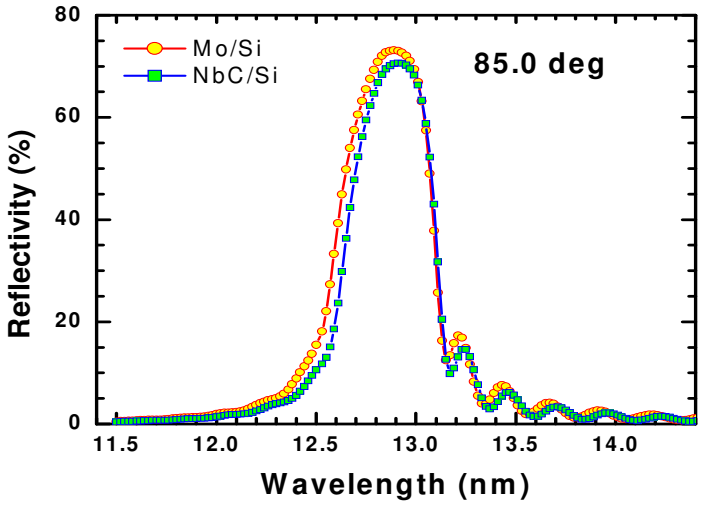

Fig. 5.3 Calculated soft x-ray reflectivity profile of Mo/Si and NbC/Si multilayers with identical structural parameters (d = 6.3 nm, Γ = 0.428, σ =0.3nm, N=51 layer pairs). At 85.0° incidence angle, the peak reflectivity of two multilayers is slightly different by ~2.5 %.

These calculations motivated us and in the present study we have examined the possibility of using NbC/Si multilayer as a replacement for Mo/ Si. We have examined the structural stability and reflectivity performance of the multilayer at high temperatures by carrying out annealing studies.

5.1.2 Experimental Details

In this work we first optimized deposition condition for depositing NbC thin films on Si (100) substrate with lowest interface roughness and highest density using developed ion beam sputtering system. Subsequently various NbC/Si multilayers were deposited for the study. High purity commercial targets were used to deposit NbC and Si layers. Film thickness was controlled by keeping the deposition time fixed for each layer. To study the thermal stability of the multilayers samples were annealed up to 700°C for 40 min in steps of 100°C in a vacuum of $< 1\times10^{-6}$ mbar.

XRR measurements were performed using Cu Kα (λ = 0.154 nm) radiation at a homemade reflectometer. GIXRD measurement was also performed of the samples after annealing. Soft x-ray reflectivity measurements were performed at Indus-1 reflectometry beamline[19] and BESSY-II storage ring facilities. At Indus-1, the multilayers were also tested near the Brewster angle in order to evaluate their polarizing properties. The details of the reflectometer are given in Ref [20].

5.1.3 Optimisation of NbC thin film deposition

Niobium carbide (NbC) is known to possess a rare combination of valuable properties like high melting point, high hardness, high toughness and Young's modulus, excellent chemical stability, together with good wear resistance which makes it interesting for a large range of applications. Niobium carbide also exhibits a high conductivity and even a superconducting phase at low temperatures [21].Our interest in NbC is because of its high melting point and excellent chemical satiability. NbC being a compound it may not be possible to deposit it in same chemical stoichiometry. Hence one may not get the same response as a bulk when deposited as thin films. To investigate these observations we first deposited thin films of NbC at various deposition conditions and characterized the films with XRR and GIXRD.

To understand the influence of discharge current and temperature on film quality, five samples of NbC films were deposited at different discharge current varying from 0.4 to 1.2 amps at room temperature with 3 cm^3/min Ar gas flow. Figure (5.4) shows the specular X-ray reflectivity patterns of the 25 nm thickness NbC thin films deposited at discharge current ranging from 0.4 amps to 1.2 amps along with best fit of the raw data. The fitting of data revealed that lowest interface roughness of 0.27 nm could be obtained in the films at a discharge current of 0.4 amps. But the density of films is good only in samples deposited at 0.6 amps and above discharge current as can be seen in the figure (5.4) (vertical line near critical angle) . Hence films deposited at 0.6 amps discharge current have lower roughness ~ 0.3 nm and highest density of ~ 6.9 g/$cc^{3.}$ At higher discharge current the number density of incident ions must have considerably increased to achieve best packing density of the film which increased the roughness of the film.

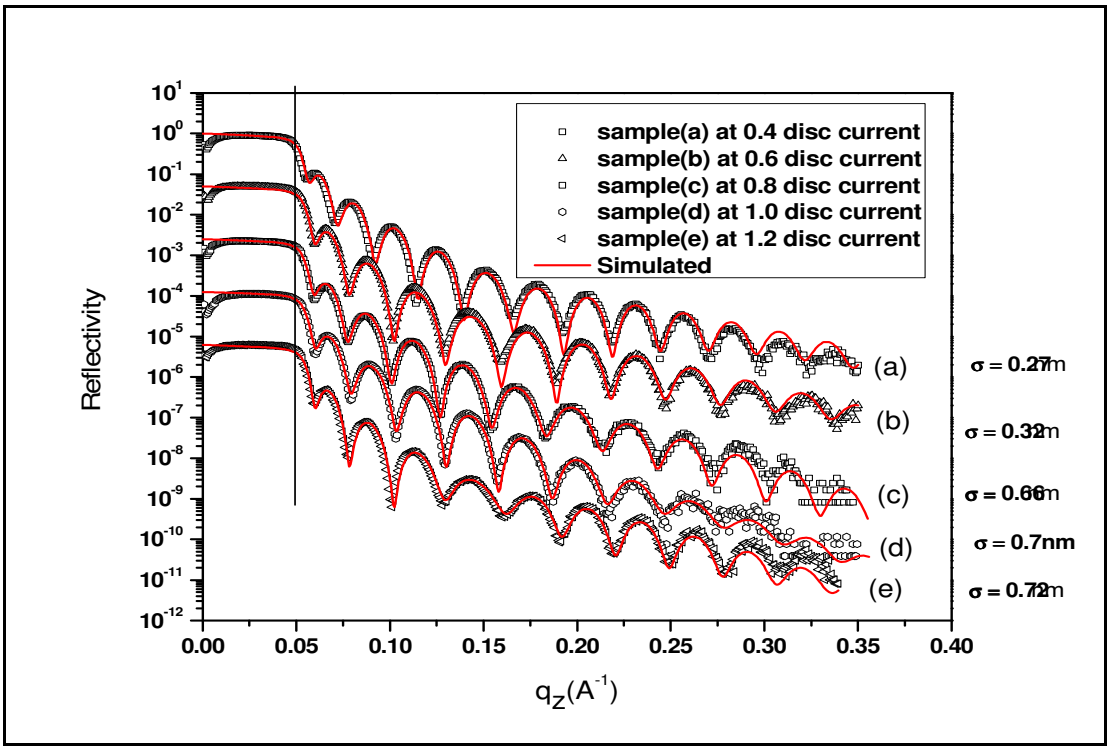

Fig. 5.4 X-ray reflectivity pattern (dots) of NbC films at various discharge current along with fitting (red line).

We further examined changes in the structure of film while depositing it at high temperatures. Similarly five samples were deposited at various substrate temperatures varying from room temperature to 200,300,400,600˚C at constant discharge current 0.6 amps using a heater mounted in place of substrate holder, as heater has some height of around 5cm

therefore the distance between target and substrate was reduced. Figure (5.5) shows the x-ray

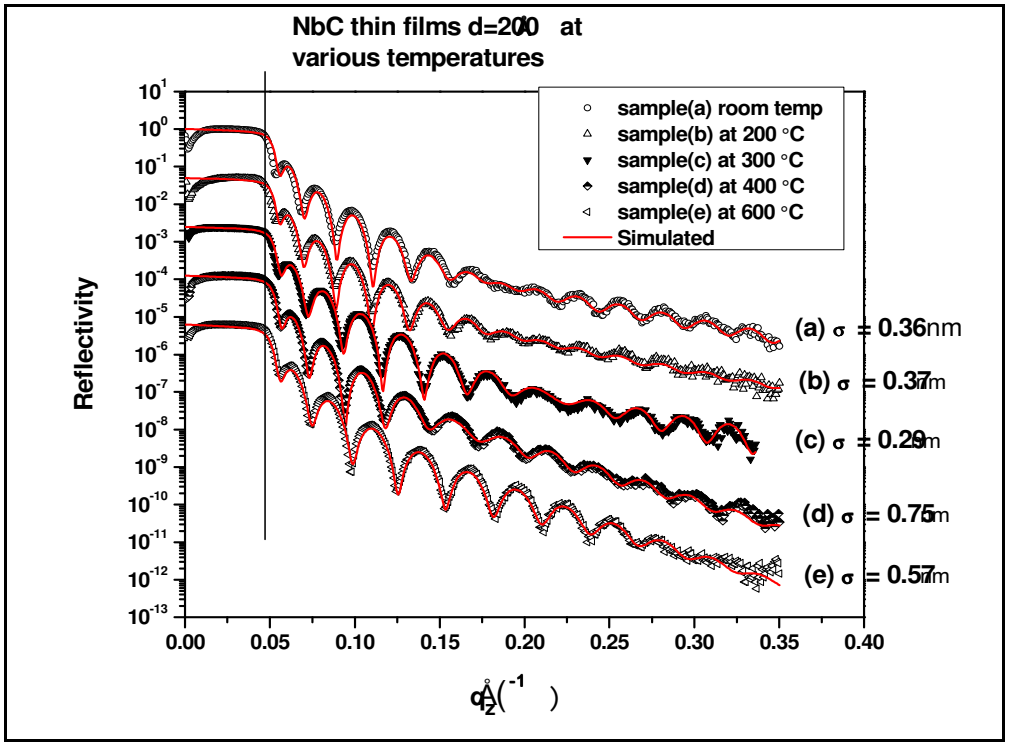

Fig.5.5 X-ray reflectivity pattern (dots) of NbC film at various temperatures along with fitting (red line).

reflectivity pattern of 20 nm samples deposited at various temperatures along with best fit line. It is clearly visible that temperature has no significant influence on the density of the film. Roughness of the does change with substrate temperature as the temperature is increased from room temperature the roughness reduces and at 300 ˚C we get the lowest roughness. On increasing the deposition temperature further increase in roughness is observed. It can be seen from XRR pattern that samples made at 400 and 600˚C show two layer structures. The second layer appears to be of a oxide layer of ~ 2.5 nm thicknesses as reveled by XRR fitting. These observations show that films deposited at temperature above 300˚C are growing in different growth mode which is increasing the roughness and simultaneously an additional layer of lower density is also forming at the top.

GIXRD of the films was carried out to examine the influence of high substrate temperature on the crystal structure of NbC layer. Figure (5.6) shows GIXRD pattern of NbC films deposited at various temperatures. It can be seen that samples deposited upto 300˚C are mixture of nearly amorphous and nano-crystalline phase. But in samples deposited at 400 ˚C and above we can see well defined diffraction peaks indicating transformations from mostly amorphous to largely crystalline state of the films. Indicating that growth mode has change

from 2D to 3D that is why the roughness of these films has increased suddenly in XRR analysis. Additionally some oxide peaks of NbO_2 are also seen in sample (e) (as marked in

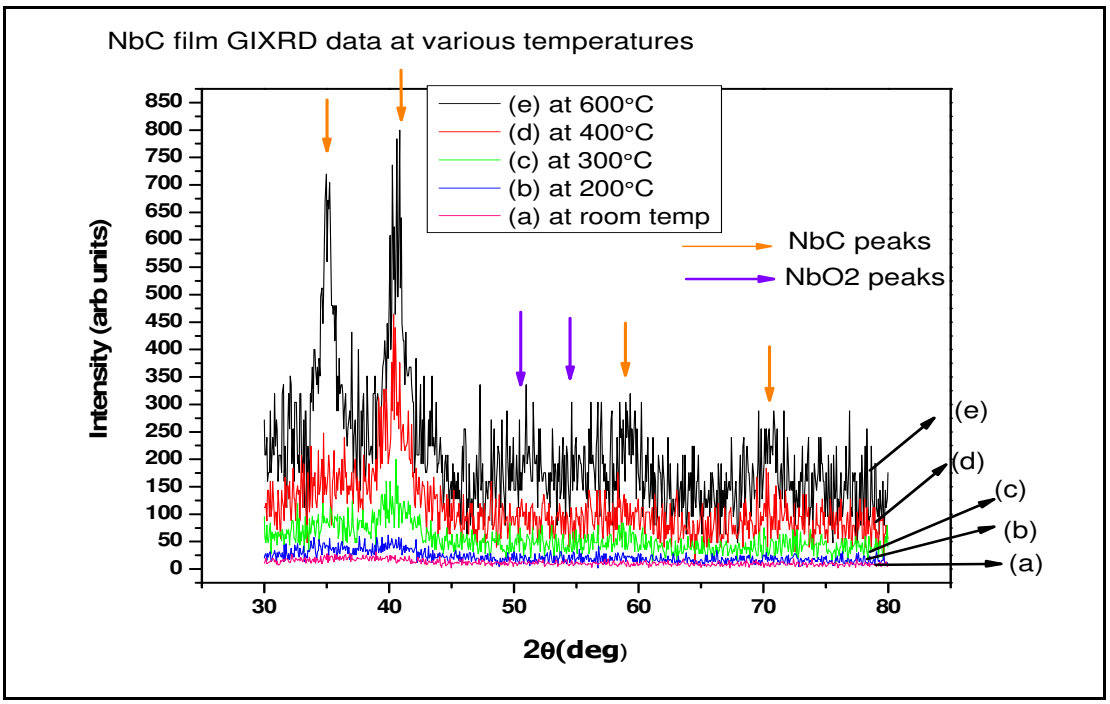

Fig. 5.6 GIXRD data of NbC films at various temperatures with peak positions of NbC and NbO_2 are marked with arrows.

figure 5.6). This explains the presence of a low density film observed in XRR analysis of samples made at high temperatures. Also on comparing the peak position of NbC layer for sample deposited at 600˚C we observe that these position match more with $NbC_{0.7}$ (PDF card no 01-074-5557) instead of NbC (PDF card no 00-038-1364). This indicates that NbC being deposited is slightly deficient in C and some Nb atoms are free which makes it possible to get oxidized while depositing at high temperature.

These optimization studies have shown that lowest roughness (0.3 nm) and highest density (6.9 g/cc3) of NbC films can be obtained at 0.6 amps discharge current deposition. Deposition at 300˚C temperature slightly reduces the roughness from room temperature deposition. NbC layer remains mostly amorphous if deposited at room at temperature and upto 300˚C above this temperature it turns to more crystalline.

5.1.4 Studies on NbC /Si Multilayers

After optimisation and characterisation of NbC film deposition we carried out our studies on NbC Si multilayers. The first sample looked at for high temperature stability was

~8 nm period 10 layer pair multilayer which was deposited at room temperature and post annealed up to 700°C in steps of 100°C for 40 minutes. The same sample was annealed every time. Figure (5.7) shows the reflectivity pattern of the same sample at room temperature and at high temperatures along with the fit line.. A noticeable feature is that the layer structure remains stable with no signature of interface degradation or any other kind of structural change. The overall reflectivity pattern with higher order Bragg peaks retained at the elevated temperatures. To carry out XRR data fitting two layer model was good at all temperatures, no interlayer was needed for fitting the XRR data. The parameter extracted from the XRR fitting of the sample are given in the table 5.1. As can be seen from this data that density of NbC is 6.9 g/cc^3 and density of Si is 2.0 g/cc^3. Density of NbC is same as observed in case of single layer, it is 12 % less than the bulk density of NbC (7.8 g/cc^3) and Si layer density is also less by 9% from bulk (2.2 g/cc^3). In thin film process it is common to have marginally reduced density with respect to the bulk value mainly because of variation in packing density. Presence of voids in between the interatomic spaces are the main cause of the reduced density which has been observed in the simulation of deposition process[22]. Another observation is that multilayer period initially expands marginally this expansion is so small that no shift is visible in first Bragg peak but shift can be observed in higher order

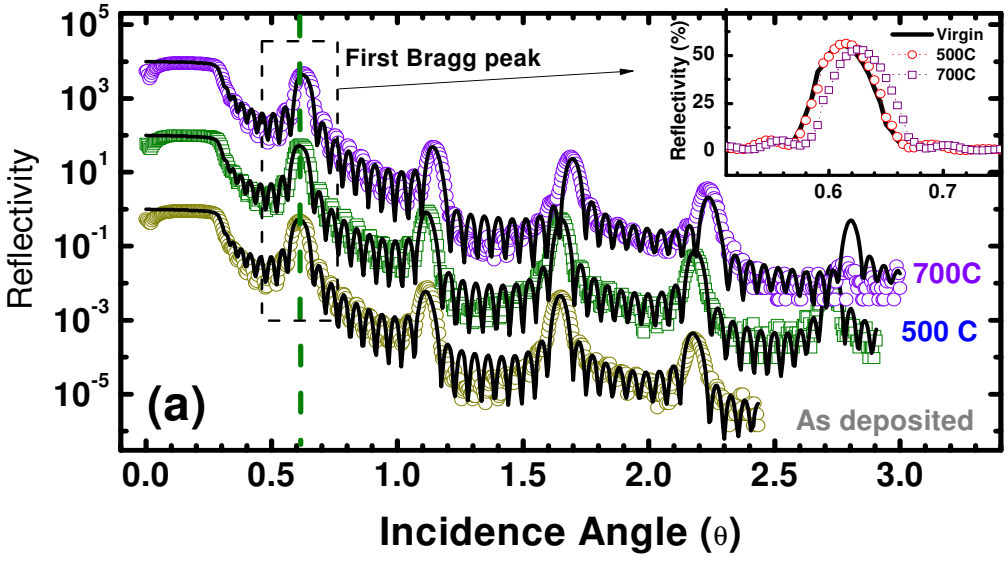

Fig. 5.7 XRR results of as-deposited and samples annealed up to 700℃ for 40 minutes Open circles represent measured data whereas best fit is shown by a continuous line. Inset

peaks. Detailed fitting revealed that period has expanded from 8.26 nm to 8.29 nm after annealing the sample at 300ºC and remained at that value till 500ºC. No significant variation was observed in the density and roughness values of NbC and Si layers till 600 ºC. After annealing at 600 ºC slight contraction from 8.29 to 8.16 nm is observed but still no detectable change in density or roughness values is observed, this indicates some compaction of layers is going on but change in density is so small that it is not detectable by XRR. Further annealing at 700 ºC showed significant reduction in the period thickness to 7.9 nm also thickness of both NbC and Si layer have reduced from 3.86 to 3.7 nm for NbC and 4.3 to 4.2 nm for Si layer. Simultaneously density of NbC layer has reduced marginally to 6.6 g g/cc^3 from 6.9 g/cc^3 where density of Si layer has increased slightly to 2.3 g/cc^3 from 2.0 g/cc^3. These observations indicate that intermixing of NbC and Si is happening across the interface at this temperature but still the structure is maintained and not very significant degradation has taken place. Annealing at 800 ºC has spoiled the structure and it was not possible to fit the XRR data from the sample. From these observation it can be concluded that NbC/ Si retains it multilayer structure till 700 ºC temperature which is a significant improvement compared to stability of Mo./Si multilayer which was stable upto 100 ^{0}C only and upto 300 ^{0}C with barrier layers[23].

Temperature (ºC)	*Thickness NbC (nm)*	*Thickness Si (nm)*	*Total Period(nm)*	*Density NbC(g/cc)*	*Density Si(g/cc)*	*Roughness NbC (nm)*	*Roughness Si(nm)*
Room temp	*3.96 ±0.03*	*4.3 ±0.03*	*8.26 ±0.06*	*6.9*	*2.0*	*0.55 ±0.07*	*0.8 ±0.08*
200	*3.96 ±0.03*	*4.3 ±0.03*	*8.26 ±0.06*	*6.9*	*2.0*	*0.55 ±0.07*	*0.8 ±0.08*
300	*3.98 ±0.03*	*4.3 ±0.03*	*8.29 ±0.06*	*6.8*	*2.0*	*0.5 ±0.07*	*0.84 ±0.08*
400	*3.99 ±0.03*	*4.3 ±0.03*	*8.29 ±0.06*	*6.9*	*2.0*	*0.5 ±0.07*	*0.85 ±0.08*
500	*3.99 ±0.03*	*4.3 ±0.03*	*8.29 ±0.06*	*6.9*	*2.0*	*0.45 ±0.06*	*0.85 ±0.08*
600	*3.86 ±0.03*	*4.3 ±0.03*	*8.16 ±0.06*	*6.9*	*2.0*	*0.48 ±0.06*	*0..85 ±0.08*
700	*3.7 ±0.03*	*4.2 ±0.03*	*7.9 ±0.06*	*6.6*	*2.3*	*0.6 ±0.06*	*0.9 ±0.08*

Table 5.1 Thickness roughness and density values of NbC Si layer after annealing.

To examine the crystal structure change happening in the samples due to annealing GIXRD of all the samples was carried out. Figure (5.8) show the GIXRD pattern of sample

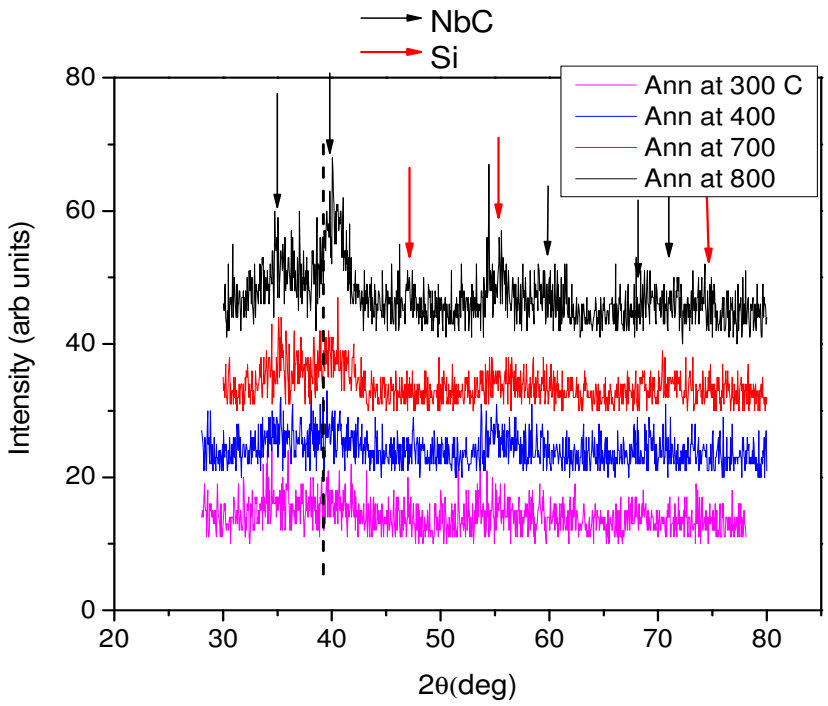

Fig. 5.8 GIXRD pattern of samples annealed at 300,400,700 and 800 ºC. Patttern have been shifted *vertically fro clarity. Peak position of NbC and Si have been marked with black and red arrows*

annealed at 300, 400, 700 and 800 ºC. Peak position of NbC and Si have been marked with black and red arrows in the figure. No peak in the GIXRD pattern of sample was seen from as deposited as well as sample annealed till 200 ºC. Slight ordering could be seen in NbC layer after annealing at 300 ºC, as (111) and (200) peaks are visible at ~35º and 40º two theta. This indicates that NbC layer is nearly amorphous in as deposited samples and becomes nano-crystalline with annealing. On further annealing these peaks grow in size and higher order peaks at 58º, 69º and 73º two theta become also visible at 400 ºC indicating increased ordering. Diffraction peaks of Si are not visible till sample annealing at 700 ºC only in samples annealed at 800 ºC we are able to Si appearance of Si peaks indicating that Si is become more and more crystalline. No other phase peak could be detected even in the samples annealed at 800 ºC confirming that no reaction is taking place between Nb and Si. Increased crystallization of NbC and Si at high temperature could be the cause of compaction and intermixing seen at 700 ºC in XRR data analysis. Cause of initial expansion is still not understood.

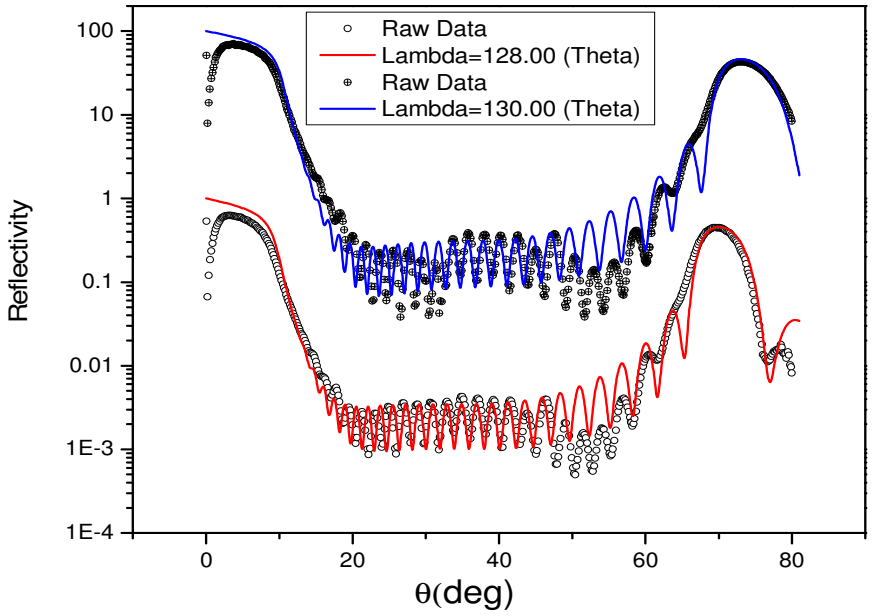

Fig. 5.9 soft x-ray reflectivity pattern of the 30 layer pair 6.98 nm period sample recoded at 12.8 nm and 13 nm along with the best fit line.

From XRR and GIXRD it can be inferred that NbC/ Si multilayer remains stable up to 700ºC annealing. To verify the normal incidence soft x-ray reflectivity performance of the multilayer mirror. We deposited another samples of NbC Si with 30 layer pairs and period of 6.98 nm. From hard x-ray XRR data fitting we found that the thickness, roughness and density of NbC layer were 2.83 nm, 0.66 and 6.7 g/cc, for Si layer these values were 4.15 nm, 0.88 nm and 2.0 g/cc. The higher roughness of the NbC layer could be due to lower thickness of this layer in this sample compared to previous samples (3.9 nm NbC). Same sample was loaded in soft x-ray reflectometer on indus-1 beam line and reflectivity of the sample was recorded at various wavelengths. Figure (5.9) shows the soft x-ray reflectivity pattern of the same sample recoded at 12.8 nm and 13 nm along with the best fit line. The soft x-ray reflectivity data could be fitted at both wavelength with same parameters as extracted from hard x-ray reflectivity only interface roughness of NbC layer had to be increased slightly to 0.72 nm and additionally one low density 4 nm carbon layer was needed to match the bump observed in the kiessig oscillations. The peak reflectivity observed from this sample was 42.45 % at 13 nm wavelength which is very good considering only 30 layer

pairs of the sample. Simulation using IMD [24] showed that if we have 45 layer pairs it would be possible to get more than 60% reflectivity. This is comparable with Mo /Si reflectivity simulated using same structural parameters. Soft x-ray reflectivity measurements were again

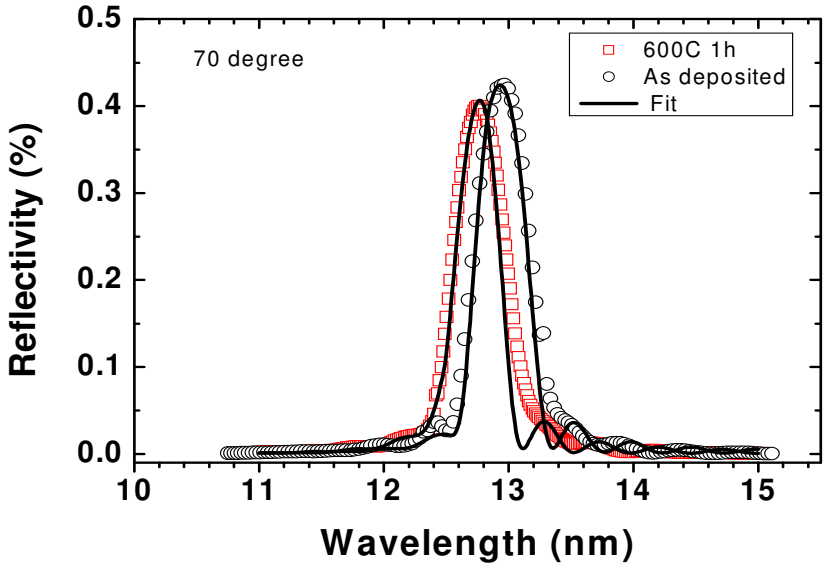

Fig. 5.10 Measured and fitted soft x-ray reflectivity spectra of as deposited and 600°C annealed sample.

carried out after annealing the same sample at 600 ºC for 1.5 hours. Figure (5.10) shows soft x-ray reflectivity wavelength scan of the sample measured at 70° angle of incidence of as deposited and 600°C annealed sample along with best fit line. After annealing the Bragg peak shifts towards lower wavelength due to period contraction from 6.98 nm of as deposited value to 6.86 nm after the 1.5 h annealing. This contraction was similar as observed in our annealing studies performed on 8.26 nm period sample in the beginning of the study. The present study suggests that, the NbC/Si multilayer has a potential to emerge as a high reflectivity mirror with extremely high stability for the 10-20 nm wavelength range. Another major advantage with this combination is that there is no chemical reaction seen between Nb and Si even after annealing at 800 ºC and complete loss of multilayer structure. No silicide formation or any other chemical species could be detected after the annealing. This proves that new combination can be used for high thermal load applications.

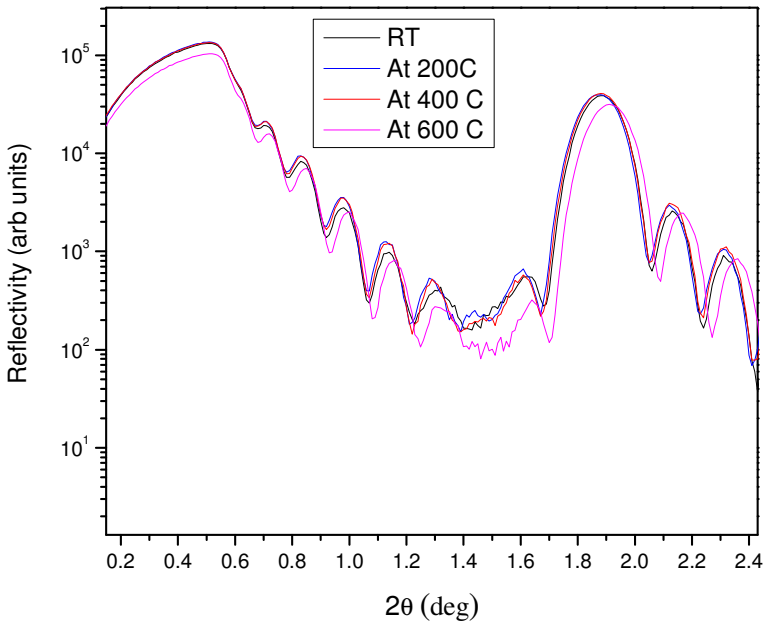

Fig. 5.11 Variation in first Bragg peak position in hard x-ray reflectivity pattern of 6 nm period sample measured in-situ at 200,400and 600 ºC.

As a further test of the performance of this combination reflectivity measurement of 10 layer pair multilayer of 6 nm sample was carried by in-situ heating upto 600 ºC and measuring the hard x-ray reflectivity on a commercial D8- Discover XRR system with MRI high temperature attachment. Figure (5.11) shows that while in-situ heating also there is no significant change in peak position up to 400 ºC only when temperature goes at 600 ºC we see a shift. These observations further confirm the high temperature stability of this combination.

5.1.5 High Temperature Deposition Studies

All these observations establish that NbC/Si indeed is a very good replacement for high heat load applications. Only problem with present mirrors is that this system has shown a low soft x-ray reflectivity performance because of high interface roughness values of both NbC and Si layers. To overcome this issue we carried out some more optimization procedures to achieve lower interface roughness and higher density contrast. To reach this objective we carried out different approaches. High thermal stability of multilayer and absence of chemical reaction between NbC and Si motivated us to try depositing multilayer at

higher temperature. So, as a first method to reduce interface roughness, we deposited the multilayer at different substrate temperature and examined the interface roughness. We deposited 10 layer pairs of 7 nm period samples on Si(100) substrate at room temp, 100,200,300,400,500 ºC. Hard x-ray reflectivity measurements were carried out to find out the interface roughness of these samples. Figure (5.12) shows the plot of interface roughness of NbC and Si layer in the multilayer deposited at various temperatures. It can be observed

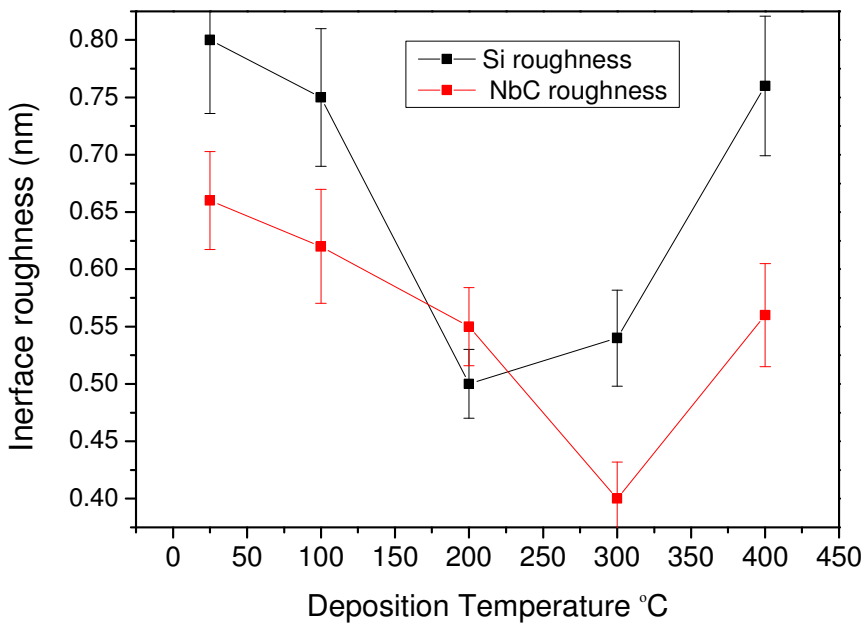

Fig. 5.12 Variation of interface roughness of NbC and Si layer in the multilayer deposited at various temperatures.

from the graph that at temperatures between 200 and 300ºC it is possible to get lowest roughness in range of 0.5-04 nm for both NbC and Si layers. We have not shown the interface roughness of the sample deposited at 500 ºC because at this temperature multilayer structure could not be formed strong intermixing of NbC and Si was observed. We also carried out post deposition high temperature annealing of these multilayers as explained earlier at various temperature for 30 minutes and carried out hard x-ray reflectivity measurements. Figure (5.13) shows that variation in first Bragg peak reflectivity with annealing temperature for samples deposited at different temperatures.

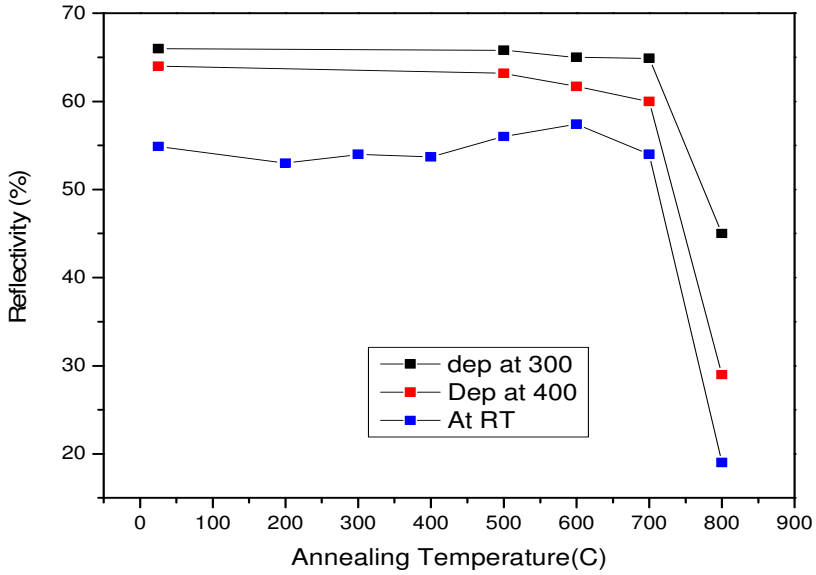

Fig. 5.13 Variation first Bragg peak reflectivity with annealing temperature for samples deposited at room temp., 300 and 400°C.

Post deposition annealing behaviour of samples deposited at high temperature is same as of the sample made at room temperature. All the samples remain stable till 700°C and at 800°C the reflectivity falls rapidly. Reflectivity of the sample deposited at 300°C is higher than the samples deposited at room temperature and at 400 °C. These observations confirm that depositing multilayer at temperature between 200-300°C we would get lowest interface roughness and high reflectivity.

5.1.6 Summary

The present study suggests that the NbC/Si multilayers have a potential as a high reflectivity and high stability mirror in the 10-20 nm wavelength range. The calculated reflectivity of this new material combination is comparable with those obtained from the conventional Mo/Si multilayer for identical structural parameters. No interdiffusion or interface degradation occurs after the heat treatment. No silicide formation or any other chemical species could be detected after the annealing. To avoid the problem of high interface roughness this combination can be deposited at high temperature between 200 to 300 °C.

5.1.6 References

1 S. Yulin, in: N. Kaiser, H. Pulker (Eds.), Optical Interference Coatings, Springer Series in Photonics, (2003).

2 M. Slaughter, P.A. Kearney, D.W. Schulze, C.M. Falco, C.H. Hills, E.B. Saloman, R.N. Watts, Proc. SPIE 1343, (1999), 73.

3 D.L. Windt, R. Hull, K. Waskiewicz, J. Appl. Phys. 71, (1992), 2675.

4 S. Bajt, D.G. Stearns, P.A. Kearney, J. Appl. Phys. 90, (2001), 1017.

5 S. Yulin, T. Feigl, T. Kuhlmann, N. Kaiser, A.I. Fedorenko, V.V.Kondratenko, O.V. Poltseva, V.A. Sevryukova, A.Y. Zolotaryov, E.N. Zubarev, J. Appl. Phys. 92, (2002), 1216.

6 M.H. Modi, G.S. Lodha, M. Nayak, A.K. Sinha, R.V. Nandedkar, Physica B 325, (2003), 272.

7 M. Nayak , G. S. Lodha, A. K. Sinha, R. V. Nandedkar and S. A. Shivashankar, Appl. Phys. Lett., 89, (2006), 182920.
8 D.G. Stearns, R.S. Rosen, Proc. SPIE 1547, (1991), 2.

9 H. Maury, P. Jonnard, J.-M. André, J. Gautier, M. Roulliay, F. Bridou, F. Delmotte, M.-F. Ravet, A. Jérome, P. Holliger, Thin Solid Films, 514, (2006), 278.

10 E. Allaria, C. Callegari, D. Cocco, W. M. Fawley, M. Kiskinova, C. Masciovecchio, F. Parmigiani, N. J. Phys. 12, (2009), 075002.

11 W. Ackermann, G. Asova, V. Ayvazyan, A. Azima, et al. , "Operation of a free-electron laser from the extreme ultraviolet to the water window," Nat. Photonics 1,(2007), 336.

12 A. R. Khorsand, R. Sobierajski, E. Louis, S. Bruijn, E. D. van Hattum, R. W. E. van de Kruijs, M. Jurek, D. Klinger, J. B. Pelka, L. Juha, T. Burian, J. Chalupsky, J. Cihelka, V. Hajkova, L. Vysin, U. Jastrow, N. Stojanovic, S. Toleikis, H. Wabnitz, K. Tiedtke, K. Sokolowski-Tinten, U. Shymanovich, J. Krzywinski, S. Hau-Riege, R. London, A. Gleeson, E. M. Gullikson, and F. Bijkerk, Opt. Express 18, (2010), 700.

13 F. Barkusky, A. Bayer, S. Döring, P. Grossmann, and K. Mann, Opt. Express 18, (2010), 4346.

14 R. Sobierajski, S. Bruijn, A.R. Khorsand, E. Louis, R.W. E. van de Kruijs, T. Burian, J. Chalupsky, J. Cihelka, A. Gleeson, J. Grzonka, E.M. Gullikson, V. Hajkova, S. Hau-Riege, L. Juha, M. Jurek, D. Klinger, J. Krzywinski, R. London, J. B. Pelka T. Płociński, M. Rasiński, K. Tiedtke, S. Toleikis, L. Vysin, H. Wabnitz, F. Bijkerk, Opt. Express 19, (2010), 193.

15 M. Barthelmess and S. Bajt, Appl. Opt. 50, (2011), 1610.

16 M.Y. Liao, Y. Gotoh, H. Tsuji, J. Ishikawa, "Compound-target sputtering for niobium carbide thin film deposition," J. Vac. Sci. Tehnolol. B 22, (2004), L24.

17 S. Barzilai, M. Weiss, N. Frage, A. Raveh, Surface and Coatings Technology 197, (2005), 208.

18 B. L. Henke, E. M. Gullikson, and J. C. Davis, "X-ray interactions: photoabsorption, scattering, transmission, and reflection at E = 50–30000 eV, Z = 1–92," At. Data Nucl. Data Tables 54, (1993), 181. http://www-cxro.lbl.gov/optical constants/.

19 R.V. Nandedkar, K.J.S. Sawhney, G.S. Lodha, A. Verma, V.K. Raghuvanshi. A.K. Sinha, M.H.Modi, M. Nayak, "First results on reflectometry beamline on Indus-1," Current Science 82, (2002), 298.

20 G.S. Lodha, M.H. Modi V.K. Raghuvanshi, K.J.S. Sawhney, R.V. Nandedkar, "Soft X-ray Reflectometer on Indus-1," Synchrotron Radiation News,17, (2004), 33.

21 E.V. Pechen, S.I. Krasnosvobodtsev, N.P. Shabanova,E.V.Ekimov, A.V.Varlashkin,V.D. Nozdrin, Physica C 235, (1994), 2511.
22, "Dependence of thin-film microstructure on deposition rate by means of a computer simulation," K.H. Muller, J. Appl. Phys. 58, (1985), 2573.

23 H. Maury, P. Jonnard, J.-M. André, J. Gautier, M. Roulliay, F. Bridou, F. Delmotte, M.-F. Ravet, A. Jérome, P. Holliger, Thin Solid Films 514, (2006), 278.

24 D.L.Windt " IMD: software for modeling the optical properties of multilayer films" Computer in Physics 12, (1998), 360.

Chapter 6

Summary and Future Scope

6.1 Summary

In this thesis we carried out both development and surface interface studies using developed instruments. The major conclusions of the thesis work are summarized below

Development of x-ray reflectometer

We have designed and assembled a moderate resolution x-ray reflectometer capable carrying out measurements on large and odd shaped samples. Instrument consists of a tube based x-ray source, collimation system, goniometer, multilayer and graphite monochromator assembly, detector and a PC for controlling and data acquisition. In this system x-ray source used is a Philips x-ray tube with Cu target. The source operates in a horizontal line focus. The effective size of the focus at a takeoff angle of 3° is 10 mm X 0.05 mm. The system can be operated with both incident beam monochromator and reflected beam monochromator or with only one monochromator as per the requirement. The performance of developed system was compared with commercial system and was fond better due to precise alignment of the system. This system is capable of carrying out GIXRD and powder XRD with very little change in optics. The developed system was used to carry out reflectivity studies on thin film and multilayer samples used for this thesis. In the later part of the thesis work we shifted this instrument to Indus -2 beamline also and carried out initial experiments.

Development of Ion beam sputtering based deposition system

We have designed and assembled an ion beam sputtering system based on Kaufman focused beam ion source. A four target holder (square block) is installed in which we can load four targets at a time for depositing thin film and multilayers of various materials. A substrate holder is also mounted on a rotary feed through which can hold four substrate at a time therefore we can fabricate four samples in a single or multiple operations without breaking the vacuum of the chamber. A substrate heater is also installed that can be used in place of substrate holder for fabricating of thin films and multilayers at high temperature (max up to 700 ^{o} C). Thickness of the film can be monitored using quartz crystal thickness monitor (INFICON IC/5). Base vacuum in the chamber is ~2×10^{-7} mbar and samples are fabricated at a pressure of the order of 4×10^{-4} to

6×10^{-4} mbar. Most of the samples used in this study have been fabricated using the same system after proper optimization.

Case studies carried out using developed system

We have carried out various case studies using developed system. The First study we carried out was x-ray reflectivity based study of pulsed laser deposited NiMnSb (alloy) thin films on Si (100) substrate. In this study, we used to XRR as a main tool to explore how the morphology of thin films is changing with thickness and confirmed the conclusion with help of TXRF and magnetization measurements. It is concluded that the presence of porous layer is the main cause of anomalous behavior of thinner films.

In second case study we have carried out analysis of growth kinetics of oxidation process on Niobium thin film in a non destructive manner using X-Ray Reflectivity. These measurements showed that an oxide layer of ~2 nm gets formed immediately after deposition which grows at a slow rate even at room temperature. We could successfully estimate the oxidation rate in the films with time. Since the growth rate of oxidation process is surface sensitive, therefore, a protective layer should be grown in-situ to avoid oxidation of Nb thin film surface.

In our investigation on Co/Si we have found that the Co layer in Co/Si multilayer system is highly oriented only for the multilayer containing low thickness of Si layers and this texture is lost as we increase the thickness of the Si layer, this thickness is ~5.6 nm. No peak due to silicide phase formation in the as-deposited Co/Si ML is seen in the XRD pattern, suggests that silicide phase is not present and even if it is present its volume fraction is so low that is presence is not seen in the XRD pattern. Magnetic measurements carried out using MOKE showed only ferromagnetic coupling between the Co layers. The hardness or softness of this ferromagnetic behavior is highly governed by Si layer thickness.All these suggest that it is the texture of the Co layer, which depends on the thickness of the Si layer that affects the magnetic properties of Co/Si system. Since silicide layer is not visible distinctly at the interface, its possible effect on the magnetic behavior of the system is not clear. Thus, structural and in turn magnetic properties of Co/Si ML system are highly governed by thickness of the Si layer and not by silicide layer

Finally we carried out Characterization of thin foil gold mirror for soft x-ray telescope ASTROSAT. This telescope is an Indian multi-wavelength Satellite telescope designed to cover

a very broad band of X-rays. Detailed X-ray reflectivity characterization of the mirrors at multiple energies was extremely important during the process of fabrication to qualify them and also to test their performance after subjecting them to various environmental tests. Developed reflectometer was used for characterization of large size curved mirrors. These measurements helped in optimizing the fabrication procedure and in predicting the imaging performance of the telescope.

All these studies have demonstrated that how x-ray reflectivity can be useful in getting details of electron density profile of the thin film structure other than just estimating film thickness and roughness. Knowledge of density profile gives finer details about the structure.

Interface analysis of short period multilayers

In this study we have studied mainly interfaces of W/Si, W/C and W/B_4C at varying periods from 9 nm to 1.5 nm. We have analyzed the influence of back scattered neutrals/ions on the growth of multilayers at short periods from re-sputtering and intermixing point of view.

The analysis of XRR, data on W/Si multilayer indicates that re-sputtering of Si layer happens during deposition and no re-sputtering of W layer occurs. Maximum thickness of Si which gets removed during deposition due to re-sputtering is ~ 0.8nm. This information about maximum thickness of Si getting lost is very useful for designing the short period multilayers and super-mirrors. Re-sputtering of Si layer stops, when the thickness of W layer on Si reaches 1.4 nm. When W layer thickness becomes greater than 1.4 nm it becomes continuous and covers the whole surface. This is observed that re-sputtering is modifying the interface and generating an asymmetry in the roughness of W on Si interface (~0.9nm) to Si on W interface(~0.5nm). It is not possible to remove this asymmetry in present setup. When thickness of Si layer goes below 1.3 nm, inter-diffusion/mixing of W into Si layers starts, due to cascade recoils produced from reflected neutrals/ion hitting the Si layer. TRIM simulations were done to confirm influence of back reflected ions and neutral hitting the Si surface. This observation points out that shortest period multilayer which can be deposited without intermixing should have W more than 1.4nm and Si more than 1.3nm. This means that shortest period of W Si layer which can be deposited is 2.7 nm.

TRIM simulations were done for damage calculations when Si, C and B_4C layers were bombarded with 100 eV Ar ions. It is observed from the calculations that both B_4C and C have much larger damage resistance compared to Si. This is happening due to large lattice binding energy, surface binding energy and displacement energy of B_4C and C compared to Si. This seems a major reason why we are able to produce multilayers with sharper interface with C and B_4C. These results were confirmed by depositing bilyers and trilayers of W/Si, W/C and W/B_4C. It was observed that in W/Si/W trilayers the interface roughness of Si layer was increasing from 0.4 in bilayer to 0.9nm in trilayer, whereas in case of W/C/W and W/B_4C/W trilayers not much increase in the interface roughness of C or B_4C was observed. This confirmed that C and B_4C being more resistant to damage by reflected neutrals should produce sharper interface.

Study on W/B_4C multilayers between 1.2 to 4 nm periods revealed following results. It is observed that when B_4C layer thickness goes below 1.0 nm intermixing of W starts in the B_4C layer. The intermixing is happening due to bombardment of high energy reflected ion/neutrals as confirmed by SRIM simulations. Lowest continues thickness of B_4C have been estimated to be 1.0 nm. Present study reveals that 1.9 nm period is the smallest period which should shows sharp interface and good thermal stability for W/B_4C combinations. This observation confirms the prediction from damage calculations that W/B4C should produce multilayer with sharper interface to achieve lower period limits.. Our studies on large layer pair samples have confirmed these conclusions. The 300 layer pair, 2 nm period sample has shown 1.2% energy resolution at 8 keV and 59% reflectivity. The measured Bragg peak reflectivity after annealing of different samples show that samples of 2.0 nm period or above do not show much degradation due to annealing in the reflectivity of first Bragg peak.

On the basis of this study we can conclude that reflected neutrals play a important role in growth of multilayer mirrors. They influence the growth in two ways (1) re-sputter the low Z layer and make it rough (2) If thickness of low Z layer is less than 1.5 nm for Si layer and 1 nm for B_4C layer than reflected neutrals produces intermixing at the buried interface below low Z layer by creating a collision cascade. It this way these neutrals reduce the contrast between low Z and high Z layers. To further extend the period to shorter lengths it would be required to reduce the damage from reflected ions /neutrals of low Z layer. Simulations using SRIM have shown that using Xe in place of Ar would reduce the number of reflected ion/neutrals to 25% of what is

expected with Ar with slightly reduced energies. But use of Xe would reduce the sputter yields of B_4C by half. The thermal stability shown by these multilayers and lack of chemical reaction between W and B_4C give an idea that depositing multilayer at higher temperatures than room temperature might help us in achieving even shorter periods with lower roughness.

Development of Soft x-ray Normal incidence mirror

In this study we have worked on a new combination of NbC/Si for normal incidence mirror application in 10-20 nm wavelength region. The calculated reflectivity of this new material combination is comparable with those obtained from the conventional Mo/Si multilayer for identical structural parameters. This study suggests that the NbC/Si multilayers have a potential as a high reflectivity and high stability mirror in the 10-20 nm wavelength range. Annealing experiments at 600°C showed a period contraction with a nominal drop of ~3% in normal incidence reflectivity at 13 nm wavelength. This combination showed no degradation in interfacial properties after annealing at temperatures up to 700 °C. No silicide formation or any other chemical species could be detected after the annealing. Only problem with NbC /Si is that it is depositing with slightly high interface roughness. To avoid the problem of high interface roughness this combination can be deposited at high temperature between 200 to 300 ºC.

6.2 Future directions

Every research work resolves our immediate problems and generates more problems for future. It is true in our case also. We have developed some understanding that reflected neutrals do have a role to play at shorter periods which was largely ignored till now. To further extend the limits one has to reduce the damage from reflected ions /neutrals of low Z layer. Simulations using SRIM have shown that using Xe in place of Ar would reduce the number of reflected ion/neutrals to 25% of what is expected with Ar with reduced energies. But use of Xe would reduce the sputter yields of B_4C by half. Doing deposition with Xe as sputtering gas, would only give the answers. One can think of using a combination. Another way to enhance the limit may be to use some other material pair in which bombardment of high energy neutrals can be reduced. For this purpose one may have to use some other material of lower Z values instead of W as higher the Z of target more is the energy of the neutrals. This might reduce the contrast but interface would become smoother. As in case of short period multilayer large number of layer

pairs take part, so loss of density contrast may be compensated by number of layer pairs. But loss of interface sharpness can not be compromised.

The thermal stability shown by W/B_4C multilayers and lack of chemical reaction between W and B_4C give an idea that depositing multilayer at higher temperatures than room temperature might help us in achieving even shorter periods with lower roughness. Issue of stresses in large layer pair multilayers have not been addressed in this thesis. Assessment stress in these multilayers would be required for depositing large layer pair stable multilayers.

In our work on NbC/Si normal incidence mirrors we have done comparison of performance variation after annealing with 30 layer pairs samples and initial results are encouraging. The problem of high interface roughness has been handled by carrying out deposition at high temperature. But still to get a complete answer one should test the performance only after depositing 50 or more layer pairs. These tests only would prove the long term use of this combination.